REPORT DOCUMENTATION PAGE

Form Approved
OMB No. 0704-0188

PLEASE DO NOT RETURN YOUR FORM TO THE ABOVE ORGANIZATION.

1. REPORT DATE *(DD-MM-YYYY)*	2. REPORT TYPE	3. DATES COVERED *(From - To)*
1 Sept 07	Final Report	1 Sept 07-31 May 08

4. TITLE AND SUBTITLE
Starfire Industries LLC
Microwave Plasma propulsion systems for defensive counter-space

5a. CONTRACT NUMBER

5b. GRANT NUMBER
FA9550-07-C-0087

5c. PROGRAM ELEMENT NUMBER

6. AUTHOR(S)
Brian E. Jurczyk

5d. PROJECT NUMBER

5e. TASK NUMBER

5f. WORK UNIT NUMBER

7. PERFORMING ORGANIZATION NAME(S) AND ADDRESS(ES)
Starfire Industries LLC
60 Hazelwood Dr
Champaign IL 61820-7460

8. PERFORMING ORGANIZATION REPORT NUMBER

9. SPONSORING/MONITORING AGENCY NAME(S) AND ADDRESS(ES)
Air Force Office of Scientific Research
875 North Randolph Street
Arlington, VA22203
New Haven. CT 06520-8286

10. SPONSOR/MONITOR'S ACRONYM(S)
AFOSR/RSA

11. SPONSOR/MONITOR'S REPORT NUMBER(S)
FA9550-07-C-0087

12. DISTRIBUTION/AVAILABILITY STATEMENT
Distribution Statement A: Approved for public release. Distribution is unlimited.

AFRL-AFOSR-VA-TR-2016-0044

13. SUPPLEMENTARY NOTES

14. ABSTRACT
The key result from this project period was measurement of plasma acceleration in both over-dense and under-dense modes with the former generating high ion currents in the 12-60 eV beam energy range and the latter generating plasma in the 50-500 eV range. As hypothesized in the Phase I proposal, resonantly exciting electrons near the peak of the magnetic nozzle expansion region leads to large ambipolar field generation and quasi-static ion acceleration. Variation in propellant mass flow and magnetic field produce observable changes in downstream ion energy. Interpretation of published literature on ECR-plasma Monte Carlo simulations suggests that high jet power efficiency exceeding 65%, rivaling modern Hall-Effect Thrusters!

15. SUBJECT TERMS
Standard terms apply

16. SECURITY CLASSIFICATION OF:			17. LIMITATION OF ABSTRACT	18. NUMBER OF PAGES	19a. NAME OF RESPONSIBLE PERSON
a. REPORT	b. ABSTRACT	c. THIS PAGE			Mitat Birkan
U	U	U	UU		19b. TELEPHONE NUMBER *(Include area code)* 703-696-7234

Part 1: Executive Summary

This final report summarizes the collaborative Phase I Small Business Technology Transfer Research (STTR) project between Starfire Industries and the University of Illinois on microwave plasma thrusters and Electron Cyclotron Resonance (ECR) plasmas with dual-use defensive counterspace (DCS) capabilities. The project met all of the Phase I objectives and demonstrated a clear pathway towards an electrode-less plasma thruster with multi-mode capability (i.e. high thrust and high specific impulse) and defensive counterspace abilities (i.e. detection and disablement). The dual-use advantages using high-power microwaves make the argument for advanced electric propulsion stronger.

The key result from this project period was measurement of plasma acceleration in both overdense and underdense modes with the former generating high ion currents in the 12-60 eV beam energy range and the latter generating plasma in the 50-500 eV range. As hypothesized in the Phase I proposal, resonantly exciting electrons near the peak of the magnetic nozzle expansion region leads to large ambipolar field generation and quasi-static ion acceleration. Variation in propellant mass flow and magnetic field produce observable changes in downstream ion energy. Interpretation of published literature on ECR-plasma Monte Carlo simulations suggests that high jet power efficiency exceeding 65%, rivaling modern Hall-Effect Thrusters!

The results from the Phase I evaluation indicates multi-modal propulsion capability:

- ECR-driven ambipolar acceleration and magnetic expansion for high specific impulse (Isp)
- Direct microwave heating magnetic expansion for moderate-Isp levels and moderate thrust
- Electrothermal physical nozzle expansion for moderate-Isp and high thrust.

Multiple configurations for DCS operations are envisioned with microwave plasma systems:

- Remote Object Detection: phase-array microwave transceiver scanning
- Illumination and Evaluation: x-ray and plasma illumination
- Disable and Negation: focused microwave beam with plasma waveguide
- Screening and Protection: local high-density plasma shielding and fouling

The proposed microwave thruster could leverage even more functionality to existing spacecraft systems laden with communication systems. Microwave sources, such as phased-array solid-state power amplifiers (and older traveling wave tube amplifiers and klystrons), are already employed on satellites for communication and data link operations in the 2-50GHz range. A large amount of mass, volume, and power are already devoted to these microwave generators for communications. If the microwave plasma thruster system could be used for propulsion, DCS applications, and communications…this would truly constitute a "multi-use" system and be a win-win scenario.

Based on these factors, there is strong support for Phase II investigation and Starfire has secured preliminary approval for future testing at Edwards Air Force Base on a thrust stand.

Based on a successful future Phase II, Starfire Industries would be positioned to commercialize a technology that would lead to near-term, flexible, efficient, and compact electric propulsion (EP) systems to meet Air Force mission requirements leverage existing MILSATCOM on-orbit capability at 2.45GHz, 7.5GHz, 14.5GHz and 45GHz. Starfire also envisions concepts for low-power nanosat defensive satellite architectures, such as ANGELS.

Furthermore, Starfire Industries has also identified a near-term commercial application of a compact microwave plasma source for fusion neutron generation. Small-diameter, high-current ion sources are needed that can function at very high voltages for applications such as neutron radiography. Starfire has identified a commercialization partner who would be willing to invest in future developments.

Part 2: Introduction

This Small Business Technology Transfer Research Phase I project addresses the technical and commercial feasibility of using a microwave electron cyclotron resonance technique for high-power electric propulsion. This type of system would have inherent defensive counter space and situational awareness capabilities.

2.1 Need For Defensive Counter Space Capability

Due to the proliferation of small inexpensive satellites, space situational awareness and object detection/negation are high priorities for protecting US space-borne assets. Nano/pico-satellites launched into space are typically used for scientific testing, space-based surveillance, navigation, and communication networks; however, there exists the possibility of future hostile applications. In particular, potential competitors could deploy this technology for applications such as shadowing, monitoring, and disabling of US assets. Due to their small size it is difficult to detect nanosats with ground-based telescopes and radar. Thus, there is a need for the capability to detect, deflect, or disable these small satellites in the event they are used for hostile applications.

Typically the propulsion system of medium- and large-size satellites occupies a significant fraction of spacecraft mass, volume, and power. So it would be advantageous if the propulsion system could also function in a DCS-mode because additional components would not be required. Starfire Industries proposed a novel microwave plasma thruster employing electron cyclotron resonance techniques for simultaneous high-power, high-efficiency electric propulsion and multiple secondary "dual-use" applications, such as object detection, illumination and imaging, and space negation.

2.2 Magnetic Nozzle Expansion

The magnetic mirror phenomenon is well known within the fusion plasma community for trapping plasma within a "magnetic bottle". This mechanism is present with any charged particles trapped on magnetic field lines. In the configuration of a diverging magnetic nozzle,

the primary means of ion acceleration is the formation of an ambipolar electric field. Electrons leaving the high-field region of the nozzle undergo acceleration by the magnetic pressure resulting from the field gradient and energy transfer due to the adiabatic invariance of the magnetic moment. The force on the electrons is proportional to:

$$F_{magnetic} = -\mu \nabla_{\parallel} B, \tag{1}$$

$$\text{where } \mu = \frac{m_e v_{\perp}^2}{2B} \tag{2}$$

is the magnetic moment and the gradient is parallel to the magnetic field lines. As the electron moves from a region of stronger magnetic field to weaker magnetic field, the component of velocity perpendicular to the field lines must decrease so that the magnetic moment is constant. In order to conserve energy, the parallel component of velocity increases as a result. Thus, electrons will accelerate out of the magnetic nozzle as shown in Figure 1.

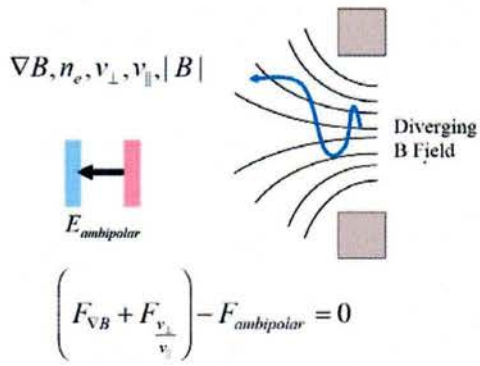

Figure 1: Electrons (blue) rapidly expand out of the high B-field region creating a natural charge imbalance from slower moving ions; the resulting ambipolar field acts as a quasi-static field for ion acceleration.

Since the trajectories of massive, unmagnetized ions are unaffected by this mirror effect, only electrons are displaced downstream of the high-field region and create an ambipolar charge separation. The resulting quasi-static field will retard the electron motion and accelerate ions downstream out of the thruster. The magnitude of this ambipolar field will depend on the force exerted on the electrons by the magnetic pressure. If the electrons have high perpendicular energy at the throat of the nozzle, then the force term can be quite large leading to a strong ambipolar field for ion acceleration.

Many plasmas with a high electron thermal temperature can expand out of a magnetic nozzle and produce thrust; however, in traditional "mirror" geometries, electrons that escape in the "loss cone" have low perpendicular energy generating little ambipolar acceleration.

2.2.1 Magnetic Nozzle Related Work

The effect of electron flow and ambipolar field generation has been observed in the nuclear fusion magnetic mirror research community. The field shape and gradient act to form a plugging

potential to minimize mirror end loss and has been termed the "dike potential". Several papers were published by Toshiro Kanejo from Tohoku University—Sendai related to this effect using ECR.[8-11] Dike potentials and ion flows with energies between 20-40eV have been reported.

There has been a flurry of interest in helicon plasmas for application to high-power electrodeless propulsion. Researchers at the Australian National University reported obtaining ion energies of 20-30 eV from a helicon double-layer thruster.[3-6] Similarly, researchers at the University of Washington reported >100eV ion acceleration with a high-power (20MW!) helicon device.[1,2] However, there has been a great deal of confusion on the ion acceleration mechanism and methods for extracting and controlling thrust for spacecraft propulsion.

Starfire Industries has been researching helicon physics for several years and believe that R-wave coupling near the lower hybrid resonance (or mode conversion of Trivelpiece-Gould electrostatic surface waves) leads to transverse electron heating near the maximum of the solenoid magnetic field. Anecdotal evidence for this effect is given by comparison between Australia and Univ. Washington's experimental evidence. Washington pulsed the helicon antenna with MW-level input power to drive large R wave amplitudes into the magnetic nozzle region and realized >100V potentials for ion acceleration; whereas Australia achieved only 20-30V potentials for kW input power levels.

2.2.2 Electron Cyclotron Resonance

This ambipolar acceleration mechanism is present in all converging/diverging magnetic mirror configurations. However, in conventional magnetic mirrors the perpendicular velocity is characteristically small in the loss cone, since only electrons with high $v_{\parallel}/v_{\perp}$ ratios can escape. Thus, electrons only expand a short distance and generate small ambipolar potentials due to the low magnetic moment (small $v_{\perp}$). However, in the presence of a forcing term, such as an electromagnetic wave, perpendicular energy can be added to the electrons such that the transverse electron temperature (energy) becomes significant. Such transverse excitation increases the magnetic moment resulting in a magnetic force sufficient to generate potentials of 10s to 100s of volts, especially if applied in a strong field gradient region.

Starfire Industries believes that the recent successes with helicon plasma thrusters at Australian National University and the University of Washington[1-6] are due to an indirect manipulation of the electron perpendicular velocity and subsequent magnetic nozzle expansion to generate anomalous "double layer" potentials downstream of the thruster. Directly controlling the perpendicular velocity (energy) of electrons in a diverging magnetic nozzle is necessary to obtain adequate ambipolar fields for exhaust velocities and power/thrust levels of interest for medium- and high-power electric propulsion. One area of this Phase I STTR project was to examine the potential for a microwave-driven plasma thruster employing electron cyclotron resonance techniques to manipulate the perpendicular electron velocity.

There are several immediate advantages to the ECR approach related to ionization efficiency and ion utilization. Direct electromagnetic injection and coupling to the plasma creates rapid ionization and wave damping in an ionization zone layer with very low ΔE/ionization cost.

Furthermore, the ionization zone can be engineered near the throat of the magnetic nozzle such that nearly all ions are accelerated downstream by the ambipolar potential. This significantly decreases wall losses and improves ion utilization efficiency, even vs. helicon systems. In addition, compact permanent magnets could be used and the system is no longer limited to a cylindrical geometry. Thus, there is a basis for scientific research to understand and control these effects.

A schematic of magnetic nozzle expansion physics for the Starfire microwave thruster is shown in Figure 2. If an electromagnetic wave were pumped into the high B-field region to induce electron cyclotron resonance both: (1) highly-localized and efficienct ionization would occur and (2) large energy would be deposited into perpendicular electron velocity by the EM wave causing large ambipolar charge separation.

1. Inject right hand circularly polarized or linearly polarized E-M waves
2. At resonance location, spin up electrons and create ionization layer.
3. Expand electrons out nozzle and generate ambipolar field.
4. Ions are accelerated out of the thruster by the ambipolar field for variable Isp and thrust.

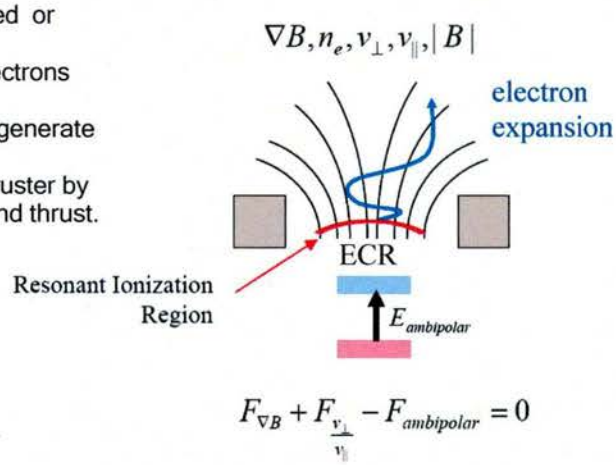

Figure 2: Illustration of EM wave and ECR interaction producing ambipolar expansion.

Starfire's innovation goal is to utilized on-board microwave energy for the direct manipulation of the perpendicular electron velocity (and thus propulsive thrust) with a propulsion system. Adding more microwave power would increase perpendicular electron motion, which yields a larger ambipolar accelerating field and more thrust. The following sections outline the major components of this innovation and discuss its application to DCS and space situational awareness.

2.3 Starfire's Microwave Propulsion System

A schematic illustrating Starfire Industries' thruster concept is given in Figure 3. Microwaves are conducted through the waveguide and launched into the discharge cavity through an optical window. Permanent or electromagnets generate a diverging magnetic field and microwaves are introduced parallel to the magnetic field lines. Propellant flows uniformly into the discharge cavity and expands downstream of the thruster. Because the electron cyclotron frequency changes with magnetic field strength, at some location in the diverging magnetic field structure, the microwave frequency will be "resonant" with the local electron cyclotron frequency. This location is termed a resonant zone because electrons resonate with the oscillating electric field of

the electromagnetic microwave and have continuous energy gain. Enough energy is gained by the electrons that the input propellant is ionized and plasma created (the ionization layer is formed). While in the resonant zone, plasma electrons continue to resonantly absorb microwave energy, then they expand downstream. There are also regimes where the electron density is sufficiently high for collective microwave absorption and heating.

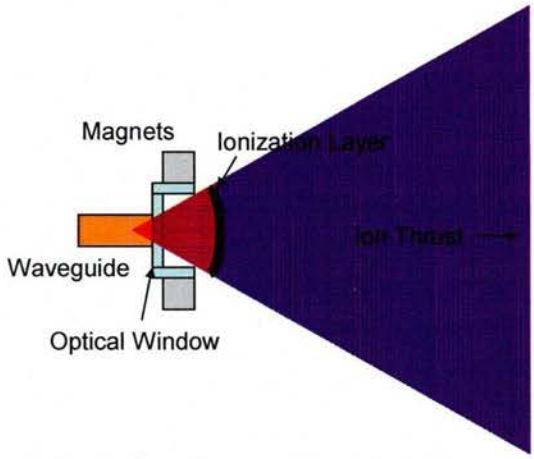

Figure 3: Component schematic illustrating microwave input, ionization zone formation, and ion exhaust.

As previously described, as electrons expand downstream in the diverging magnetic field, their perpendicular energy is converted into parallel energy. Because electrons are less massive than the ions, an ambipolar field is generated due to the charge separation. Ions are then accelerated by the ambipolar field and expelled downstream to generate thrust.

The components of the microwave thruster are fairly simple and straightforward. There are no electrodes in contact with the plasma since it is a wave interaction phenomenon which generates and sustains ionization. The ionization zone is located in the high-field section of the magnetic nozzle such that nearly all ions which are formed will be utilized and accelerated downstream in the ambipolar potential; this minimizes ion wall loss and decreases ΔE/ionization cost.

Based on this understanding, Starfire Industries is highly optimistic about the potential for a microwave-driven thruster technology to achieve highly-efficient electric propulsion at multiple thrust and specific impulse levels. Furthermore, using high-power microwaves may enable a host of object detection, remote imaging, and space negation options for defensive counter-space operations. These are described in the following section.

2.4 Defensive Counter Space Capability

The microwave thruster concept has inherent application as a DCS system for object detection, identification and disabling. Starfire has identified at least three possible configurations that utilize these DCS capabilities and they are: 1) wide-angle microwave; 2) x-ray inspection; and 3) focused microwave operation. These three concepts are shown schematically in Figure 4 and discussed further in the following sections.

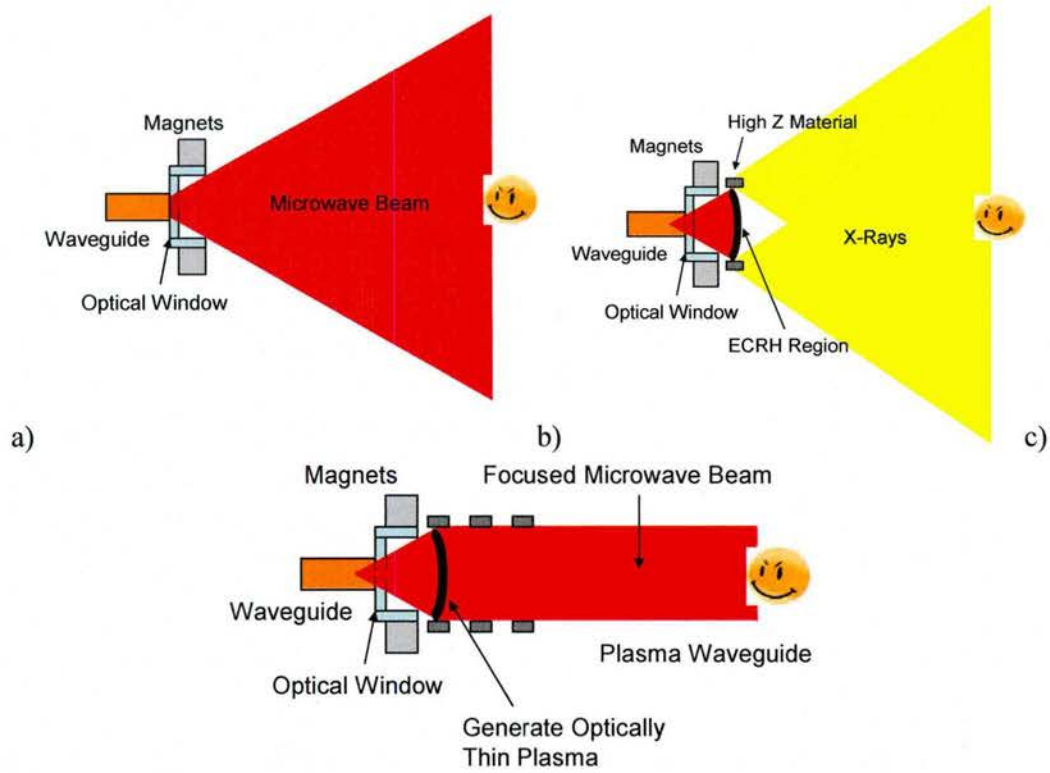

Figure 4: Schematic illustrating the DCS capabilities of the proposed microwave thruster in a) wide-angle microwave, b) x-ray inspection, and c) focused microwave operation.

2.4.1 Wide Angle Microwave Operation

Perhaps the easiest and most obvious DCS application of the thruster is active microwave scanning and detection of pico/nano-satellites. Figure 4a shows a hostile low-cost pico/nanosat under broad-area illumination from microwaves. In this configuration, propellant flow is shut-off and only the microwave power supply is operated. Microwaves are launched through the thruster waveguide, but plasma is not created and an ion beam is not expelled. The microwaves simply propagate away from the thruster and impinge on any object within the viewing area. In this configuration the thruster is functioning as a microwave transmitter, similar to radar on conventional ground- and space-based systems. The transmitted signal is reflected by an object and then detected back at the transmitter. Detectors would be placed strategically on the satellite for reflected waves and used to determine relative position and ranging.

2.4.2 X-Ray Inspection Operation

Another DCS application is the use of the microwave thruster plasma to generate x-rays for object detection, imaging and analysis, Figure 4b. Electromagnetic emission in the x-ray range can be produced by two main effects. First, when an electron is slowed down it emits

bremsstrahlung, or braking radiation. If the braking is severe (i.e.; if a high velocity electron impacts a target and is slowed to zero velocity) it will emit radiation in the x-ray range. Second, x-rays can be emitted by electrons in the target atom orbital shell. If a high energy electron knocks an inner-shell electron off, then an outer-shell electron will replace it. The first method emits radiation in a wide range of frequencies, while the second method emits at specific frequencies. Therefore, the x-ray emission spectrum from a target is typically a continuous range of frequencies from the first method superimposed with sharp peaks from the second method.

In the wide-angle x-ray configuration, propellant flow is input into the discharge cavity, the microwave power supply is operational, and plasma is produced. If the microwave frequency is tuned to ECR resonance, electrons gain considerable perpendicular energy in the zone. In a near collisionless (low-pressure) regime, electrons will resonantly gain energy through the ECR process, spiral outwards with increasing Larmor radii, impact a high-Z (atomic number) material, and create x-rays through the mechanisms described above. Efficiency of x-ray production increases with increasing electron energy and the spectral emission will be determined by the target material composition and average electron energy.

The use of x-ray fluorescence as a shorter range detection system complements the microwave system above that has a minimum distance due to resolution of reflected waves from outgoing waves (based on minimum transit time). Alternating use of the two would provide detection abilities in the short and long ranges. In addition, material composition can be determined from backscattered spectroscopy techniques.

2.4.3 Focused Microwave Operation

The third DCS application uses the microwave thruster plasma as a lens to focus the microwaves into a beam that can impinge, heat, and disable a satellite, as shown in Figure 4c. A target satellite could be heated or "cooked" to high temperature, disabling important electronic components. Further, it can be used to blind sensors and detectors on hostile satellites. For extended range and focusing of microwaves onto the target the plasma exhaust stream could be adjusted with a density minimum on-axis such that the index of refraction is less and microwaves are reflected and focused toward the object. This effect is well-described by Chen.[8] Such a high-power microwave beam could be used for a variety of DCS applications.

2.4.4 Integrated Propulsion, DCS and Communications Bus

The use of a microwave thruster could add even more functionality to existing spacecraft systems. Microwave communications sources, such as phased-array solid-state power amplifiers and antennas (and older traveling wave tube amplifiers and klystrons), are already employed on satellites for communication and data link operations in the 2-50GHz range. A large amount of mass, volume, and power are already devoted to these microwave generators for communications. If the microwave plasma thruster system could be used for propulsion, DCS applications, and communications…this would truly constitute a "multi-use" system and be a win-win scenario.

An ambitious goal stemming from a successful STTR would be to develop an advanced EP-based power, propulsion, guidance, navigation, control, and communication module to serve as the basic building block for future satellites. Essentially, this would be a new spacecraft bus that would serve as a common platform for mission planners and satellite designers. This is shown in Figure 5 below.

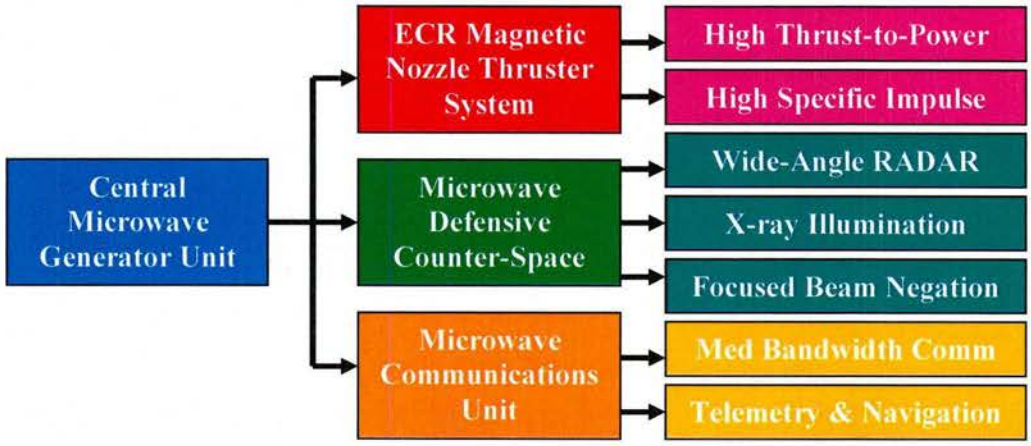

Figure 5: Multi-mode microwave-driven satellite architecture.

This approach to commercialization with the development and flight testing of a standardized platform would be ideal, i.e. phased-array microwave transmitter blocks could be directly utilized. Starfire Industries could supply flight-ready components to satellite integrators and build a sustainable revenue-based business servicing the USAF and other US agencies. In addition, the common block spacecraft bus could be extended to commercial spacecraft systems and could even incorporate advanced Orbital Express refueling, attachment, and other common mode block infrastructure items.

Part 3: Phase I Technical Objectives

The primary Phase I technical objective was to verify the generation of an ambipolar potential drop generated in a diverging magnetic nozzle with the application of microwave radiation and ECR in a small experiment. The secondary objectives were to perform analytical and computer studies to examine the propulsion parameter space and qualify the defensive counter-space aspects of the overall approach. This was accomplished with an integrated experimental and computational investigation.

A small-scale proof-of-principle experiment was used to validate the plasma acceleration propulsive capabilities of the thruster. This experiment drew upon previous experience with radio frequency (RF) and helicon plasmas, and made use of a microwave waveguide, power supply hardware, and a graduate student provided by the Univ. of Illinois. Numerical simulations were used to further study thruster operation and clarify experimental results. The

DCS capabilities of the microwave thruster were investigated analytically and numerically during this Phase I STTR. In summary, to the goals of the Phase I STTR were:

- Perform a series of small-scale plasma experiments with magnetic nozzle (< 1kW) on microwave/ECR plasmas to measure plasma parameters as a function of input variables.
- Demonstrate ion energy modification by varying input variables (|B|, grad B, P_{ECR}) to influence the $\mu\nabla B$ magnetic force and resulting quasi-static ambipolar field.
- Analytical and computational investigations of electron-to-EM wave coupling and potential formation, with resultant ion acceleration and plasma detachment analysis.
- Analytically study DCS methods to determine required microwave power, maximum detection distance, and required electron energy for x-ray applications.
- Select a suitable thruster design to allow the rapid fabrication of components and assembly of hardware for testing in a large vacuum test facility, e.g., AFRL, should a Phase II be awarded.

Part 4: Phase I Results

To investigate the properties of the microwave plasma system, an experimental testing and modeling simulation plan was developed. The following sections outline the experimental setup, diagnostics, measurements and data analysis on an ECR plasma system and magnetic nozzle operation.

4.1 Microwave Plasma and ECR Testing

4.1.1 Experimental Facility Setup

The basic facility is the Starfire 1-m diameter chamber. This cylindrical vacuum chamber was acquired in 2005 through a surplus sale and it is equipped with two Wheeler doors on both sides of the chamber for excellent access to the internal regions for probe positioning, experiment mounting, etc. There are two CTI Cryogenics 8F cryopumps located on the top and bottom ports on the central cylinder section. These surplus sale pumps were originally from semiconductor processing equipment and are connected to two external compressors with helium coolant. The approximate pumping speed for argon gas is 1,200 L/s for each pump. Pressure is monitored on a side port by a Pfeiffer full-range vacuum gauge. This pressure measurement is baffled not in contact with the plasma beam, and it measures only the background equilibrium pressure. Actual pressures within the flow channel for gas injection are slightly higher

The centerpiece of the ECR plasma source is the microwave applicator. It consists of five main components: 1) magnetron with cylindrical waveguide; 2) circulator with a water-cooled dummy-load; 3) directional coupler; 4) three-stub tuner; and 5) a transverse electric (TE) to transverse magnetic (TM) mode converter. A Hitachi 2M120 (running at 750W) magnetron generates 2.45 GHz microwaves that propagate into a cylindrical WR430 waveguide. A

standard 60 Hz wall transformer removed from a microwave oven is rectified and used to power the magnetron. More details regarding this type of operational setup are provided in the results section. The microwaves are converted from the cylindrical TE_{10} mode to the circular TM_{01} mode before propagating through a quartz window into the vacuum vessel. Reflected power is directed to the water-cooled dummy-load by the circulator. Reflected and forward power were measured using a Boonton Electronics 4231A RF power meter connected to the directional coupler. Matching between the microwave applicator and plasma discharge was made possible by the three-stub tuner. A photograph of the setup is shown in Figure 6.

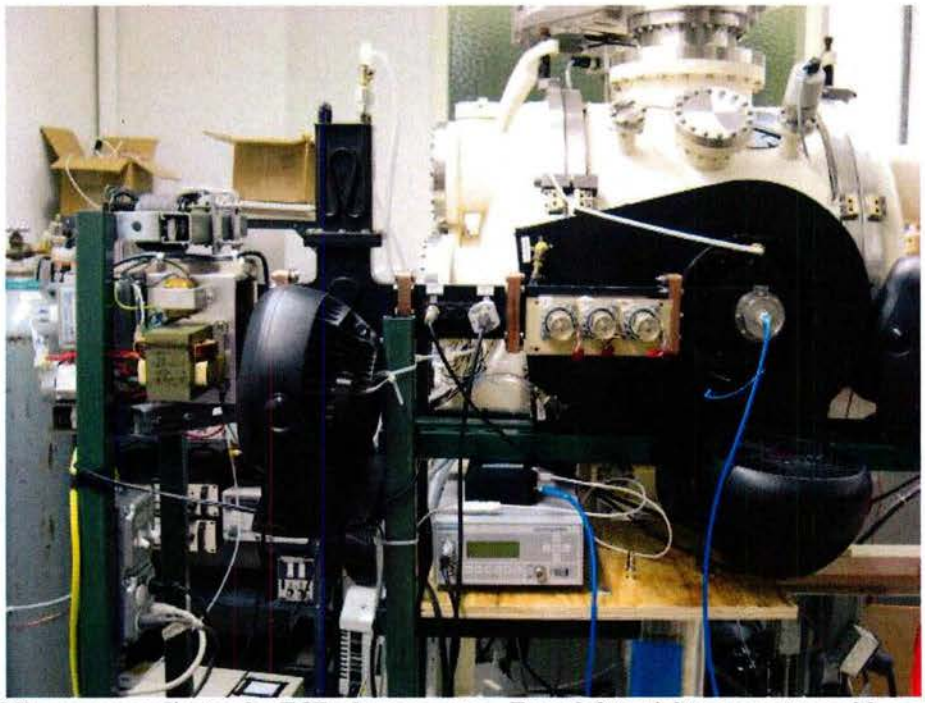

Figure 6: Microwave applicator for ECR plasma source. From left to right: magnetron with power supply, wave guide, circulator, directional coupler, three-stub tuner, and mode converter.

ECR requires the interaction of microwaves with electrons immersed in a magnetic field. The magnetic field of the plasma source is provided by two cylindrical water-cooled electromagnets driven by an ESS 80-185 power supply. The power supply is current-controlled by an external voltage source. Electromagnet current and, therefore, magnetic field strength is controlled by varying a potentiometer on the voltage source. The shape of the magnetic field is solenoidal through the center of the electromagnets and expands with axial distance. A plot of the magnetic field with the potentiometer set at 7.0 is shown in Figure 7.

Figure 7 also shows a schematic of the internal vacuum chamber setup, along with the coordinate system used for this experiment. The electromagnets fit around a feedthrough port on the vacuum vessel. Internal to the vacuum chamber, a glass tube is inserted into the feedthrough port to decrease plasma interaction with a conducting boundary within the ECR region. This also decreases the concentration of impurities within the plasma.

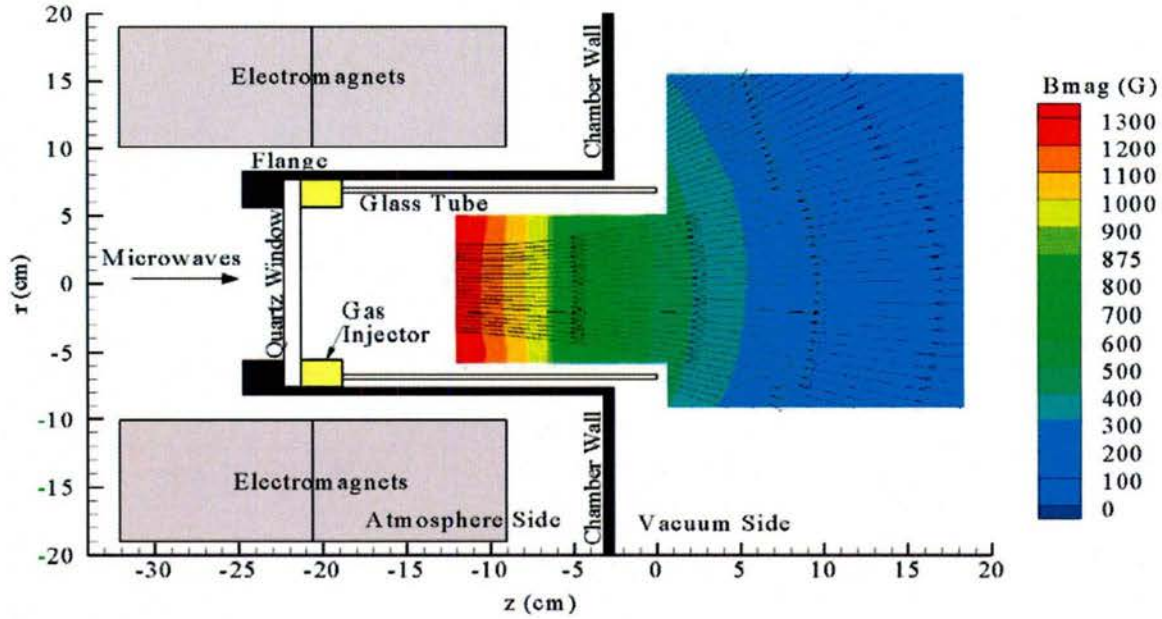

Figure 7: Experimentally measured magnetic field for a 7.0 potentiometer setting. This figure also shows the experimental setup and coordinate system for the experiment.

The relationship between the power supply potentiometer setting, electromagnet current, axial location of the resonant 875 G magnetic field line, and the magnetic field strength at the exit of the glass tube is given in Table 1. As expected, as the potentiometer is increased, the electromagnet current increases and the magnetic field strength at the exit-plane of the glass tube increases. Furthermore, as the potentiometer is increased, the 875 G magnetic field line moves downstream toward the chamber wall. In the following sections, the potentiometer setting will be adjusted as an independent variable. The user is referred back to Table 1 to determine how the electromagnet current and magnetic field have been quantitatively affected.

Table 1: Relationship between the electromagnet power supply potentiometer setting, electromagnet current, axial location of the 875 G magnetic field line, and exit-plane magnetic field strength.

Potentiometer Setting (-)	I (A)	875 G Line Axial Position (cm)	Exit-plane Magnetic Field (G)
4.5	84.3	-11.5	326
5.0	93.5	-10.3	350
5.5	102.7	-9.1	376
6.0	111.8	-8.2	406
6.5	121.0	-7.3	437
7.0	130.1	-6.5	475
7.5	139.3	-5.6	504
8.0	148.4	-4.8	538
8.5	157.6	-4.0	574
9.0	166.8	-3.4	615
9.5	175.9	-2.9	660

Finally, neutral argon gas was input into the system through a custom feedthrough at the quartz window. Gas is fed into an annular gas manifold with ~1-mm-diameter holes spaced azimuthally around the manifold. Each of the holes is oriented in the radial direction toward the centerline so that uniform gas injection is obtained. The input gas then flows through the tube and out into the vacuum vessel. It is important to note that the gas pressure will actually be higher within the quartz tube injector region since pressure measurement only measures equilibrium pressure.

4.1.2 Microwave Plasma Operation

The microwave ECR plasma source was operated at a variety of pressures and magnetic field strengths. The downstream plasma properties were analyzed as the source operation was adjusted. In the following sections, the ECR source operation is described, along with the results from the downstream Langmuir probe and retarding potential analyzer (RPA) diagnostics.

Operation of the ECR plasma source is accomplished by energizing the electromagnets, supplying gas flow, and then energizing the magnetron. The magnetron voltage and forward and reflected power as a function of time during typical plasma source operation at 1.0 mTorr pressure and 8.0 electromagnet potentiometer setting is shown in Figure 8. Figure 8a shows the magnetron operating voltage as a function of time. The magnetron does not produce a continuous supply of microwaves, but oscillates at 60 Hz with a 50% duty cycle. At time 0 msec, the voltage decreases to -3.5 kV. As time increases, voltage continues to decrease further and obtains a minimum of -4.2 kV at 5.5 msec. At 8.2 msec the magnetron voltage increases abruptly to 0 V. This result is due to the standard microwave oven transformer power supply used to drive the magnetron. In microwave ovens, the power supply is designed to operate the microwave magnetron at 50% duty cycle at 60 Hz to minimize thermal loads. This type of supply is used to operate the ECR plasma source magnetron.

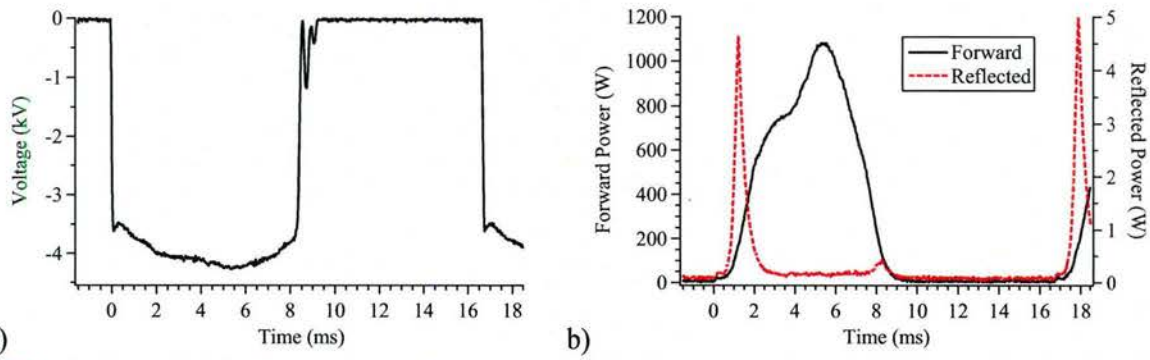

Figure 8: Example microwave plasma source operation. A) Magnetron voltage and b) forward and reflected power as a function of time.

Figure 8b shows the forward and reflected power as a function of time. These results correspond with the magnetron voltage output in Figure 8a. At time 0 msec, the magnetron begins to operate and the reflected power spikes up to 4.7 W. Reflected power quickly decreases and

forward power increases as the plasma discharge is formed and better matching is achieved between the plasma and microwave applicator. A peak forward power of ~1100 W is obtained at 5.5 msec and corresponds to the voltage minimum on the magnetron. Forward power decreases to 0 W as the magnetron voltage decreases to 0 V.

The 60 Hz oscillatory nature of the plasma is acceptable in this laboratory experiment because this frequency is much lower than the response time of the plasma. Plasma frequencies within the GHz range are common, so during the 8 msec magnetron pulse width the plasma has reached equilibrium. Ideal operation of a space thruster will likely not incorporate this 60 Hz oscillation because the time required increasing to peak power and decreasing from peak power would represent losses in efficiency. A space thruster would likely be operated in a continuous microwave mode. Finally, because the plasma oscillates, the plasma diagnostics must be timed to only record data when the plasma is on. Specifically, both the Langmuir probe and RPA voltage sweeps are triggered to only record data at the peak in the forward power signal (~5.5 msec).

As pressure and magnetic field were adjusted during this investigation, the matching properties between the plasma and microwave applicator changed. This is typically due to changes in plasma properties, which affect the coupling of microwave power from the applicator to the plasma. Therefore, each time that the source operation was adjusted (i.e., pressure or magnetic field adjusted) the matching network required re-tuning. The re-tuning process involved adjusting two stubs of the three-stub tuner to minimize reflected power. A measure of the time-averaged power in the forward and reflected direction was done using the power meter. Forward and reflected power was monitored as pressure and magnetic field were adjusted. These results are shown in Figure 9. These results represent the minimum attainable reflected power. Based on repeatability, the error of these measurements was estimated at 5% and 15% for the forward and reflected power, respectively.

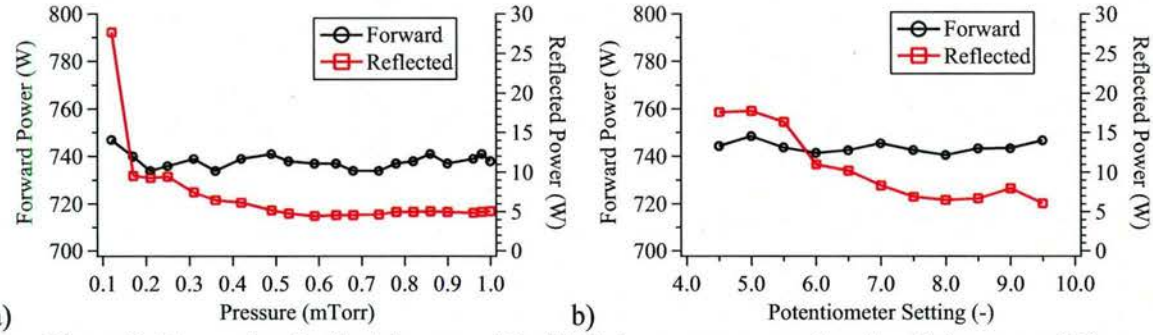

Figure 9: Forward and reflected power of the ECR plasma source as a function of a) pressure (7.0 potentiometer) and b) magnetic field strength (0.2 mTorr pressure).

Figure 9a shows that as pressure decreased, the forward power remained relatively constant at approximately 740 W, while the reflected power started to increase at approximately 0.5 mTorr. As pressure decreased below 0.5 mTorr, the reflected power continued to increase and showed a significant increase at the lowest pressure point of 0.1 mTorr. At the lowest pressure condition, reflected power was 27.6 W and forward power was 747 W. Operation at a pressure below 0.1 mTorr was initially attempted, but the reflected power continued to increase. Significant

reflected power has the potential to damage the microwave applicator system and is therefore undesirable. For the results presented here, reflected power was always less than 5% of the forward power.

Figure 9b shows the forward and reflected power as a function of the electromagnet power supply potentiometer setting. The correspondence between the potentiometer, electromagnet current, and magnetic field was given in Table 1. For all magnetic field cases the forward power remained relatively constant at 745 W. Reflected power increased with decreasing magnetic field strength. For the strongest magnetic field (9.5 potentiometer setting) the reflected power was 6 W. The reflected power remained relatively constant until a potentiometer setting of 7.5. At this point, reflected power begins to increase as magnetic field continues to decrease. For the weakest magnetic field case described in this work (4.5 potentiometer), the reflected power was 17 W, which is only 2% of the forward power. A data point at a potentiometer setting of 4.0 was initially attempted, but the reflected power for this case increased to 86 W. This was 11% of the forward power and significantly above our criteria of 5% maximum reflected power.

Photographs of the ECR source being operated at high and low pressure are shown in Figure 10. Gas and plasma flow in these photographs is out of the tube from right to left. The crossed mesh pattern visible in the plume is a result of the photograph being taken through a wire mesh screen that covers the viewport. This screen is necessary to eliminate microwave leakage out of the vacuum vessel. Comparison of the two photographs shows visible differences in the ECR plasma plume. Specifically, at high pressure the plume appears more dense and purple in color. The plasma internal to the glass tube shows a blue color near the exit of the tube, with a white appearance farther upstream. Furthermore, plasma is created and expelled from the region between the glass tube and chamber. At low pressure the plume appears less dense and white or blue in color. The color internal to the tube is also lighter. Also, the plasma emanating from between the glass tube and chamber is gone. Much of these changes in the visible nature of the plume are attributed to 1) fewer collisions at lower pressure and 2) hotter plasma at lower pressure.

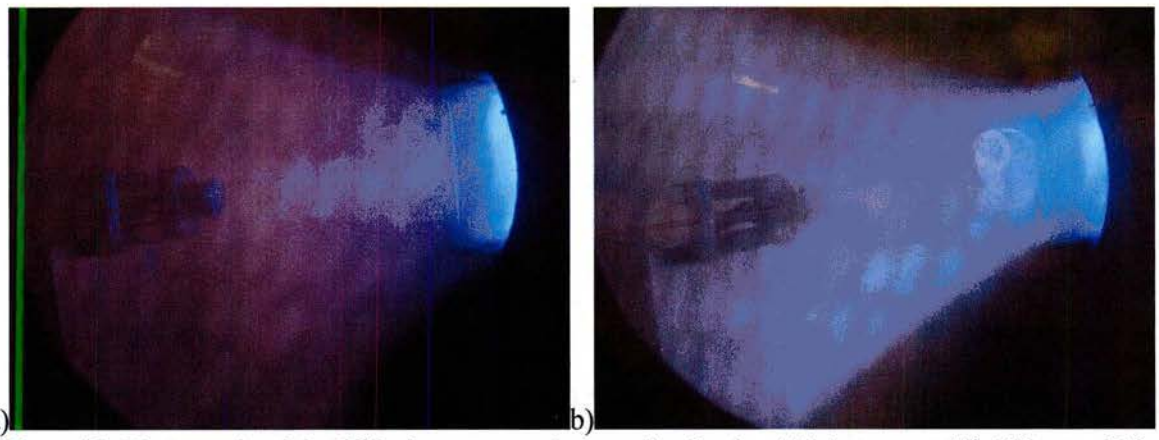

Figure 10: Photographs of the ECR plasma source in operation for the a) high-pressure 1.0e-3 Torr and b) low-pressure 1.0e-4 Torr operating conditions.

4.1.3 Plasma Diagnostics Setup

The experimental apparatus is configured with a fixed-location retarding potential analyzer and an adjustable-location (axial) Langmuir probe (LP). A single, cylindrical Langmuir probe was constructed using tungsten wire and alumina tubing. The tube and wire were bonded using ceramic epoxy. The diameter of the probe tip was 0.38 mm and the length was 3 mm, yielding a collection area of 3.6 mm^2. Current is measured as a voltage drop across a 997 ohm shunt resistor.

A Kimball Physics RPA was used to measure ion energy-per-charge distributions. This RPA has floating, electron suppression, and ion retarding grids. For all experiments, the electron suppression grid was operated at -50 V, while the ion retarding grid was swept from 0 to +90 V with respect to ground. To decrease the plasma density internal to the RPA, such that the grid spacing meets the space-charge criteria,[21] two layers of stainless steel wire mesh were placed over the orifice. Probe voltage for both the Langmuir probe and RPA were swept at 1kHz using a function generator connected to a bipolar supply.

Figure 11 shows a photograph of the thruster system operating at 30 sccm flow rate of argon gas. The RPA and LP diagnostic assembly is mounted on a linear motion feedthrough to sweep across the plasma plume for measurement of local density, temperature and particle energies. The microwave energy is fed into the chamber through a TM_{01} waveguide into a cylindrical quartz tube approximately 25 cm in length. Argon gas is fed into this region through an annular manifold to maximize density inside the quartz tube for ionization and plasma formation.

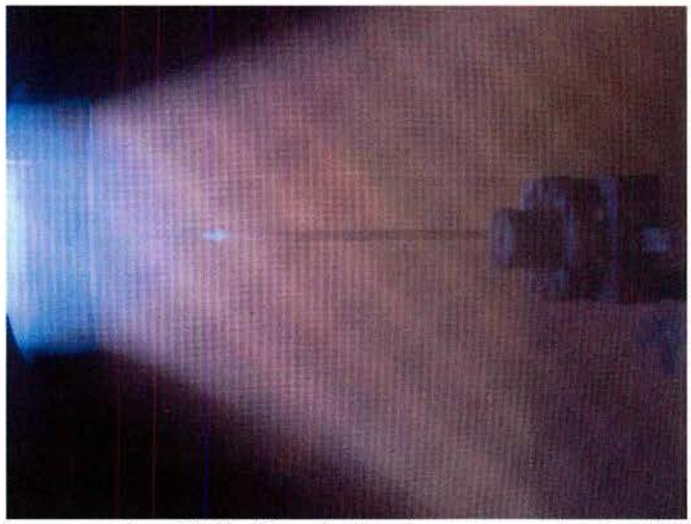

Figure 11: ECR plasma running at 0.19mTorr Ar chamber pressure showing LP and RPA in plume.

As mentioned in the previous section, the 2.45 GHz power supply is a conventional high-power magnetron generator operating on wall-plug AC power. The input voltage signal is stepped up to several kilovolts through a transformer and half-wave rectified for magnetron operation yielding 60 pulses/sec. Looking at the magnetron cycle time (60Hz) multiplied by a FWHM value of approximately 5.5 msec leads to a 33% duty cycle. This is shown in Figure 12. The forward transmitted power measured before the 3-stub tuner in the rectangular waveguide measures

approximately 750 W. Thus, the instantaneous power averaged over each magnetron pulse is ~2.25 kW.

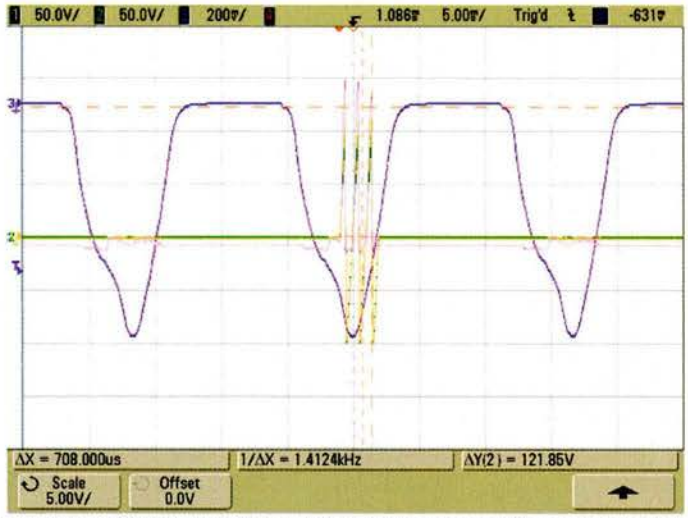

Figure 12: Magnetron pulsing at 33% duty (purple) and triggered voltage sweeps (green/pink) for analysis.

As a result, the plasma is discontinuous and re-ignites every cycle due to the pulsed nature of the magnetron power supply; therefore, the RPA and Langmuir probe data was obtained by triggering the oscilloscope and function/sweep generator to the peak forward power. Three sweep cycles are performed, as shown in Figure 13, since the function generator starts at zero, and the region of interest is the first continuous voltage interval. The oscilloscope is centered about the peak in forward power and data obtained at this level with average change in power <10%. Note, due to the periodic nature of the magnetron and interaction with the plasma load there are frequent mismatching and fluctuations in total power and the noise level is fairly high. To obtain smoothed pulses, 1024-2048 waveforms (17-34 seconds worth of data) were averaged to yield extractable data.

Figure 13: Triggered voltage sweep centered about peak forward power indicator.

A continuous microwave power amplifier would be ideal to provide steady-state plasma production and ion acceleration without the difficulties of jitter and trigger timing to reduce noise levels. However, for this Phase I investigation the available magnetron supply has been sufficient. As noted in the original proposal, Starfire's partnership with the University of Illinois will grant access to a larger 6kW continuous system for high-power studies in a future Phase II study.

4.1.4 Initial Experimental Results

4.1.4.1 Retarding Potential Analyzer Measurements

The RPA was positioned on centerline of the plasma source at an axial location of 21 cm downstream of the glass tube. Ion retarding grid voltage was swept from 0 to +90 V with respect to chamber ground. Electron repelling grid voltage was set at -50 V and the collector electrode was grounded through a 9.96 kOhm resistor. The derivative of collector current versus retarding grid voltage yields the ion energy-per-charge (or voltage) distribution function. A key feature of the energy-per-charge distribution function is the location of the peak(s), corresponding to the most-probable-voltage(s). The error associated with these methods is estimated at 10% based on the repeatability of the measurements. In this first test with the RPA, magnetic field was fixed at a 7.0 potentiometer setting and data recorded for different facility pressures. Results are shown in Figure 14.

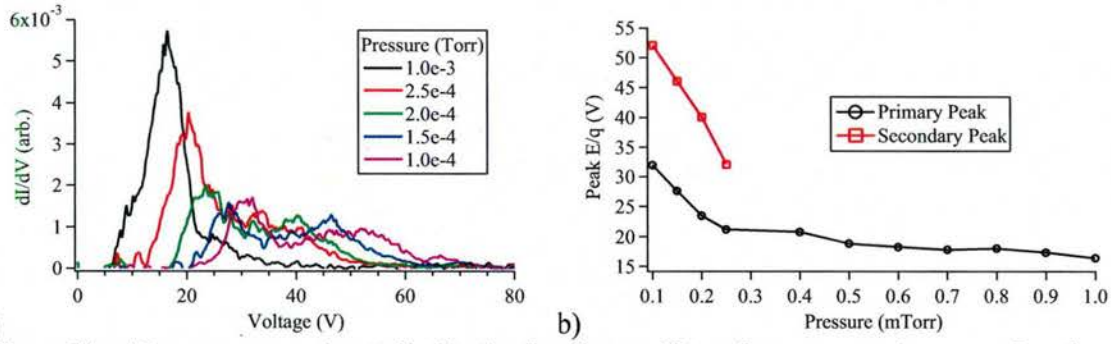

a) b)

Figure 14: a) Ion energy-per-charge distribution functions and b) peak energy-per-charge as a function of pressure.

Figure 14a shows the ion energy-per-charge distribution function for different pressures. For the high pressure case of 1.0 mTorr, the distribution function shows a single primary peak at approximately 16 V. As pressure decreases, this primary peak shifts to higher voltages and decreases in magnitude. At a pressure of approximately 0.25 mTorr, a second peak in the distribution function appears at 33 V. As pressure decreases further, the primary peak continues to shift to higher voltages and decrease in magnitude, while the secondary peak shifts to higher voltages and remains relatively constant in magnitude. At the 0.15 mTorr pressure point the magnitude of the peaks are approximately equal. The primary peak is at 27 V and the secondary peak is at 46 V.

Figure 14b shows the effect of pressure on the peaks in the energy-per-charge distribution functions. As pressure decreases, both the primary and secondary peaks shift to higher voltages. The primary peak is a result of ions gaining the plasma potential as they accelerate through the sheath in front of the RPA. Comparison of Figure 14b and Figure 17a shows nearly identical magnitude and trend between the primary peak voltage and plasma potential. The secondary peak is a result of an ion beam component present in the plasma. Further discussion about the effect of pressure on peak energy-per-charge is given in the discussion section below.

It is important to note that in these experiments, not all of the ions expelled from the microwave/ECR thruster are measured at the RPA. With the detector being 21-cm downstream from the quartz tube exit, there is a significant chance that an ion will collide with the background gas before reaching the detector. This can result in either the ion changing direction (and missing the RPA), or in a symmetric charge transfer reaction that leaves a fast neutral and slow ion. As an estimate of the importance of this effect, for a pressure of 0.2 mTorr the density of gas atoms is 6.4×10^{18} m^{-3}. For Ar^{+}-Ar scattering at 30 eV, the momentum transfer cross section is $\sim8\times10^{19}$ m^2.[1] The mean free path of the expelled ions, i.e. the average distance ions travel between collisions with a background gas atom, is therefore $\lambda=(n\sigma)^{-1}=19$ cm. This is less than the distance to the RPA, and explains why there is considerable degradation in ion current at the detector location. In fact, when the detector is moved to the rear of the vacuum chamber, very little ion current is resolvable. It is important to note that the calculation of ion energy degradation and charge exchange reactions is complicated due to the fact that there is significant variation in the momentum transfer cross section over the energy ranges of interest (1-100eV). The flux of ions transmitted without colliding will vary with distance according to $\phi(x)=\phi_0 e^{-x/\lambda}$. In order to make accurate thrust predictions, future experiments will need to be carried out in a space environment facility for testing at very low base pressures.

At the same spatial location, the pressure was fixed at 0.2 mTorr while the magnetic field was changed by adjusting the electromagnet power supply potentiometer and RPA data recorded. Figure 15 shows the results. Similar to the results that will be shown in Figure 18 for the Langmuir probe, magnetic field does not significantly affect the energy-per-charge distribution function either. Figure 15a shows that for all potentiometer settings except 4.5, the distribution function is relatively unaffected. Primary and secondary peaks are located at 23 V and 39 V, respectively. This is in good agreement with the 0.2 mTorr case shown in Figure 14a. The magnitude of the peak in the distribution function decreases 30% from a potentiometer setting of 9.0 to 8.0. Operation at a magnetic field potentiometer setting of 4.5 showed a single peak that was 60% larger in magnitude and shifted to a lower voltage of 19 V; this suggests non-resonant behavior where the peak magnetic field is less than the 875G required for 2.45GHz ECR.

Figure 15b shows the effect of magnetic field on the peaks in the energy-per-charge distribution function. In general, changes in the magnetic field over this range had little effect. The primary and secondary peaks remained constant at 23 V and 39 V, respectively. This is in good agreement with the trends for the Langmuir probe, which also showed that magnetic field has little effect on the plasma properties. Specifically, the trend and magnitude for the primary peak in Figure 15b and the plasma potential in Figure 18a are nearly identical.

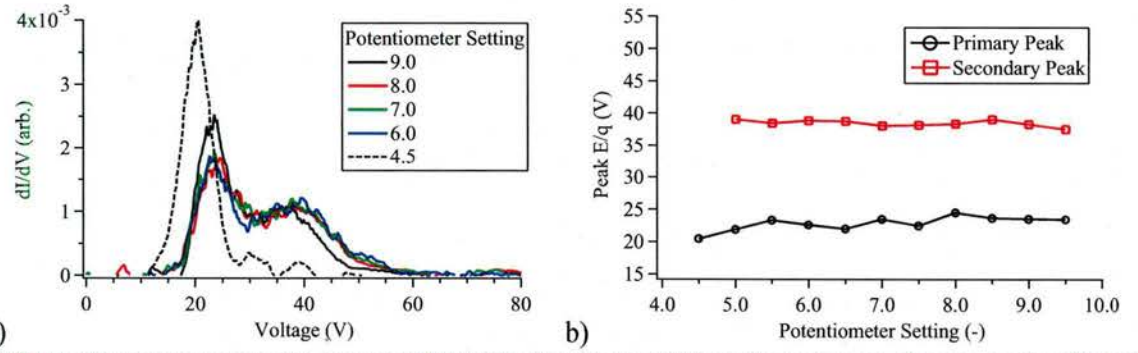

Figure 15: a) Ion energy-per-charge distribution functions and b) peak energy-per-charge as a function of magnetic field potentiometer setting.

More recently, the experimental campaign has concentrated on investigating the spatial change in the ion energy-per-charge distribution. Some preliminary results are shown in Figure 16 below. These data were collected at an axial location of 21-cm downstream, based on the coordinate system described above.

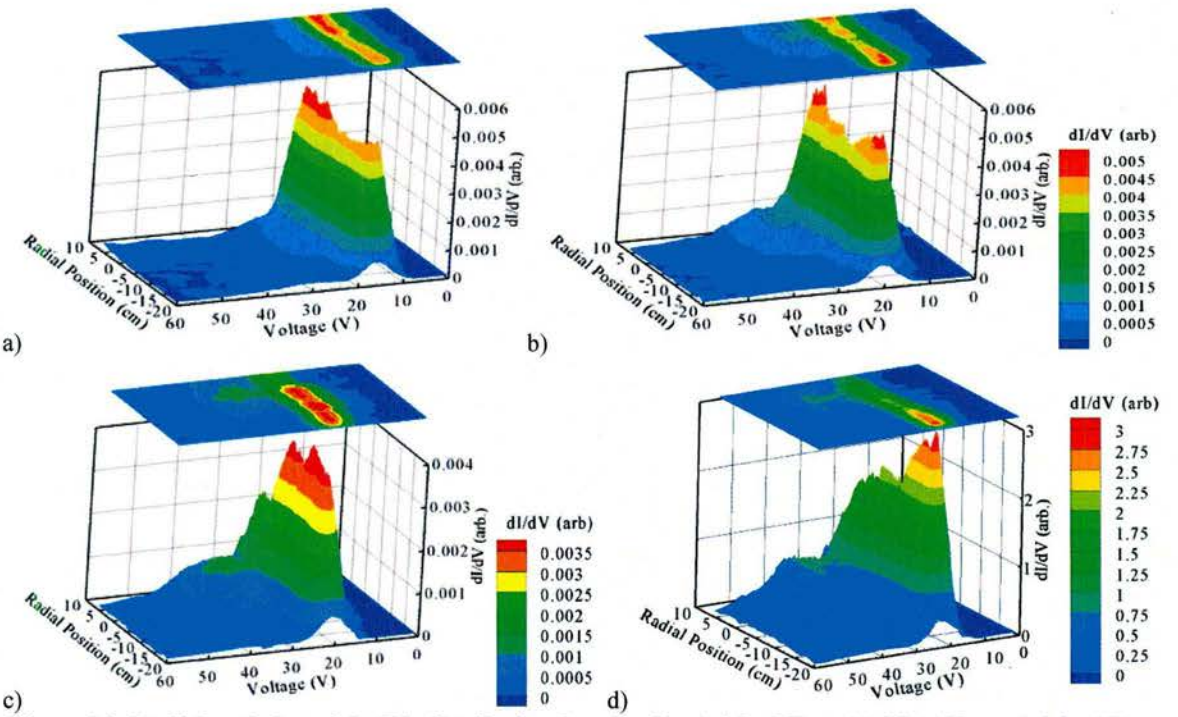

Figure 16: Radial variation of the E/q distribution function for a) 1.0e-3 Torr, b) 4.0e-4 Torr, c) 3.0e-4 Torr, and d) 2.0e-4 Torr.

Ion energy-per-charge distributions show two peaks during low pressure operation (2.0e-4 Torr). The first peak corresponds with the plasma potential and represents ions falling through the plasma sheath. The second peak is at higher energy and is attributed to an ion beam component within the plasma. This second peak has values of 30-50 V and increases with decreasing pressure.

4.1.4.2 Langmuir Probe Measurements

Initial Langmuir probe data were analyzed based on a collisionless, thin-sheath assumption without the presence of charged particle beams. This assumption serves as a basic starting point for analysis because the plasma Debye length is much smaller than the radius of the probe ($\lambda_D \ll r_p$) and the mean free path is much larger than the probe radius ($\lambda_{MFP} \gg r_p$). For the thin sheath analysis, the ion saturation regime of the probe trace yields the ion number density. We assume quasi-neutrality, so the ion number density is also the electron number density. The reciprocal of the slope of a log-linear fit to the electron retarding region yields the electron temperature. The floating potential was calculated as the probe voltage when no current was collected by the probe. Finally, the plasma (or space) potential was calculated as the intersection of the log-linear electron retarding region with a linear fit to the electron saturation region of the probe trace. This is the standard interpretation of the Langmuir probe I-V characteristic for low temperature plasmas.[22-24] Error estimates using these techniques are ~50% for number density and ~25% for electron temperature. Results using this analysis procedure are described as follows.

The Langmuir probe was positioned on centerline of the plasma source at an axial location of 19 cm downstream of the glass tube. Probe voltage was swept from -50 to +90 V with respect to chamber ground. Magnetic field was fixed at a 7.0 potentiometer setting and probe data recorded for different facility pressures. These results are shown in Figure 17. Figure 17a shows the plasma potential and floating potential as a function of facility pressure from 1.0 to 0.1 mTorr. As pressure decreases, both the plasma and floating potentials increase. Specifically, at 1.0 mTorr the plasma and floating potentials are 7.0 and 6.2 V, respectively. At 0.2 mTorr the plasma and floating potentials are 14.8 and 13.5 V, respectively. The plasma potential is consistently a few (1-2 V) higher than the floating potential.

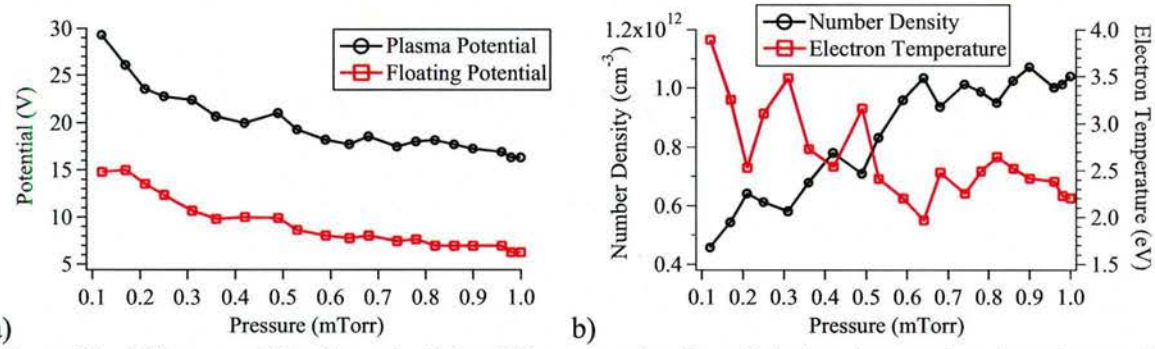

Figure 17: a) Plasma and floating potential and b) number density and electron temperature downstream of the ECR ion source.

Figure 17b shows the number density and electron temperature as a function of facility pressure for the same range. As pressure decreases, number density decreases. For the 1.0-mTorr high-pressure case, the number density is 1.0×10^{12} cm^{-3}, and it decreases to 6.2×10^{11} cm^{-3} at 0.2 mTorr pressure. There is considerable noise in the electron temperature results due to the data analysis procedure; however, a trend is noticeable that shows the electron temperature increasing with decreasing pressure. Over the entire pressure range investigated, electron temperature values are between 2-4 eV. The highest temperature occurs at 0.1 mTorr and is 3.9 eV.

At the same spatial location, the pressure was fixed at 0.2 mTorr while the magnetic field was changed by adjusting the electromagnet power supply potentiometer and Langmuir probe data recorded. Results for this test are shown in Figure 18. The correspondence between the potentiometer setting, electromagnet current, axial location of the resonant 875 G magnetic field line, and exit-plane magnetic field strength is given in Table 1.

Figure 18a shows the effect of changing the magnetic field on plasma and floating potential. In general, both the plasma and floating potential are relatively unaffected by changes in the magnetic field and remain constant at 23 V and 12 V, respectively. Only at a 4.5 potentiometer setting do the plasma and floating potential decrease to 20 V and 8 V, respectively. Lower magnetic field strengths were not investigated because the reflected power increased beyond the acceptable limit of 5% of the forward power. Comparison with the 0.2 mTorr data point in Figure 17a shows good agreement. Specifically, the data at 0.2 mTorr in Figure 17a show plasma and floating potential of 23 V and 13 V, respectively. This is similar to the relatively constant values obtained in this test and shown in Figure 18a.

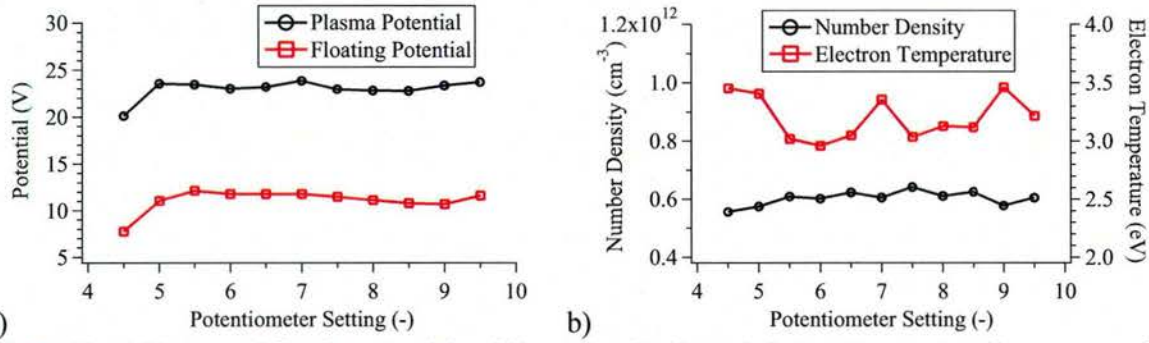

Figure 18: a) Plasma and floating potential and b) number density and electron temperature downstream of the ECR ion source.

Figure 18b shows the results for the number density and electron temperature as magnetic field was adjusted. Electron temperature and number density are relatively constant over the range of magnetic field investigated. Number density is 6.0×10^{11} cm^{-3} and shows a relatively constant value. More noise is present within the electron temperature data, and the average value was determined to be 3.3 eV. Comparison of these results with Figure 17b shows good agreement for number density. Specifically, at 0.2 mTorr, a density of 6.5×10^{11} cm^{-3} was obtained in Figure 17b. Due to the noise in the electron temperature data, the results in Figure 17b yield a value of 2.5 eV. However, a linear fit to the data in Figure 17b yields an electron temperature of 3.1 eV at 0.2 mTorr, in close agreement with the data in Figure 18b.

4.1.5 Later Experiments with Improved Facilities

In Section 4.1.4 above, Starfire Industries showed evidence of ambipolar ion acceleration from the microwave ECR plasma with ion energies up to 20 eV greater than the local plasma potential at an operating pressure of 0.2 mTorr (15sccm). However, a factor of 2-3 change higher in operating pressure would degrade this distribution considerably, presumably from ion collisions leading to gas heating. Therefore a second CryoTorr 8F was added to the 1-m cylindrical

chamber for subsequent testing at twice the pumping rate with an overnight base pressure of 2e-6 Torr. With the improved setup, a similar Ar flow rate of 18 sccm produced an ECR discharge at 0.11 mTorr chamber pressure, which is roughly half of the value in Section 4.1.4.

Additionally, in this second experimental campaign, spatially resolved Langmuir probe data was to be taken and analyzed in more detail. Therefore, higher-temperature cables were used for diagnostics (both the Langmuir probe and the retarding potential analyzer) to stop the cable melting issues experienced previously, which would have prevented sufficient operating time to take spatially resolved data. This set of RPA and Langmuir probe data was analyzed more rigorously than that in Section 4.1.4.2, taking into account the presence of charged particle beams in the analysis. As shown in detail, this latter correction to diagnostic data is important for evaluation of I-V traces.

4.1.5.1 Mode of Operation

During operation above ~0.1 mTorr, at flow rates exceeding 18 sccm, the plasma discharge was found to be operating in the overdense regime in the quartz central cavity. The overdense regime is defined as the mode where electron density is large enough for collective bulk response to the incident microwave energy leading to rapid attenuation and plasma heating, especially downstream of the resonance location where $\omega_{ce} < \omega_o$. The critical density for 2.45 GHz microwaves is 7.45×10^{10} electrons/cm^3 from the following expression:

$$n_{critical} = \frac{4\pi m_e \varepsilon_o}{e^2} f^2 = 7.45\times10^{10}\, electrons/cm^3 \,@\, 2.45GHz \quad (1)$$

In this scenario, the microwave energy entering through the waveguide and quarter-wave plate at the rear of the chamber port is attenuated into the bulk plasma over several skin depths. With axial injection of microwaves along the magnetic field, the rigid B upstream of the resonance zone limits the collective response of the plasma somewhat.

As shown in the subsequent RPA and LP data sets, operating in overdense mode resulted in high plume densities with ambipolar ion acceleration up to 80eV with argon plasma. For higher flow rate and chamber pressure, the average ion energy signal is reduced due to neutral gas collisions and charge exchange processes, as well as $<T_e>$ cooling. It is important to note that during measurements in this mode, the electron suppression electrode on the RPA had to be adjusted in excess of 200 V to minimize the electron beam contribution from magnetic nozzle acceleration. It is a well known phenomenon that electrons accelerated to high energies can "run away" from collisions, while their counterpart ions still suffer collision with neutral gas at low pressure. Thus it is not surprising to observe 150 eV electrons with only 75 eV ions following closely behind. A key point for thruster design is that average ion energy can be controlled by the appropriate propellant flow rate combined with the applied microwave power, thus there is a jet power spectrum vs. specific impulse for a given propellant and magnetic field configuration.

The transition regime between overdense and underdense mode occurred at an argon flow rate of approximately 12 sccm, corresponding to a chamber pressure of 0.09 mTorr. At this point the

gas density in the ECR region is sufficient to strike plasma that ramps up into an overdense regime. However, the high degree of ionization and acceleration from the region rapidly depletes neutral gas quenching the discharge into an underdense state until additional argon gas is injected through the gas manifold. A series of oscillations on forward microwave power are observed during this transition regime where quasi-periodic bursts of high-density plasma measured on the diagnostics (rendering measurement impossible). The 0.2-0.5msec oscillation period is consistent with neutral gas pumping and depletion timescales for $v_{thermal} \sim 400$ m/s over a length scale of 10 cm.

Further decreasing mass flow to 8 sccm would achieve stable underdense plasma operation (i.e. no transition to overdense mode and mismatch in plasma load conditions) at an operating pressure of 0.05 mTorr. In this mode, the plasma in the quartz channel upstream of the resonance region is optically thin to the microwave energy; and the EM radiation reaches the 875 G line region with significant amplitude for resonant electron acceleration. An electron making a single pass through the resonance region can obtain hundreds of eV over multiple gyro orbits.

4.1.5.2 Retarding Potential Analyzer Measurements

As shown below, operating in underdense mode resulted in very high energy electron acceleration greater than 500eV! The initial RPA ion traces were swamped negative by the high-energy electron beam exceeding the secondary electron suppression voltage of -250V in addition to loading down the Kepco ion repeller. To attempt to achieve a readable ion current signal, the RPA was physically modified with the insertion of an additional electron beam repeller before the inlet aperture and tested with a -1kV bias, as shown in Figure 19 below.

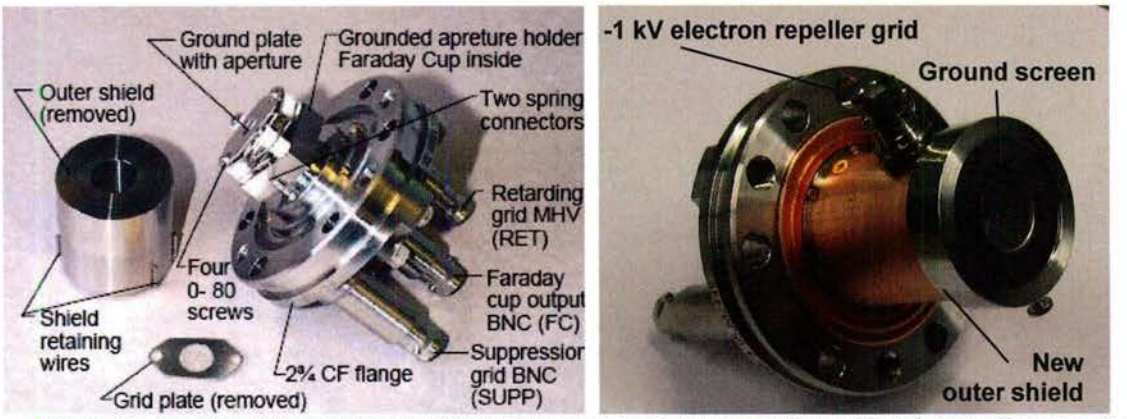

Figure 19: Modified Kimball Physics RPA with entrance electron repeller grid and grounding structure

Several experimental runs were performed with the RPA and LP for different ECR system conditions; see Figure 20 to Figure 30. It is important to note that Data Sets (1-2), (3-4), (A1-4), (A5-6) and (B1) were taken on different days with slightly different setups, particularly oscilloscope triggering conditions. While efforts were made to maintain similar conditions between data runs, excessive heating and melting of internal probe cables led to several shorts and rebuilds of the diagnostic assembly. Data sets 1-4 have an additional grounding screen cover decreasing current signals.

Figure 20: RPA Data Set 1 (Overdense)

Pressure (Ar)	MFC	B Field Current	RPA Location
0.11 mTorr	18 sccm	7 turns (pot)	21 cm from exit plane

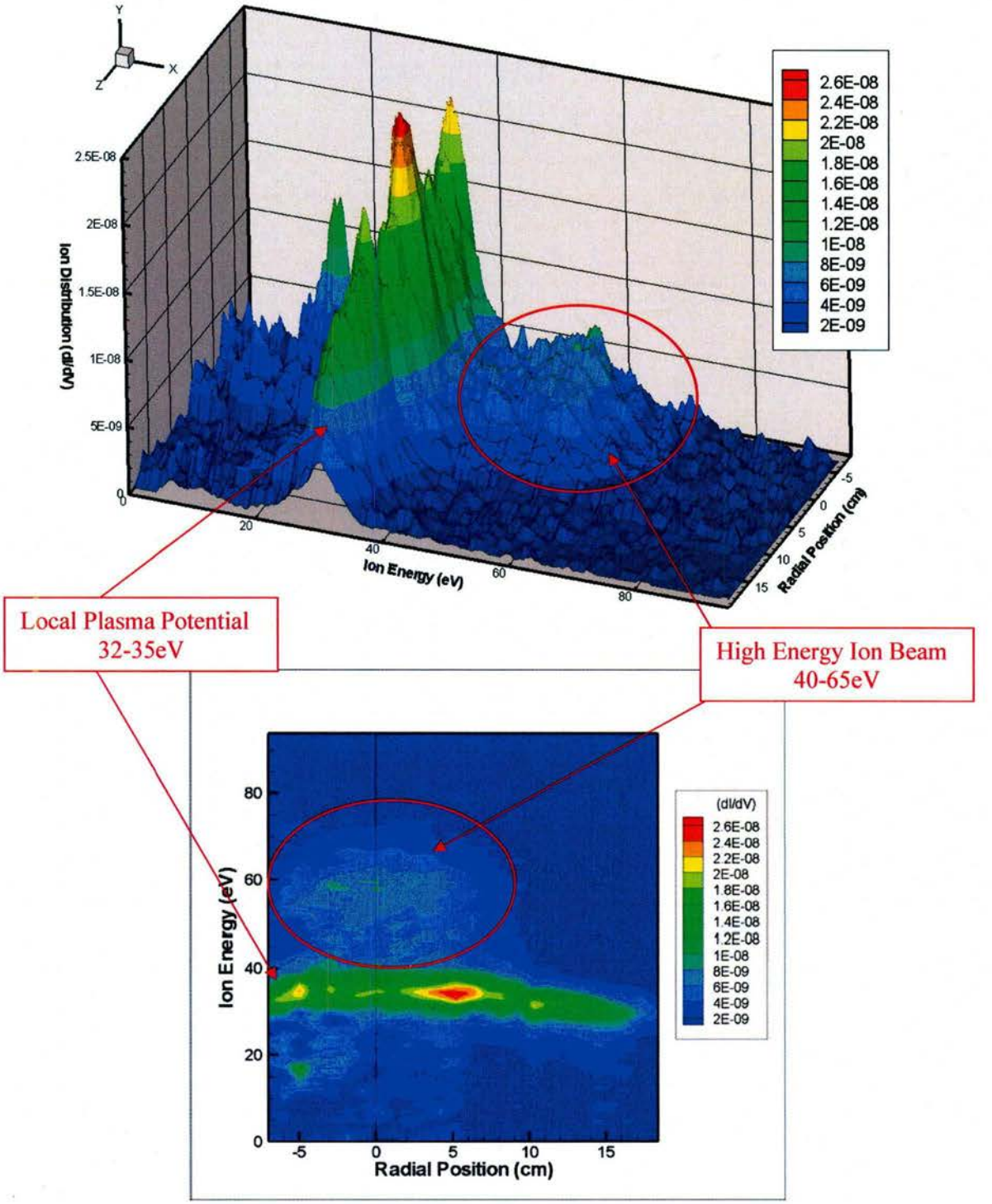

Figure 21: RPA Data Set 2 (Overdense)

Pressure (Ar)	MFC	B Field Current	RPA Location
0.11 mTorr	18 sccm	9 turns (pot)	21 cm from exit plane

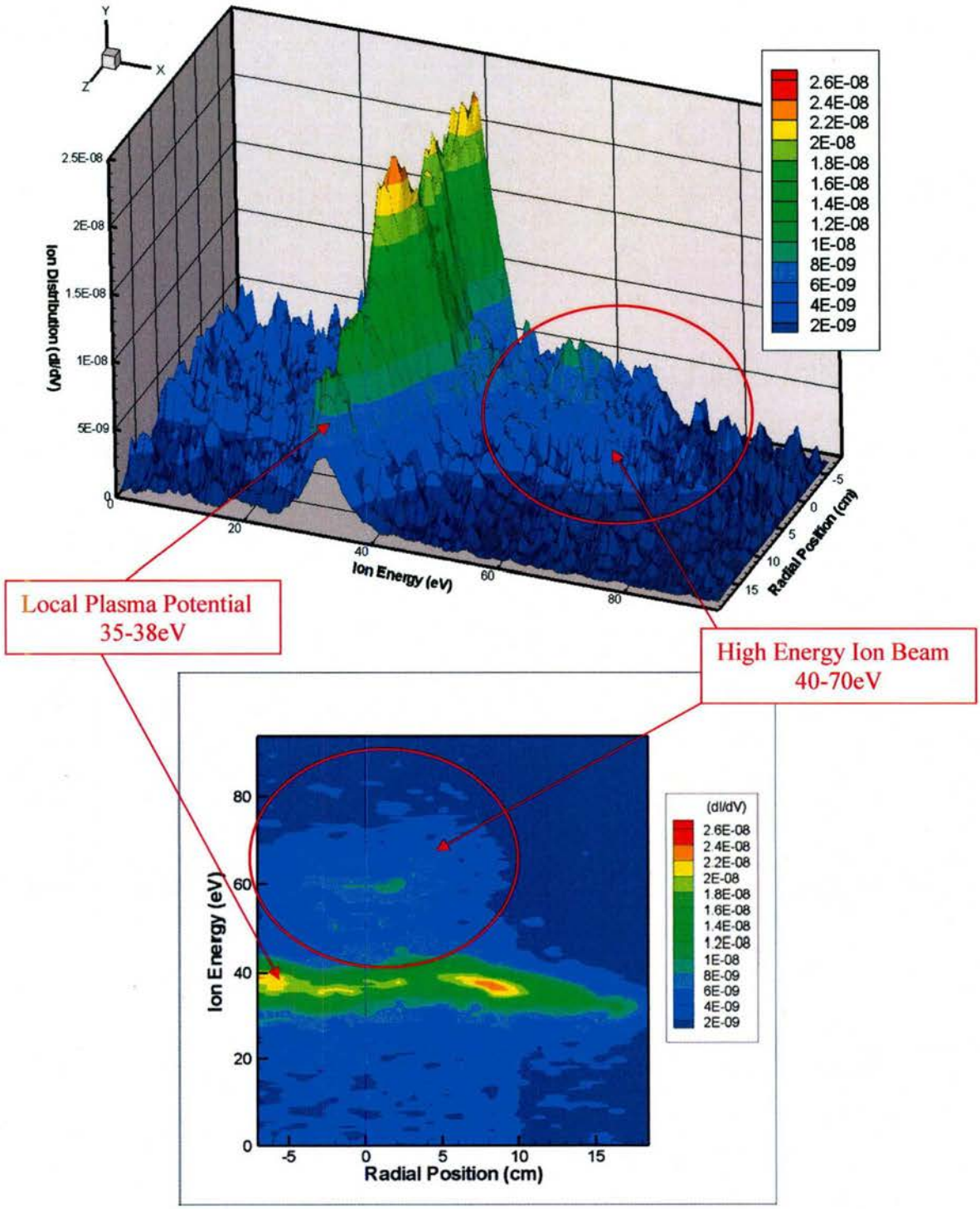

Figure 22: RPA Data Set 3 (Overdense)

Pressure (Ar)	MFC	B Field Current	RPA Location
0.19 mTorr	30 sccm	7 turns (pot)	21 cm from exit plane

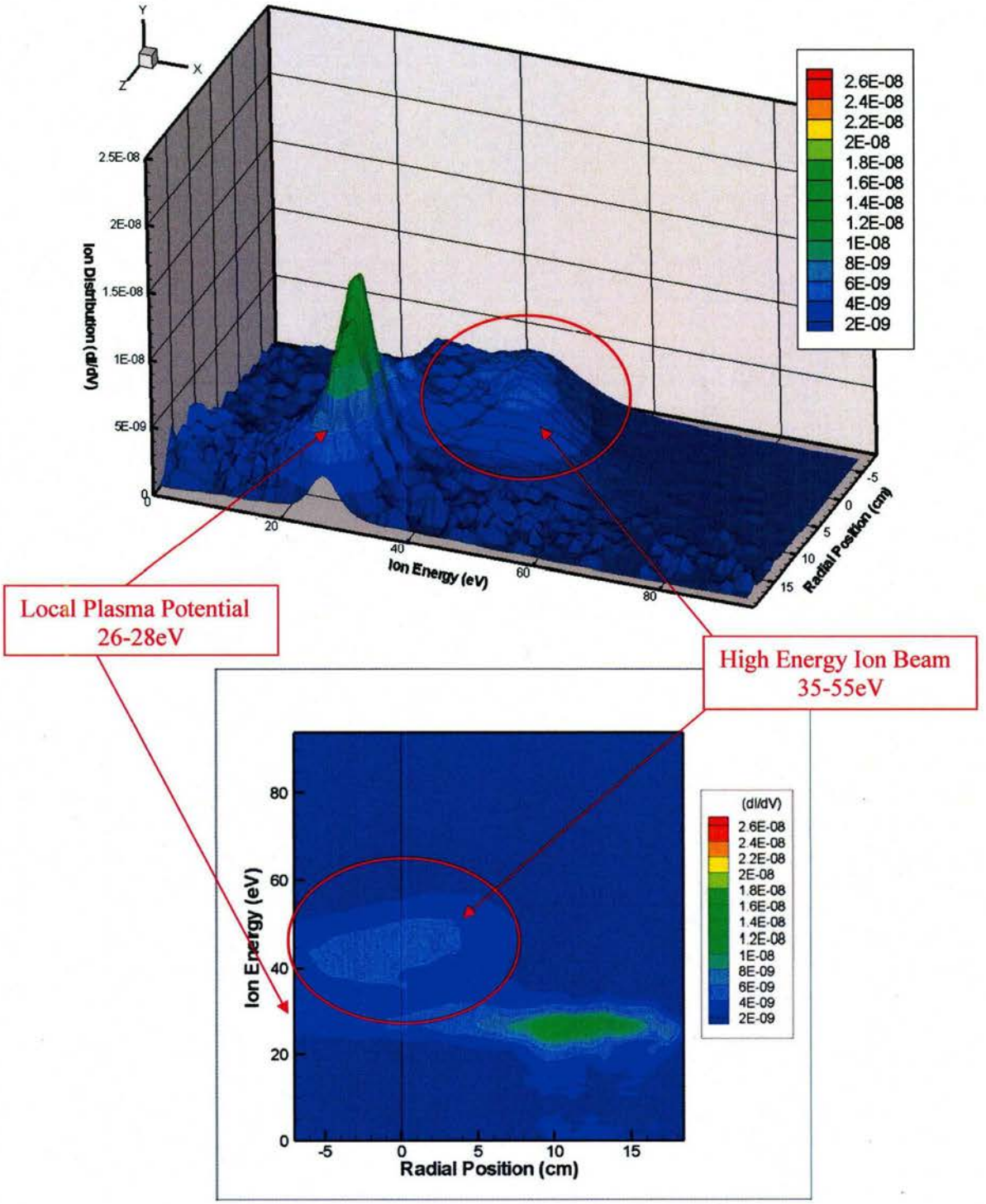

Figure 23: RPA Data Set 4 (Overdense)

Pressure (Ar)	MFC	B Field Current	RPA Location
0.19 mTorr	30 sccm	9 turns (pot)	21 cm from exit plane

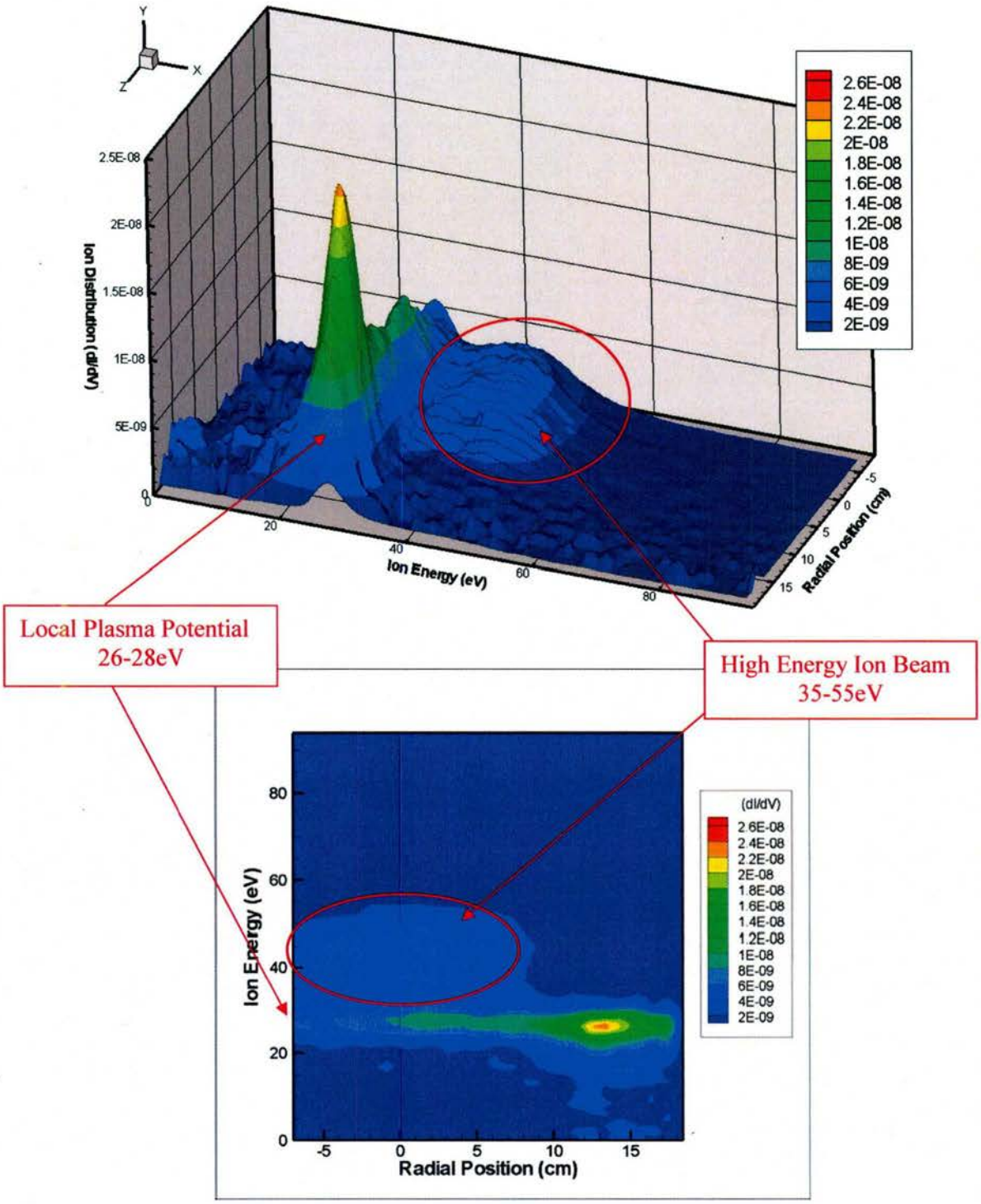

Figure 24: RPA Data Set A1 (Overdense)

Pressure (Ar)	MFC	B Field Current	RPA Location
0.18 mTorr	30 sccm	7 turns (pot)	21 cm from exit plane

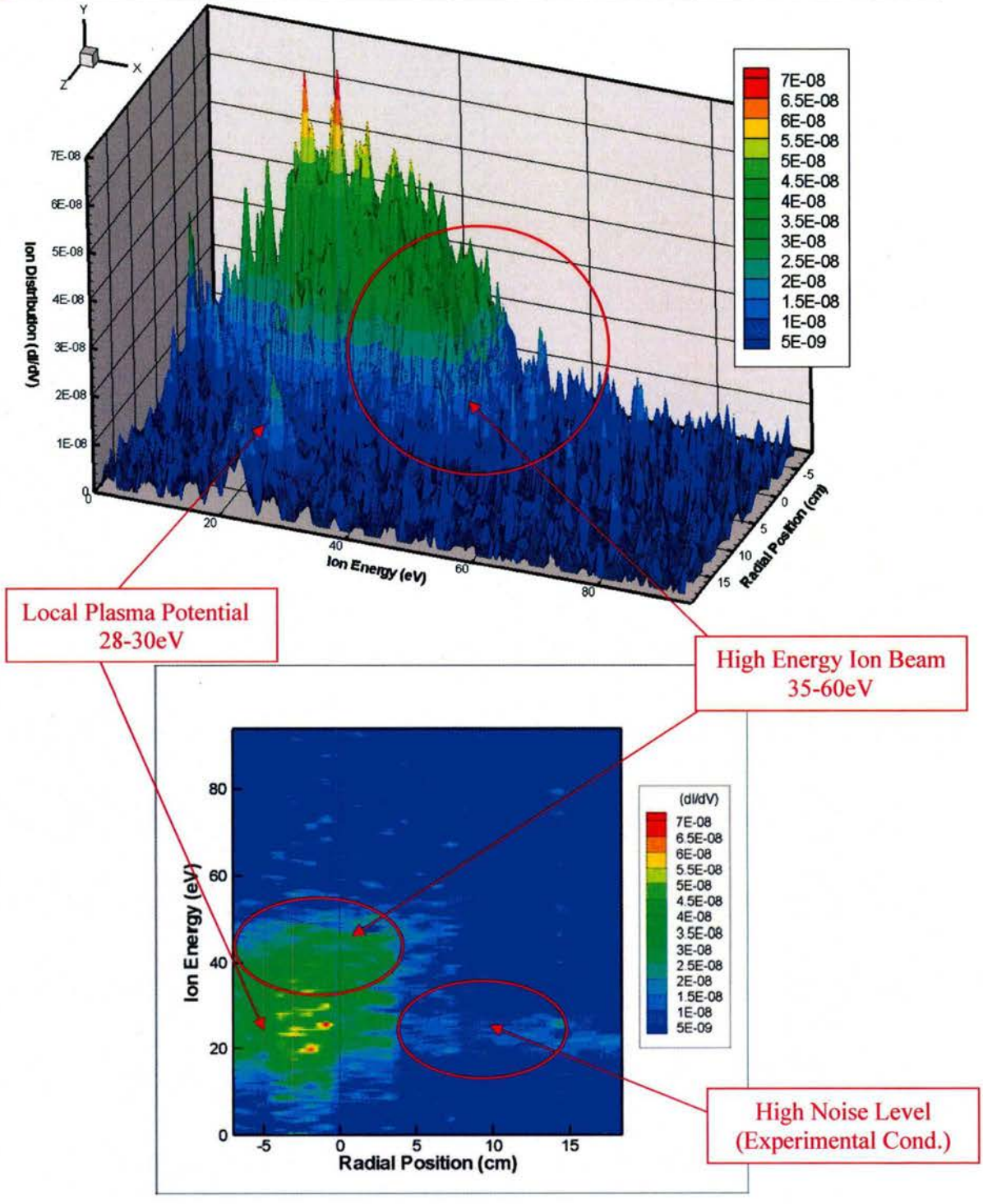

Figure 25: RPA Data Set A2 (Overdense)

Pressure (Ar)	MFC	B Field Current	RPA Location
0.18 mTorr	30 sccm	9 turns (pot)	21 cm from exit plane

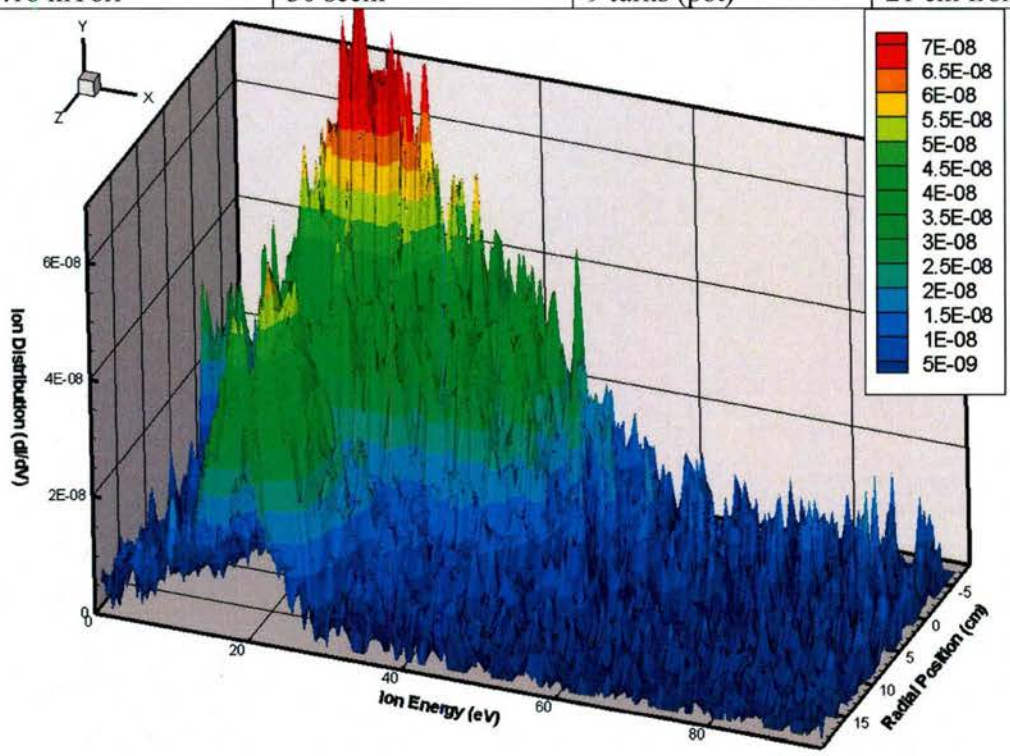

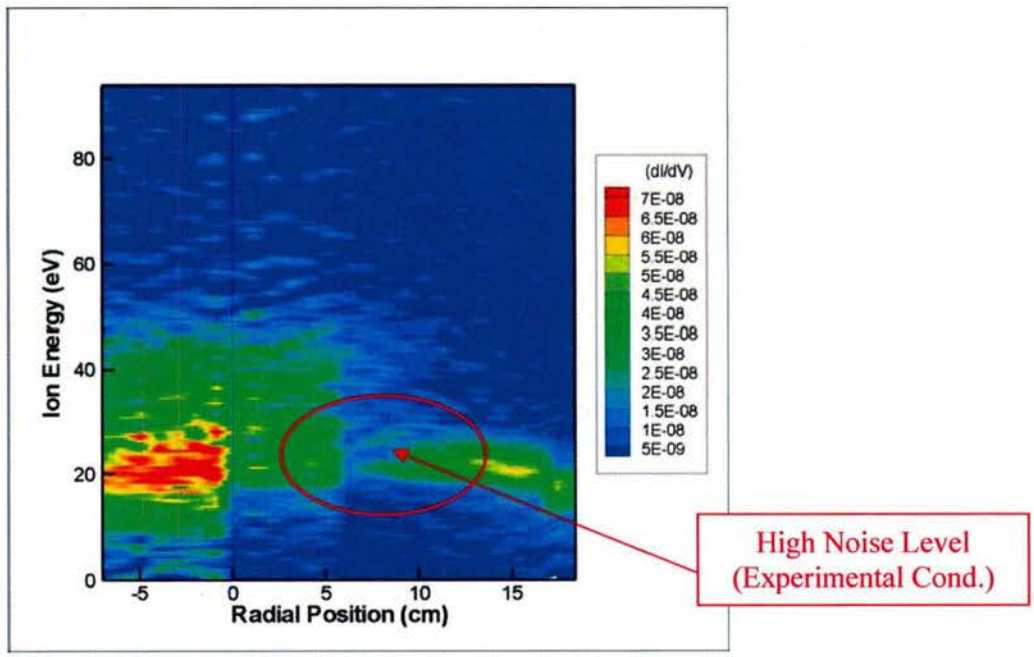

Figure 26: RPA Data Set A3 (Overdense)

Pressure (Ar)	MFC	B Field Current	RPA Location
0.10 mTorr	18 sccm	7 turns (pot)	21 cm from exit plane

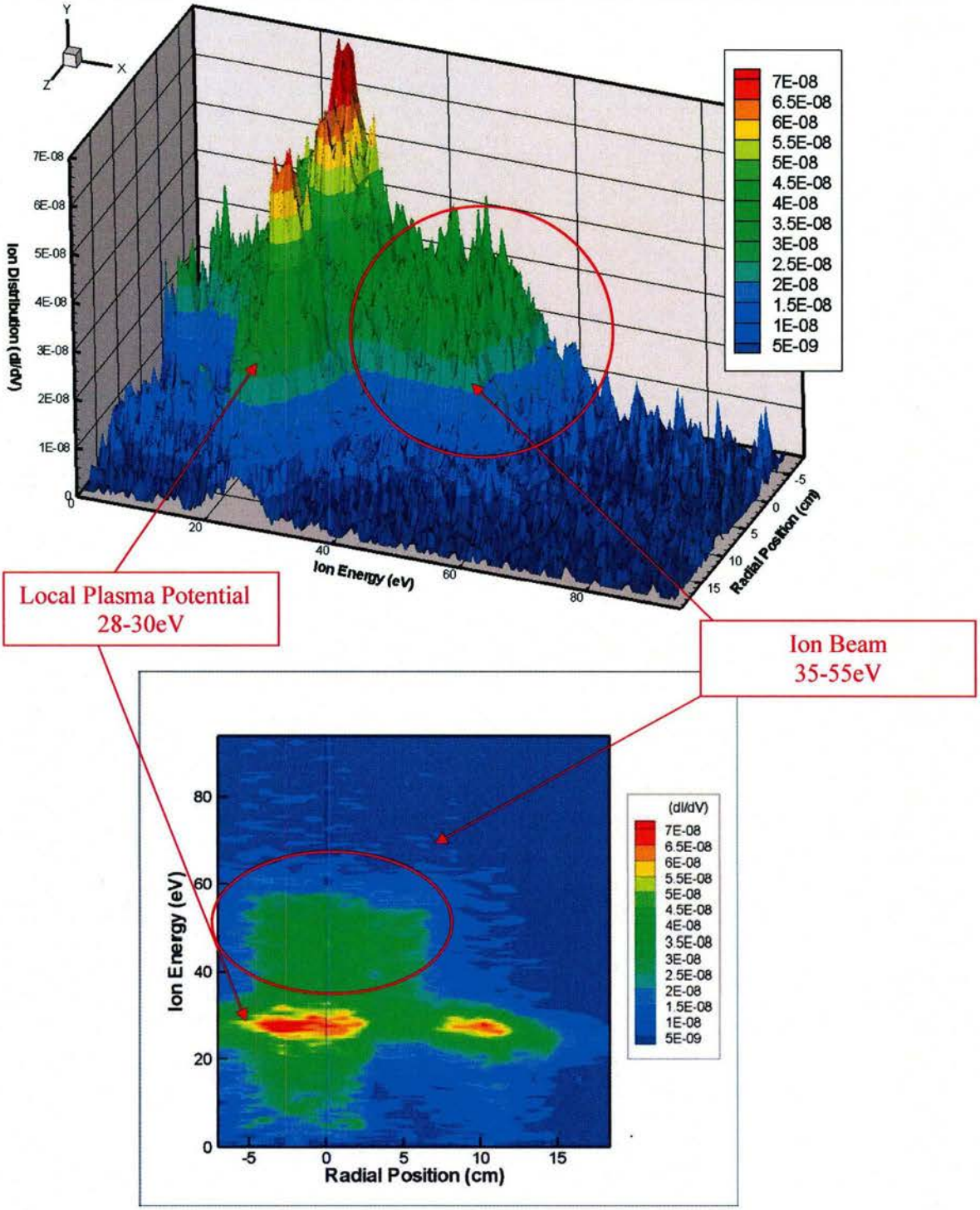

Figure 27: RPA Data Set A4 (Overdense)

Pressure (Ar)	MFC	B Field Current	RPA Location
0.10 mTorr	18 sccm	9 turns (pot)	21 cm from exit plane

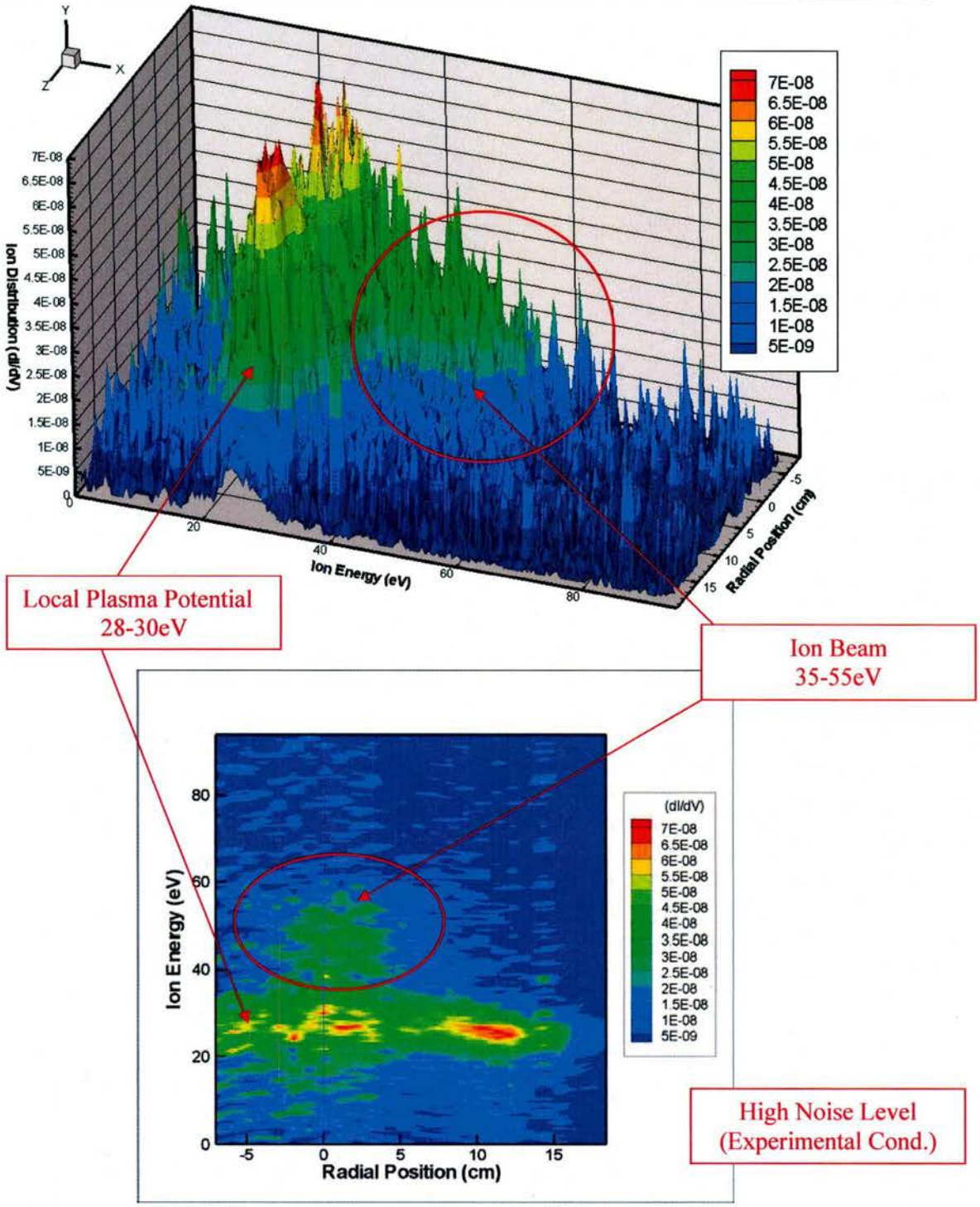

Figure 28: RPA Data Set A5 (Overdense)

Pressure (Ar)	MFC	B Field Current	RPA Location
0.16 mTorr	30 sccm	7 turns (pot)	48 cm from exit plane

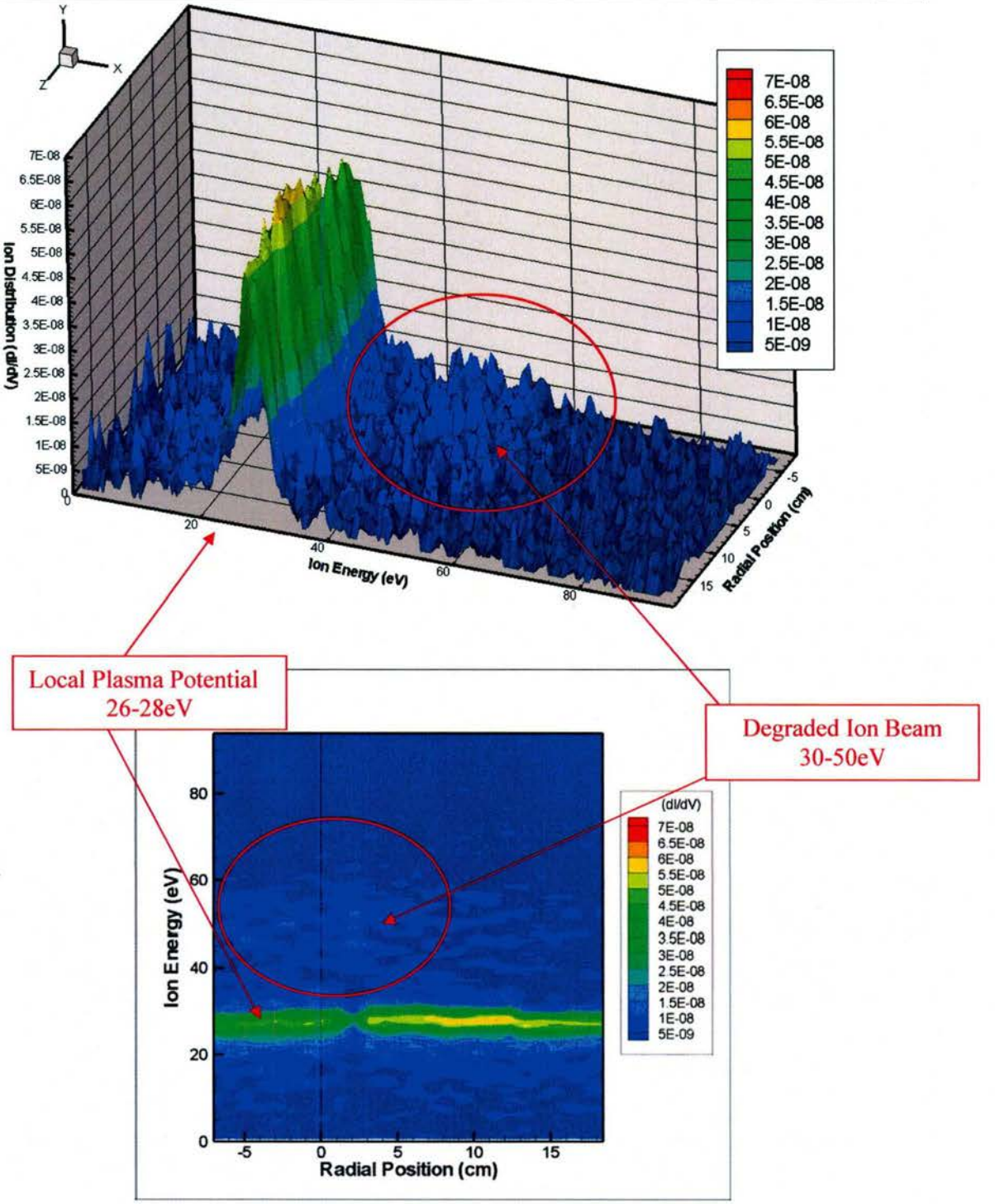

Figure 29: RPA Data Set A6 (Overdense)

Pressure (Ar)	MFC	B Field Current	RPA Location
0.16 mTorr	30 sccm	9 turns (pot)	48 cm from exit plane

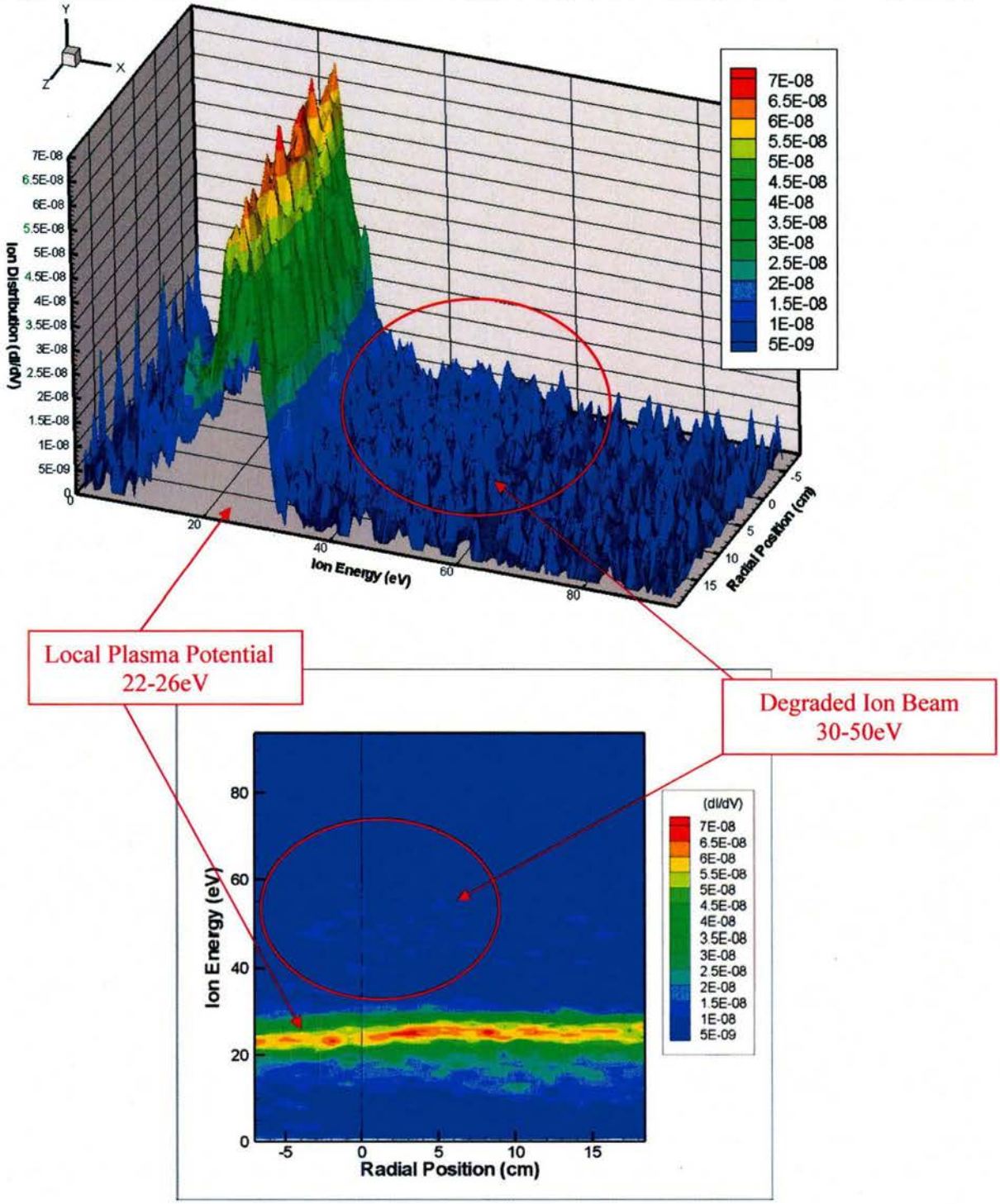

Figure 30: RPA Data Set B1 (Underdense)

Pressure (Ar)	MFC	B Field Current	RPA Location
0.069 mTorr	12 sccm	9 turns (pot)	48 cm from exit plane

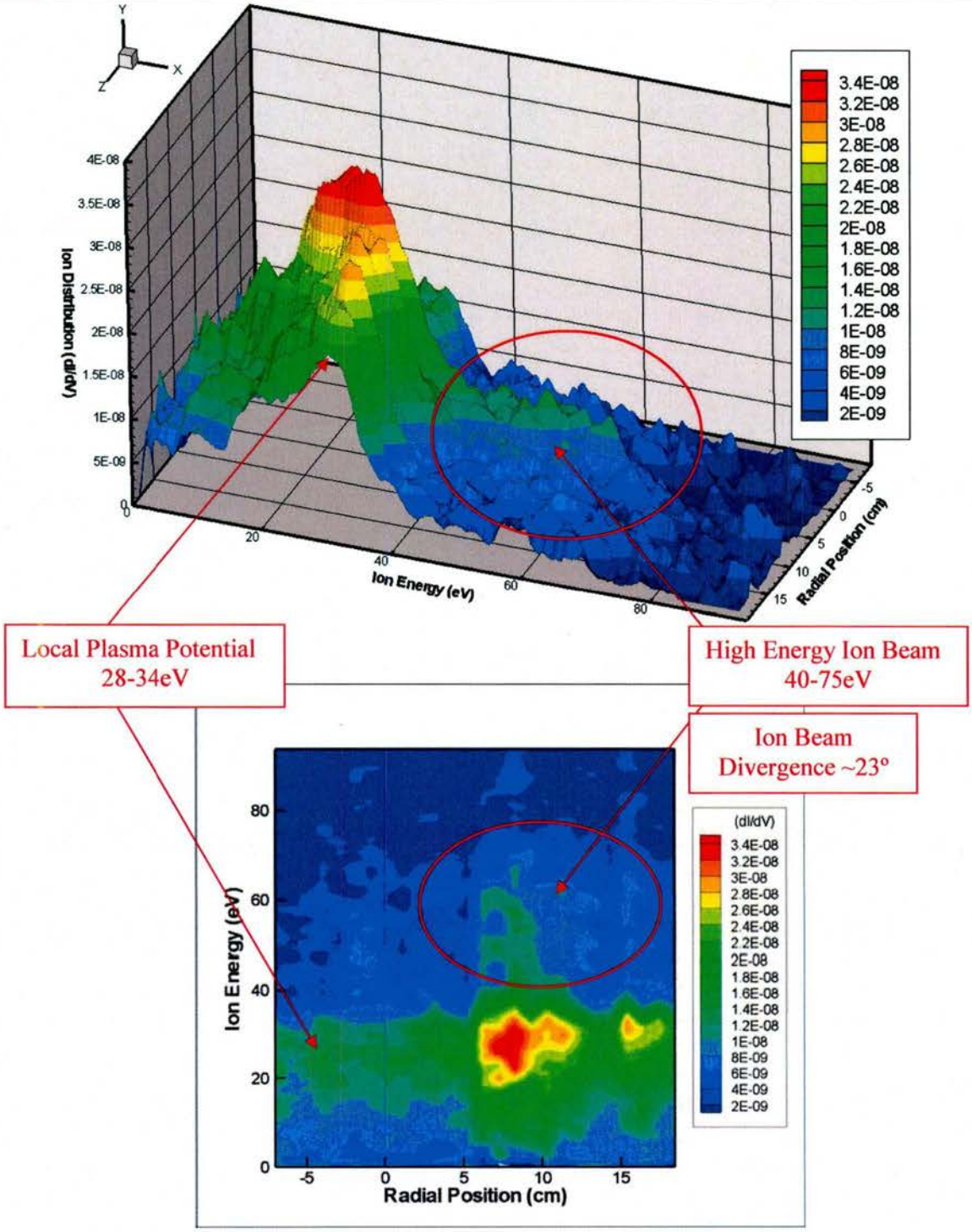

Examining the RPA data from the overdense plasma regime, there is a clear distinction of the local plasma potential at the probe location denoted by a solid line across the 2D plots. For cases of higher magnetic field, there appears to be high ion average energy and higher currents measured on the collector. This is presumably from increased density from higher electron confinement and ionization. Interestingly at higher flow rates of 30 sccm Data Sets 3-4 show decreased overall signal with a higher fraction of energetic ions; whereas, Data Sets A1-A4 show mixed results depending on flow rate. Again the higher magnetic field rule applies.

A key point in data interpretation is that plasma is accelerated in the microwave thruster, not just a single species as in a Hall effect thruster or gridded ton thruster. Thus, there are contributions for high energy electrons, as well as, high energy ions striking the RPA collector plate producing a zero or negative net current as ion motion is degraded preferentially vs. electrons. As mentioned earlier, the secondary electron suppression electrode was increased to -150 to -250V to repel incoming electrons in the beam to obtain a clear ion signal, as shown in the electron RPA trace in Figure 31 below.

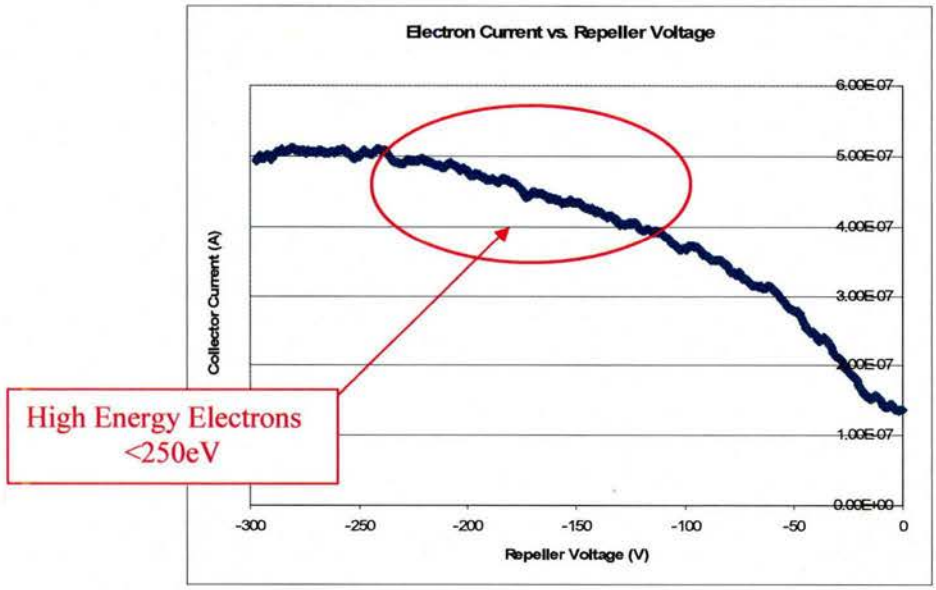

Figure 31: RPA configured for electron measurement at 30 sccm argon flow rate.

Local plasma potentials appear consistently in the 25-35eV range demonstrating a hot Maxwellian electron temperature distribution (see the LP data in the following section). The ion energy distribution appears to be truncated at less than 80eV and highly concentrated on the central axis. At first this was thought to be a highly-directed beam; however, since the RPA is mounted on a linear motion axis at high angles relative to the exit plane the entrance solid angle into the detector is diminished or even occluded (at the extreme ends).

To counter this effect, the diagnostic assembly was moved from the central chamber position (21 cm distance from quartz tube exit plane) to the rear chamber position with a corresponding 48 cm distance to the diagnostics suite. Data Sets A5-A6 show very little fast ion energy distribution downstream of the thruster, presumably due to increased collisions with background gas since the mean free path for charge exchange at 0.2mTorr is less than 20 cm. Data Sets A7-

A8 at 0.1mTorr were interrupted by difficulty striking and maintaining a plasma, possibly caused by intermittent failure of the magnetron or gas injection problems which is still under investigation.

An important fact is that visibly there is some detachment from the magnetic field lines since the visible plasma does not curl around and strike the exit plane side of the chamber. So there is some confidence that energetic plasma expansion out of the magnetic nozzle will separate from the spacecraft.

Operating the microwave/ECR thruster at lower pressure in the underdense regime produced vastly different results. Most notable was the appearance of a very high energy electron beam up to 600eV! This high electron current saturated the RPA collector with a large negative signal and washed out the incoming ion signal, until the new RPA design added the electron repeller grid. Increasing the negative bias on this repeller up to -750V eliminated the electron signal. Thus, there is a significant high-energy electron component when the thruster is operating underdense in an ECR mode.

Unfortunately, the ECR system would not operate stably in this underdense regime due to neutral gas depletion, frequent mismatching (high standing wave ratio) and inability of the plasma to strike and stay lit. The periodic nature of the magnetron system (60Hz) is the problem and the ECR unit was designed for operation at significantly higher gas pressures for semiconductor processing. A continuous microwave amplifier circuit would provide the ideal method for investigating this important operational regime.

Starfire was fortunate to obtain Data Set B1 at 0.069 mTorr pressure (12 sccm) at the far probe location. Here ion energies truncated at <80eV were again observed with the very high energy electron beam <600eV. However, the peak in the ion energy distribution is not centered on the axis, rather peaked in an annulus at 8-12 cm. **This would correspond to an ion divergence angle of approximately 23 degrees from the exit plane location.**

4.1.5.3 Langmuir Probe Measurements

The campaign of Langmuir probe experiments discussed in Section 4.1.4.2 were continued with the improved experimental setup to obtain plasma properties as a function of radial distance from the centerline of the ECR discharge tube at several axial locations. In Section 4.1.4.2, the plasma on the centerline was found to have temperatures of 3-4eV, plasma potentials of 25-30V, and plasma densities of $4\text{-}7\times10^{11}/cm^3$ for pressures between 0.1 and 0.2 mTorr. As expected, density increased with increasing pressure while temperature and plasma potential decreased.

Figure 32 shows the plasma potential as a function of radial distance from the centerline of the plasma source at three axial locations (2, 17 and 44 cm from the exit plane of the quartz tube) with a mass flow rate of 30 sccm (a facility pressure of ~0.17 mTorr) and a magnet potentiometer setting of 9.0 (a field of 615 Gauss at the quartz tube exit plane). In the 2-cm axial location, the plasma potential drops off near the radial boundary of the quartz tube (~±8 cm) because the tube limits the radius of the plasma at this location. Farther from the exit plane and within the radius of the tube the plasma potential lies between 25 and 30 V, which corresponds to

previous data taken only on the centerline of the plasma. This data also agrees with the plasma potential of 25-30 V obtained from the retarding potential analyzer at similar conditions.

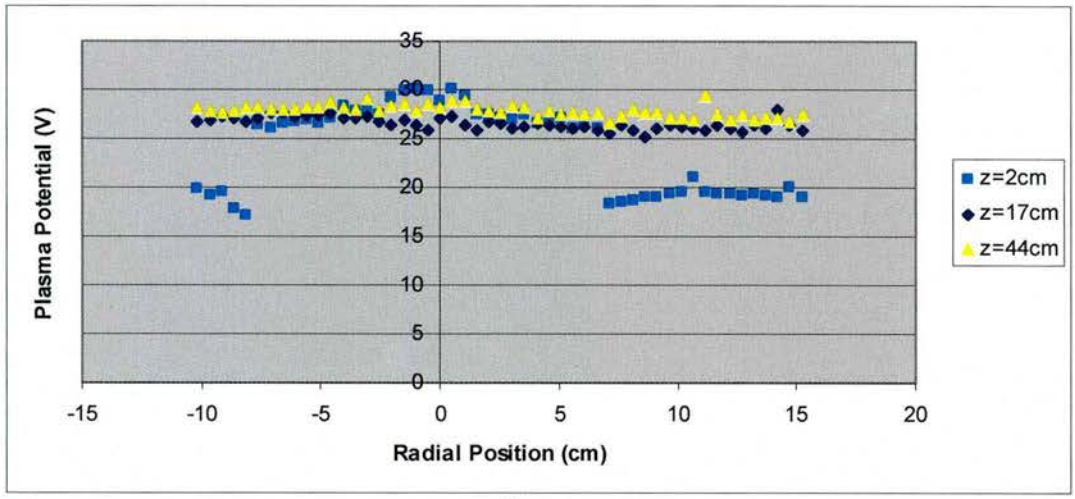

Figure 32: Plasma potential as a function of radial distance from the centerline of the ECR source at 2, 17, and 44 cm from the exit plane of the quartz tube with a mass flow rate of 30 sccm and a magnet setting of 9.0.

Figure 33 shows the plasma density and Figure 34 shows the electron temperature, from the same set of data. These data also show the effect of the quartz tube limiting plasma radius at the 2-cm location. Another, more interesting feature is the change in temperature and density as a function of position. The density at 2 cm is $7.0\times10^{11}cm^{-3}$ with a temperature of 5.2eV, the density at 17 cm is $5.1\times10^{11}cm^{-3}$ with a temperature of 6.9eV, and the density at 44 cm is 8.2×10^{11} cm^{-3} with a temperature of 3.7eV. This is depicted in Figure 35 below.

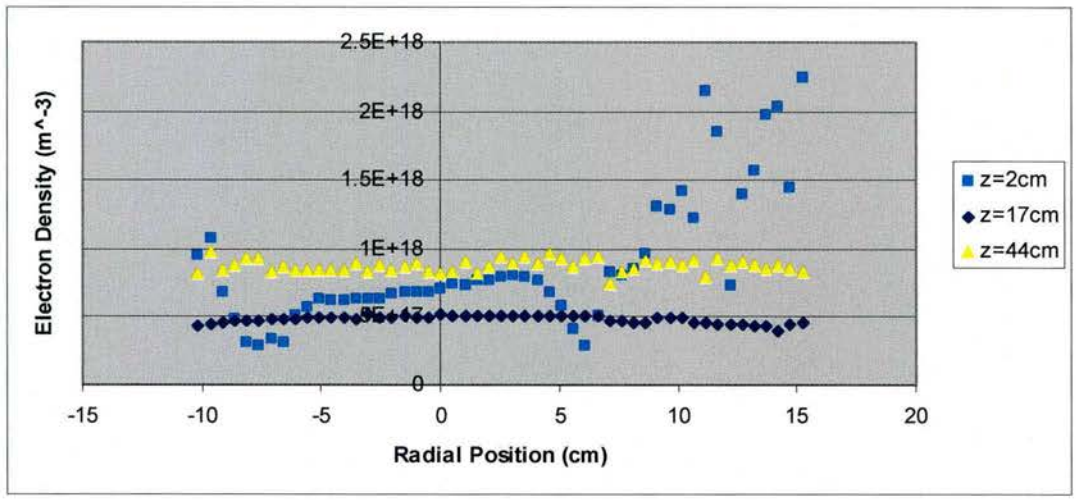

Figure 33: Plasma density as a function of radial distance from the centerline of the ECR source at 2, 17, and 44 cm from the exit plane of the quartz tube with a mass flow rate of 30 sccm and a magnet setting of 9.0.

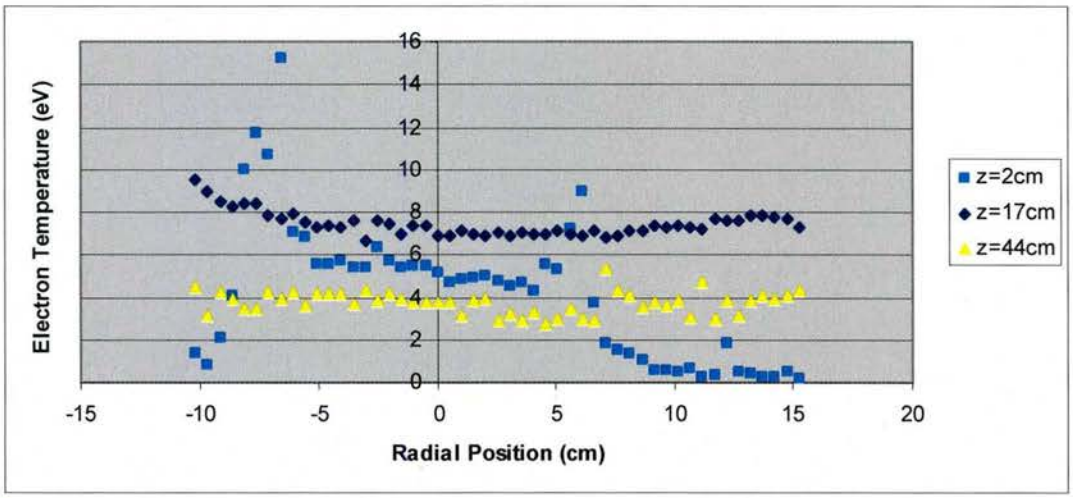

Figure 34: Electron temperature as a function of radial distance from the centerline of the ECR source at 2, 17, and 44 cm from the exit plane of the quartz tube with a mass flow rate of 30 sccm and a magnet setting of 9.0.

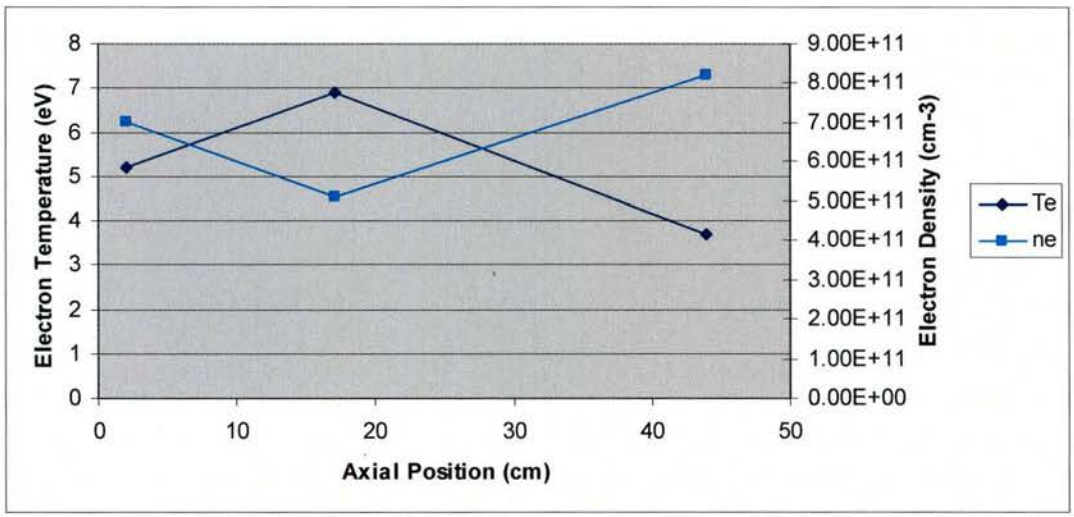

Figure 35: Centerline density and temperature as a function of axial distance from the exit plane of the quartz tube with a mass flow rate of 30 sccm and a magnet setting of 9.0.

The interesting aspect of Figure 34 is that the temperature initially increases as the density decreases from the exit plane to the middle location, but this is followed by a decrease in temperature and an increase in density beyond the initial density at the exit plane. The cause of this behavior is acceleration of the electrons from the exit plane to the middle location by the diverging magnetic field. Acceleration increases temperature, and plume divergence decreases density. As the accelerated electrons penetrate further into the chamber and reach the 44-cm location, they cause ionizations, which cool the electrons and increase density. Thus plasma is accelerated by the diverging magnetic field, which is the premise of the proposed thruster. However, there is more subtlety involved than simple expansion through a nozzle. A close examination of the Langmuir probe traces reveals a beam component to the electron energy distribution. Figure 36 shows the centerline probe traces at the three axial locations.

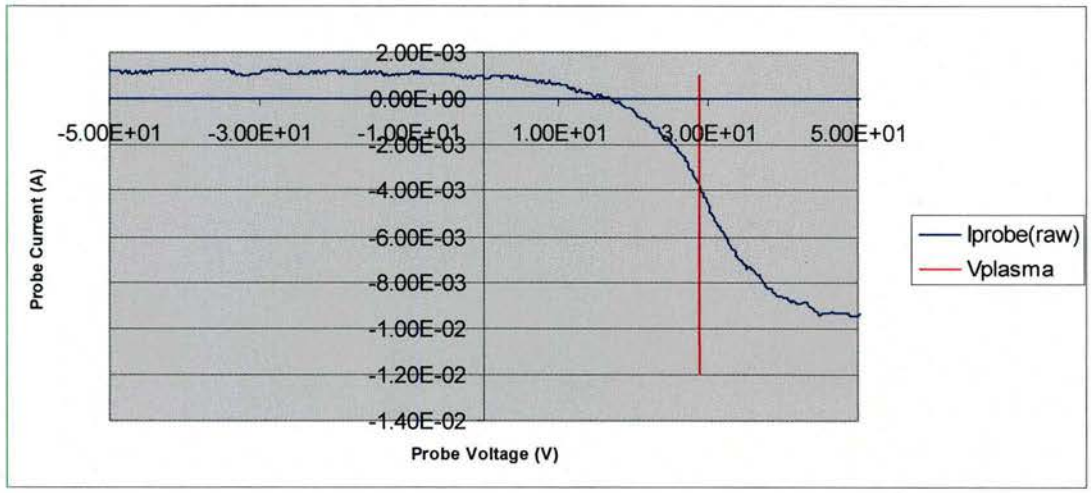

(a)

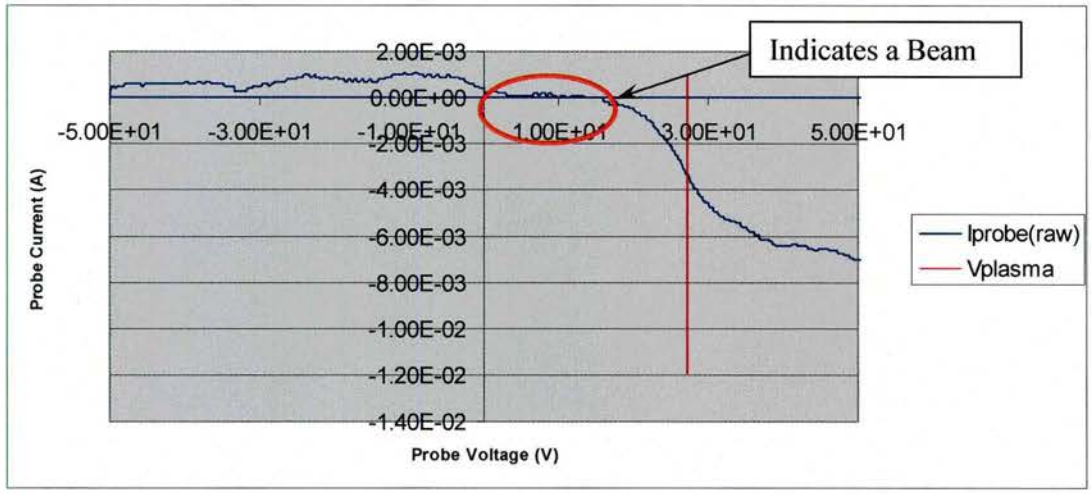

(b)

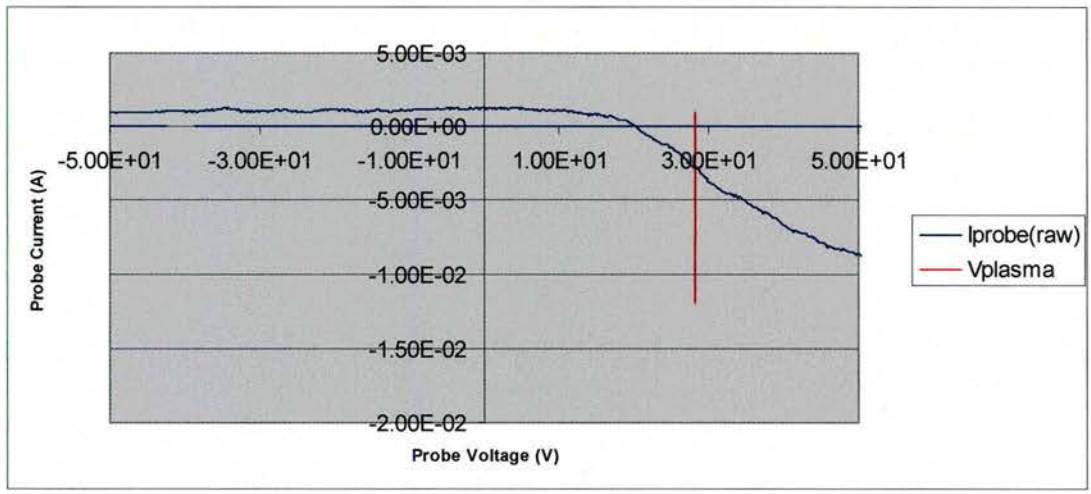

(c)

Figure 36: Langmuir probe I-V traces at (a) 2-cm, (b) 17-cm, and (c) 44-cm locations.

The 2-cm location and the 44-cm locations appear very ordinary and yield a good fit to a Maxwellian energy distribution; however, this is not the case for the 17-cm location. At 17 cm, a flat portion of the trace, i.e. current does not change as probe bias changes, indicates the presence of a beam. The flatness of this region also indicates that the beam is not only non-Maxwellian, but also directed, presumably along the axis in the direction of the magnetic field gradient. Also of interest is that **the beam characteristic is at the floating potential – an equal number of ions and electrons are striking the probe over a range of probe bias voltages. Thus, this is not just an electron beam, but also an ion beam; demonstrating that a microwave/ECR thruster functions as a plasma accelerator rather than an ion accelerator or electron accelerator.** This affirms the hypothesis in Starfire's Phase I proposal that electrons are accelerated by the diverging field as their perpendicular energy is converted to axial beam energy, setting up an ambipolar electric field that also accelerates ions. **An microwave thruster would therefore be a very simple electrode-less thruster – a tube with a magnetic field – that accelerates and expels plasma with no need for a neutralizing electron source.**

The energy of the beam component and the temperature of the background plasma can be found by subtracting the probe voltage at which this beam knee occurs from the plasma potential. This energy varies slightly with radius, but is an average of 12eV. The beam energy as a function of radial distance from the centerline of the ECR source is shown in Figure 37. After identifying the beam knee, the remainder of the trace can be used to find the ambient electron temperature in the usual way by calculating the reciprocal of the slope of the natural logarithm of the electron current.

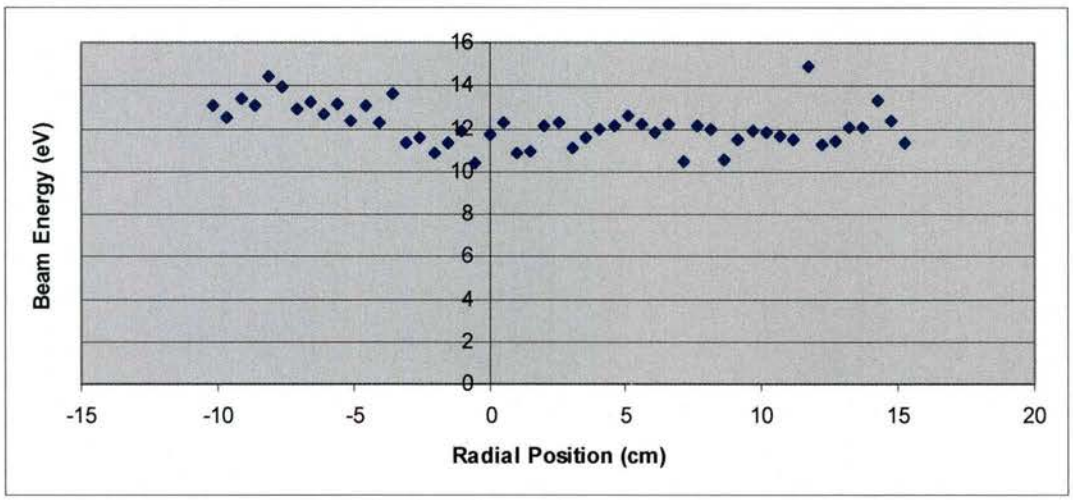

Figure 37: Beam energy as a function of radial distance from the centerline of the ECR source at 17 cm from the exit plane of the quartz tube with a mass flow rate of 30 sccm and a magnet setting of 9.0.

The beam energy data is further supported by retarding potential analyzer measurements of the high-energy ion component, which show ion energies centered around ~40eV at the middle location (21-cm axial location for the RPA which is slightly behind the Langmuir probe) for the same mass flow and magnet conditions. When the beam energy measured by the Langmuir probe is added to the plasma potential energy, an ion beam energy of 40eV is expected, which

correlates very well with the RPA data at a similar axial location. Further away from the exit plane, the RPA shows additional acceleration due to further expansion of the magnetic field. At this point, the electrons have cooled and the beam component has disappeared, resulting in a 3.7-eV temperature.

Since the electron energy is degraded by collisions with the background gas, a lower chamber pressure should result in higher beam energies and, thus, higher ion energies. To confirm this, a second set of Langmuir probe experiments was carried out at the 2-cm and 17-cm locations for the same magnet configuration (9.0 setting) and a mass flow rate of 18 sccm (chamber pressure of 0.11 mTorr. Comparing the centerline locations, the plasma potential at the 2-cm location was 36.6V with a temperature of 16 eV, and the plasma potential at the 17-cm location was 38.1V with an electron temperature of 7.8eV. The densities were $4.3\times10^{11}cm^{-3}$ and $4.8\times10^{11}cm^{-3}$ at 2-cm and 17-cm, respectively. The beam energy at the 17-cm location was 14.4 eV on the centerline with an average of 14 eV across the radial measurement. Figure 38 shows the beam energy as a function of radial position at the 17-cm location.

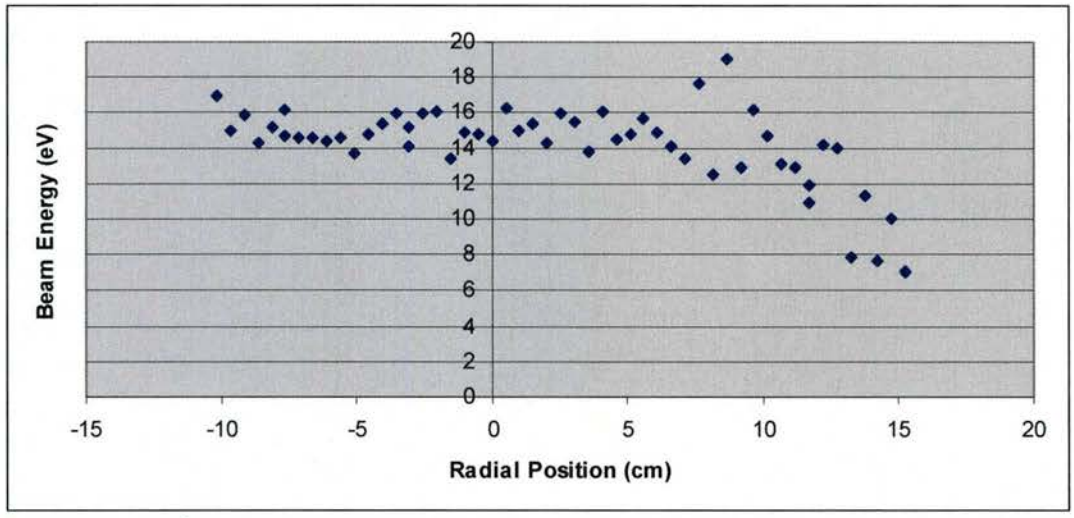

Figure 38: Beam energy as a function of radial distance from the centerline of the ECR source at 17 cm from the exit plane of the quartz tube with a mass flow rate of 18 sccm and a magnet setting of 9.0.

Comparing this data with that of the retarding potential analyzer data for the same flow rate and magnet configuration confirms this data. The RPA shows a plasma potential of 38V and a fast ion component centered about 50 eV. When the energy resulting from the plasma potential and beam energy measured with the Langmuir probe are summed (38eV + 14eV), an expected fast ion signal of 52eV results, which confirms that lower pressure operation allows greater ion acceleration, and that the plasma is accelerated, not just ions or electrons.

In principle, the energy obtainable by the plasma is limited only by the perpendicular energy attainable by the electrons. In ECR devices, as will be discussed below, electrons with energies of greater than 1keV can be obtained; therefore, **a wide range of plasma energies can be obtained with the same simple and robust thruster.**

4.1.6 Overdense and Underdense Operation Modes

A common misconception regarding ECR plasma sources operating in the overdense regime is that electrons are only heated in the 875 G resonance zone through cyclotron action; rather, the additional process is through collective EM wave absorption akin to lower-frequency RF plasma sources. The plasma skin depth can be written from the following expression, where the electron conductivity is wrapped into the ratio of collision-to-microwave frequency.

$$\delta_o[m] = \sqrt{\frac{2m_e}{e^2\mu_o}}\sqrt{\frac{\nu_c}{n_e\omega_o}} = 7.5\times10^6\sqrt{\frac{\nu_c}{n_e\omega_o}} \tag{2}$$

The electron collision frequency can be written from the following the following expressions:

$$\nu_{ce} = 2.91\times10^{-6}\frac{n_e \ln\Lambda}{T_e^{\frac{3}{2}}},\ where\ \ln\Lambda \approx 10-12 \tag{3}$$

$$\nu_{cn} = n_{gas}\sigma_{e-n}\sqrt{\frac{kT_e}{m_e}} \tag{4}$$

$$\nu_c = \nu_{ce} + \nu_{cn} \tag{5}$$

For a gas pressure of 0.2 mTorr, $T_e \approx 7$ eV and electron densities of 10^{18} electrons/m^3, the electron-electron collision frequency dominates and the ratio of ν_c/ω_o is $\approx 1.2\times10^{-4}$. Thus, the skin depth for attenuation of the ordinary mode of EM wave propagation (E parallel to B) is approximately 82.5 micrometers. However, due to the heavy magnetization of the plasma in the transverse direction and corresponding loss of electron conductivity, the perpendicular conductivity (i.e. collision frequency) can be modified by:

$$\nu_{c\perp} = \nu_c\frac{\nu_c^2+\omega_o^2}{\nu_c^2} \tag{6}$$

For the case where $\nu_c/\omega_o \ll 1$, the perpendicular skin depth can be re-expressed as:

$$\delta_o[m] = 7.5\times10^6\sqrt{\frac{\nu_c}{n_e\omega_o}\frac{\nu_c^2+\omega_o^2}{\nu_c^2}} = 7.5\times10^6\sqrt{\frac{\omega_o}{n_e\nu_c}} \tag{7}$$

For the same plasma conditions, the extraordinary mode propagation (E perpendicular to B) results in a perpendicular attenuation length of 68.5 cm! Microwave energy is rapidly attenuated along the magnetic field since electrons can respond to the fluctuating EM field; whereas, the stiff magnetic field lines inhibit the collective plasma response to extraordinary wave propagation.

In the present experimental setup, at B_{pot}=7.0, the 875 G line is located about 15 cm downstream of the quartz EM injector wave port. Almost immediately, microwave energy will be attenuated

into the local plasma within the first millimeter of the quartz window surface. However, a portion of the EM field will still propagate down the channel to reach the ECR zone layer. This field would attenuate ($1- e^{(-15/68.5)}$) on the way to the resonance zone downstream, losing 20% into the bulk plasma through collective absorption. Therefore, it is possible for some microwave energy to propagate down the channel. If we assume a 45° EM launch angle at the wave guide mode converter, 40% of the transmitted microwave power will reach the resonance layer.

For higher gas pressures and plasma densities (collision frequency), the fraction of power that reaches the resonance zone will decrease due to heavier attenuation on the way there. In the overdense mode where the electron density exceeds the critical density and approaches full ionization (i.e. $\sim 10^{13}$ electrons/cm^3), the skin depth shrinks even further and is mostly dependent on electron temperature. In this scenario, little microwave energy reaches the resonance layer for transverse electron cyclotron heating.

This makes perfect sense for an ECR plasma source from a semiconductor processing viewpoint, where little microwave energy is desired to escape the plasma or reach the resonance zone to generate very high energy electrons (>100eV). Thus, a long quartz tube >15cm (which is installed on the system from the University of Illinois) would serve to attenuate the incident microwave energy before reaching the wafer while still generating high density plasma. Therefore the RPA and LP results showing up to 12-30eV plasma acceleration could be mostly due to isotropic thermal plasma expansion, not resonant ECR heating and expansion!

This is VERY IMPORTANT for using higher-frequency microwaves in magnetic nozzle structures that cannot achieve sufficient B-field for ECR. Propulsion is still viable with direct microwave "heating" of the plasma; it is just that the heating is transferred into isotropic bulk motion vs. perpendicular energy for conversion into magnetic nozzle expansion at energies of 12-30eV (based on T_e and magnetic gradient). With sufficient electron confinement time, microwave energy can be deposited into a local region for electron heating.

For space propulsion applications, maximizing the perpendicular electron energy will grant the greatest expansion in the magnetic nozzle and corresponding generation of a large ambipolar gradient for ion acceleration. The method of EM power injection becomes important as to the mode of bulk plasma heating (e.g. cavity resonators, beamed EM energy to the magnetic nozzle, etc.). If electrons are heated perpendicular to magnetic field lines through cross-field EM heating, then power could be more readily used for ambipolar expansion. Thus, there is considerable room for engineering design and system optimization for thrust and Isp.

If the plasma can be run near resonance, then EM energy can be directly coupled into perpendicular electron velocity and expanded into thrust in the magnetic nozzle. Power coupling efficiencies >95% are possible for this configuration since it is a resonant phenomena. For bulk microwave drive heating, a maximum power transfer efficiency of 65% is possible; this is still good for multi-functional propulsion systems with DCS capability.

Also, if the length of the resonance or heating zone is sufficiently small, the plasma can be optically thin to microwave energy and a microwave beam can be directed out of the thruster. In several circumstances, the microwave radiation was directed into the probe assembly causing

local heating and melting of BNC connectors and cabling. In essence, demonstrating an attractive feature for defensive counter-space operations—directed energy absorption in a nearby object.

Further experimental study is required to gain optimization criteria for designing the ECR zone location, injected EM radiation pattern and power, magnetic field shape, gas pressure and electron temperature, etc.

4.1.7 Experimental Summary

The Phase I critical goal of demonstrating a potential drop across the magnetic nozzle was completed. Measurements of current density and ion energy downstream of the thruster estimate nearly full ionization of the propellant and high energy ion generation. Based on observation of plasma behavior, variability in ion energy and thrust level should be possible with an microwave/ECR-based propulsion system. No electron cathode or neutralizer is needed. There are no electrodes to erode, sputter or damage. Measurement of a 23° ion divergence angle in the plume region suggests manageable divergence angle and thrust contribution along the centerline axis. This addresses some concerns regarding a high magnetic field system and plasma detachment.

As reported, the present experimental setup with long quartz tube has many field lines intercepting the tube walls leading to electron depletion and wasted power density. Having an ECR thruster setup with magnetic coils located inside the vacuum chamber or a uniform field region with low loss would be ideal. With appropriate field geometry and electron confinement, average ion production energy will drop close to the theoretical minimum cost for impact ionization (as determined by propellant). Propellant choice is completely up to the end user with some consideration given to molecular species rotational and vibrational energy states; however, with very high temperature plasmas and full dissociation this may become a non-issue.

Phase I investigations have also showed that there are a diversity of EM launcher configurations that can achieve the microwave propulsion and DCS capabilities. Further study is needed!

4.2 Modeling of Microwave-Plasma Interaction

Starfire's exploratory research into ECR thruster design is focused on exploiting a feature of the magnetic nozzle expansion, namely the conservation of magnetic moment and adiabatic invariance. This is a property whereby as a charged particle expands out of a diverging (or the opposite in case of converging) magnetic nozzle, the particles perpendicular velocity is converted into parallel velocity as the particle moves through the changing B field. Since electrons are lighter and more responsive compared to ions in the system, electrons will experience the most force and expansion from bulk plasma in an expanding magnetic nozzle and a separation of charge will result. A restorative ambipolar field will result from this charge separation and the magnitude is governed by the following equations.

$$F_{MagneticNozzle} = -\mu \nabla B_{\parallel} = -\frac{mv_{\perp}^2}{2B_z}\frac{\partial B_z}{\partial z} \tag{8}$$

$$F_{Ambipolar} = qE_a \tag{9}$$

In quasi steady state, these equations can be equated and rewritten to yield the stationary ambipolar field that will exist across the magnetic nozzle region. This electric field will serve to accelerate ions out of the thruster, where Te is measured in eV.

$$E_a(z) = \frac{mv_{\perp}^2(z)}{2qB_z(z)}\frac{\partial B_z(z)}{\partial z} = \frac{T_{e_{\perp}}(z)}{B_z(z)}\frac{\partial B_z(z)}{\partial z} \tag{10}$$

The key terms are the transverse electron temperature, the magnetic field and the gradient in the field. For a full treatment of the problem, these equations need to be differenced and integrated over expansion region of the magnetic nozzle to compute an exact solution. However, this basic formulation can be used to compute initial values of the ambipolar field to zero-order to gain some insight into the key problems associated with engineering the Starfire ECR Thruster.

Let's assume a simplified thruster magnetic field and expansion profile as shown in the following figure. There is a well defined resonance zone at the top of the magnetic potential hill where the electron will gain a fixed transverse energy, a linearly declining B field that is over a fixed distance so as to yield a constant slope dB/dz. From this, we can compute what the steady-state ambipolar field and integrated voltage drop across the magnetic nozzle to obtain a zero-order estimate on ion energy.

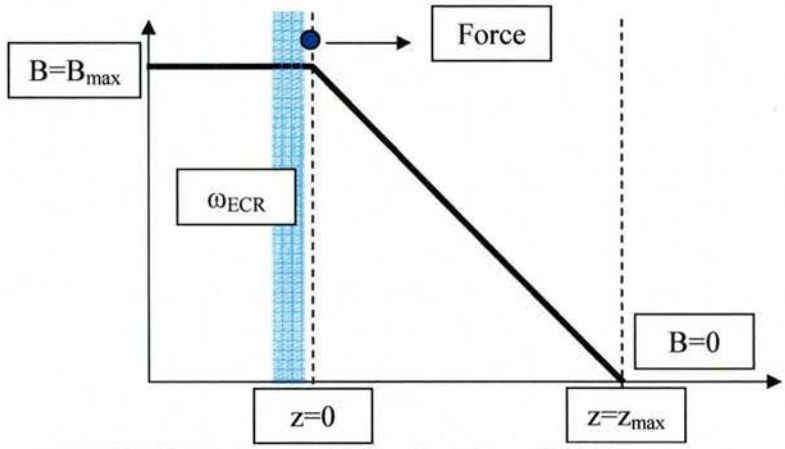

Figure 39: Simple illustration for calculation of ECR thruster setup.

For S-band ECR magnetron running at 2.45GHz, we have a resonance zone magnetic field of 875G (0.0875T). For the X-band mini ECR system running at 10GHz, we have a field of 3500G or 0.35 Tesla. Let's assume that the magnetic field will fully disappear over a distance of 10 cm. This is a sharp magnetic gradient and could be achieved with the use of a specialized pole piece or magnet arrangement. If the transverse electron energy is 5 eV, then the electric field and total

potential drop will be only 5 V. Notice that in either the 2.45GHz or 10GHz system, the result is the same.

$$E_a = \frac{5\text{V}}{875\text{G}}\frac{875\text{G}}{0.1\text{m}} = 50\frac{\text{V}}{\text{m}} \tag{11}$$

$$\Delta\phi = 5\text{V} \tag{12}$$

This makes complete sense since the adiabatic invariance will convert the perpendicular energy into axial energy. In the above example there is only 5 eV of energy to convert into parallel energy.

Thus, for an ECR system to develop any appreciable amount exhaust velocity, it will need to impart a significant amount of perpendicular energy to the electrons in the system as they fall into the magnetic nozzle region. Similar to HET systems, lighter propellants (than Xe) will increase the effective exhaust velocity for a given acceleration voltage. However, a good question is "Are 100s of eV of perpendicular energy feasible?"

If an electron drifts into the resonance zone it will begin to gain energy from the wave and field coupling. In the absence of collisions, the energy that can be gained depends on the electrons residence time in the zone and the number of wave cycles applied to the electron. Since the electron is continually gaining energy from the field, the average energy gain per pass is proportional to

$$KE_{pass} = \frac{1}{2}mv^2 = \frac{q^2E^2}{2m}\Delta t_{res}^2 \tag{13}$$

Thus, it appears that the energy gain goes as the applied E field squared. Having a lower initial velocity in the resonance region is good to have more time to gain energy, as well as, having a longer resonance zone region.

What is the electric field of the wave injected into the vacuum chamber? Literature from a 1.1-kW microwave oven magnetron lists the electric field in the opening of the WR340 waveguide is 25 kV/m. If we assume that the resonance region is 1-mm wide and an electron entering this region has 1-eV parallel energy, the time spent in the region will be about 1.7 nsec. Using the above equation, the energy gain from one pass through this region will be 156 eV! This is encouraging; however, collisions with background gas and ions will limit this energy gain and lead to increased plasma heating and scattering out of the resonance zone.

There also is a collisionless heating limit when the wave energy is attenuated away into the electron and the E field amplitude drops across the resonance zone. A full spatial wave treatment is necessary to account for this wave-plasma coupling even at densities below the critical threshold for overdense transition.

The significance of this is that electrons can be heated to keV energies provided that the resonance zone width is sufficiently long to yield a long electron confinement time, or a

magnetic bottle arrangement is used to trap electron axial velocity and allow radial heating. If electrons are heated to high temperatures via ECR heating, then they can be directed into a high-Z target for the production of x-rays via Bremsstrahlung reactions. Alternatively, very high Isp magnetic nozzle expansion can be achieved for high efficiency propulsion.

4.2.1 Simulation of X-Band (10 GHz) System

To simulate the ECR thruster conditions and ascertain the value of the anticipated exhaust velocity for a given set of field conditions (B_r, B_z, E_r, E_z, etc.), we use the object-oriented particle-in-cell code OOPIC-Pro. Figure 40 shows the simulation volume comprising a cylindrical waveguide, which is 2-cm in radius and 3-cm long, expanding into free space. The mesh spacing is set to be 1-mm by 1-mm using a 128 by 96 grid spacing. This corresponds to a simulation volume in the (r,z)-symmetric coordinate system to be 12.8-cm long in the z-axis and 9.6-cm long in the r-axis. An initial distribution of electrons and ions were loaded, with a radial weighting to account for the increased cell volume near the outer edge of the simulation space (using a built-in function) at a density of 10^8 electrons/cm3.

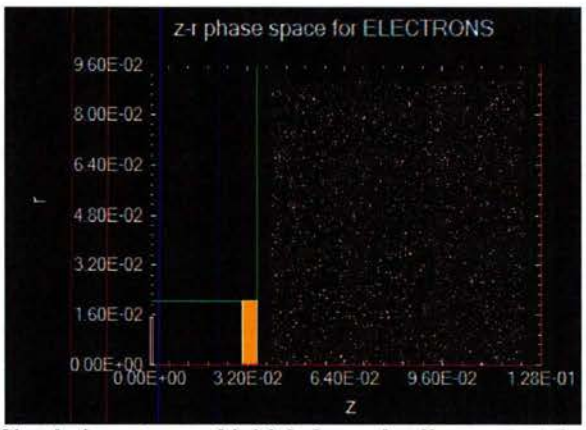

Figure 40: Simulation setup and initial plasma loading to start the simulation.

On the left most edge of the waveguide cavity is a radial voltage source that has an applied 10GHz current pulse applied. The radial length of the source is $\lambda/4 = 1.5$ cm. This generates and launches a TM_{01} wave into the waveguide that propagates along a perfect conducting tube through a quartz quarter-wave dielectric window into free space. The conductor also serves as the boundary of the spacecraft in the simulation that is kept at ground potential (a condition of the OOPIC-Pro EM field solver model). The axial and radial axes are exit boundary conditions where particles and EM fields leave and do not commute back to the simulation volume. Figure 41 shows the electric field profiles from the TM_{01} launcher. The choice to use 10GHz was made to decrease the size of the simulation space since the larger 12-cm wave would have made the simulation mesh size more cumbersome.

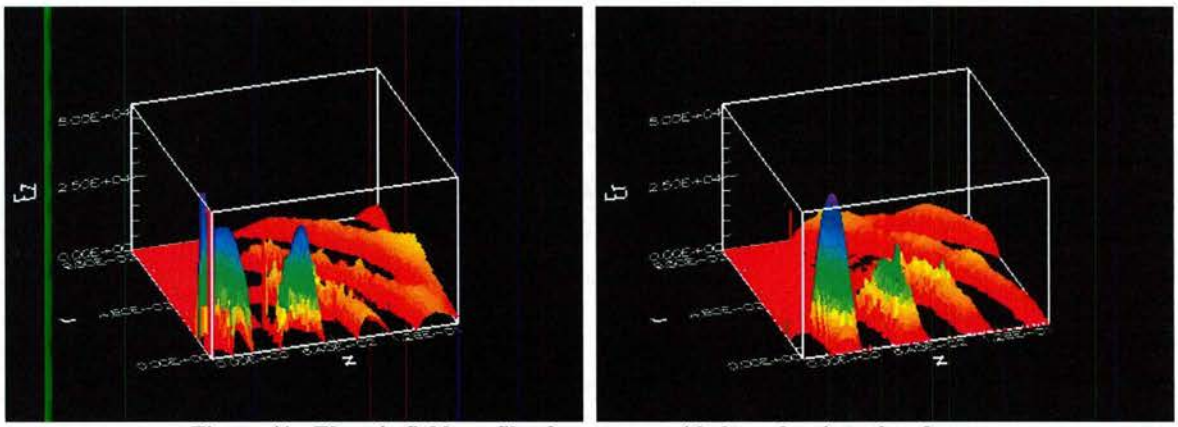

Figure 41: Electric field profiles from waveguide launcher into the plasma.

The peak values are adjusted to yield ~20-40kV/m electric field amplitudes commensurate with a 0.25-1kW magnetron at the exit of the WR90 waveguide (0.9-in by 0.4-in) given by the following simplified expression.

$$Power = \frac{|E \times H|}{A} = \frac{E_{peak}^2}{Z_{freespace} A_{waveguide}} \tag{14}$$

Since OOPIC-Pro does not have a built-in solver for complex-geometric static magnetic field shapes, a suitable input file for the magnetic field must be used to define the local B_z, B_r values per grid point and mesh spacing. Note that OOPIC uses mesh cells and not grid references in its input file, so a 128 x 96 grid spacing corresponds to a 127 x 95 mesh cell array. Using an EM field solver code developed internally, a solenoidal coil configuration envisioned with a 2-cm x 2-cm rectangular cross section at an inner radius of 4 cm was simulated. The field maximum was chosen to create a 3500 Gauss equipotential line a short distance from the exit of the waveguide. Figure 42 shows the actual static fields used in the simulation. The actual solenoid sits behind the conducting boundary.

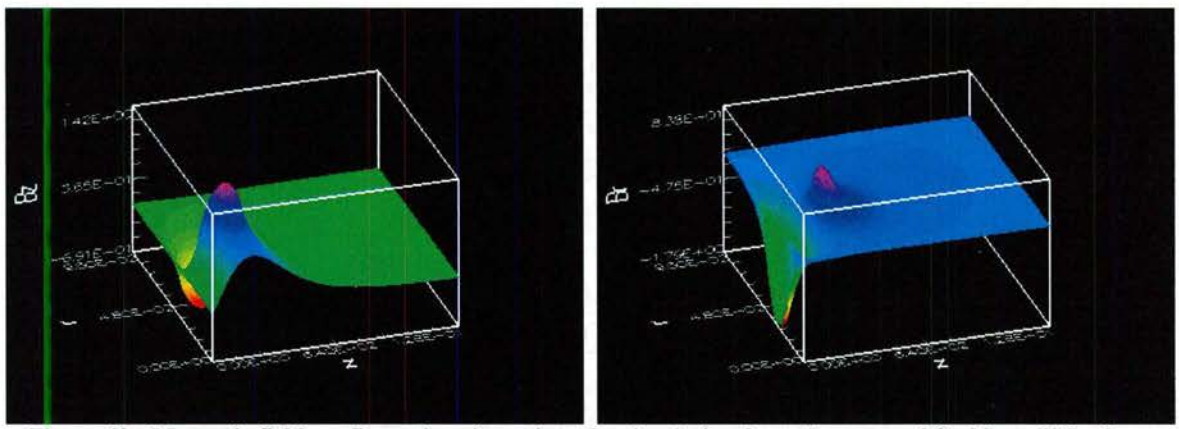

Figure 42: Magnetic field configurations input into the simulation from the external Stubbers EM solver.

The simulation input file used hydrogen (atomic weight A=1) atoms to speed up the simulation time and actually move ions within an appreciable amount of time, versus argon (A=40) atoms which would take 6-7 times as long. Monte Carlo gas collisions and ionizations were scored using OOPIC-Pro's internal routine for a non-uniform neutral gas loading. To approximate the neutral gas expansion away from the spacecraft, a linear weighting was used across the z-axis of the simulation with a peak value of 10mTorr on the left boundary and 0.1mTorr on the right. Figure 43 shows the initial gas distribution and the plasma number density over 4 microseconds of simulation.

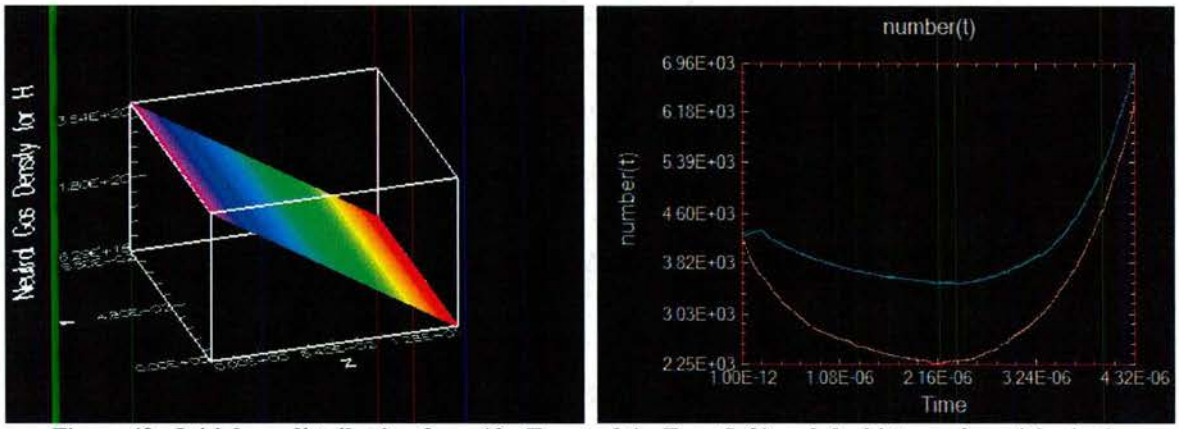

Figure 43: Initial gas distribution from 10mTorr to 0.1mTorr (left) and the history of particles in the simulation space showing electron heating and ionization after 2usec.

A time step of 1E-12 seconds was used in the EM model that was tested for numerical stability. The following figures detail results from the simulation space after 4 microseconds of simulation time. The electron and ion phase space plots denoting position of PIC super particles is shown in Figure 44(a-b). Note that the majority of plasma follows the magnetic field lines near to the conducting surface on the left side. This is an artifact of the higher gas density for the Monte Carlo collision subroutine. Subsequent simulations will employ an improved gas distribution as a function of z and r to improve the validity of the simulation.

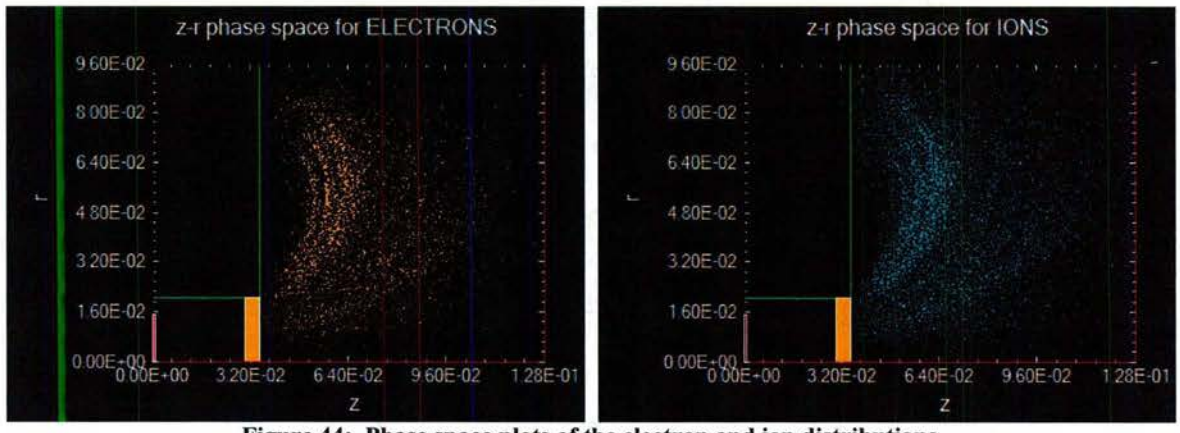

Figure 44: Phase space plots of the electron and ion distributions.

Examining the velocity space distributions tells the most information about the makeup of the plasma potential and the ambipolar acceleration terms. Figure 45a shows the axial component of velocity as a function of z position in the simulation system. The scale has been zoomed in to observe the ion distribution and it has a characteristic Espstein-like shape with a higher-energy tail on the right. This is an important result, since it shows ion acceleration and velocity out of the thruster.

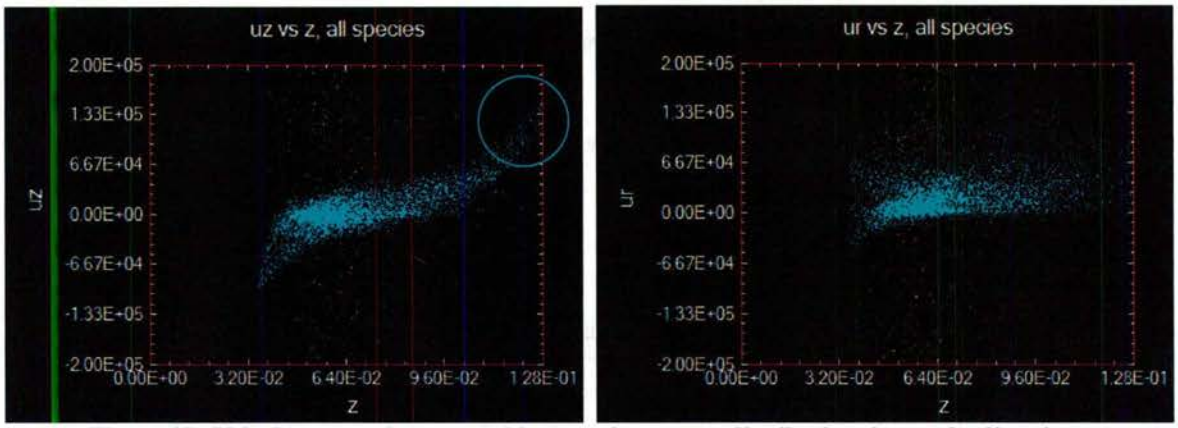

Figure 45: Velocity space plots zoomed in to see ion energy distributions in z and r directions.

The minimum in the velocity on the left corresponds to the effective plasma sheath potential immediately before striking the dielectric and conductor surfaces on the spacecraft. A velocity of -1E5 m/s roughly corresponds to a max ion energy of 52eV for hydrogen gas, thus we can conclude that the plasma potential is quite high. The exit velocity for ions on the opposite simulation exit boundary is 1.5E5 m/s, corresponding to a max energy of 117eV.

$$E_{plasma} = \frac{1}{2} m v_{ion,wall}^2 \tag{15}$$

$$E_{ambipolar} = \frac{1}{2} m v_{ion,exit}^2 - E_{plasma} \tag{16}$$

Assuming that the plasma potential has come to near-equilibrium (which is a poor assumption with only 4 microseconds of elapsed time), subtracting both values yields a net ion acceleration due to the ambipolar field to be approximately 65eV. This can be confirmed in the OOPIC-Pro graphical outputs in Figure 46 for the ions on the exit boundary diagnostics, showing distribution in energy space up to 120 eV. Note, there is a lot of scatter in the data due to the initial low-temperature plasma loading in the thruster getting expelled from the simulation space.

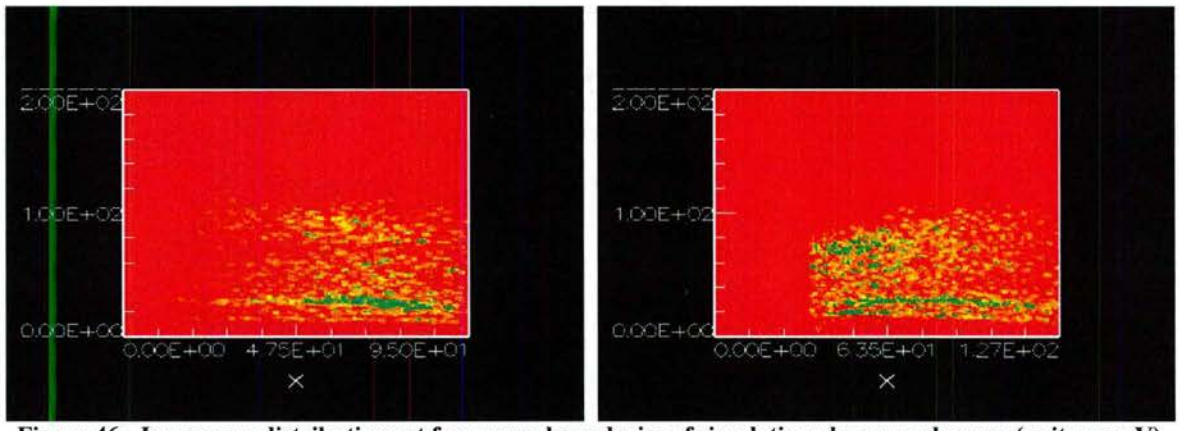

Figure 46: Ion energy distributions at free-space boundaries of simulation along z and r axes (units are eV).

The resulting simulations show that there is promise for modeling the ECR magnetic nozzle expansion conditions present in a conceptualized system. Since the magnetic fields are rather large (and radial) and the plasma electrons are highly-magnetized (and the hydrogen ions are to a small degree too in the simulations), an improved geometry that has a wider resonance zone with lower power microwave fields would be ideal to generating ionization locally in a high pressure gas-injection region, and then expansion out a small magnetic nozzle.

4.2.1.1 Refined Mesh and EM Injection

Additional numerical simulations were performed with the OOPIC-Pro particle-in-cell code for the TM01 electromagnetic launcher configuration, approximating the current experimental geometry to zero order. An improved computational mesh from 6.4cm to 12.8cm was designed with a better axial-diverging magnet configuration. Again, the 10-GHz frequency was modeled with a simulated TM01 waveguide and quarter-wave injector quartz plate. Even this setup took days to simulate on a high-end workstation due to the Courant-condition timesteps for EM propagation and high particle count.

Resonant plasma formation occurs approximately along a ring-like surface with vanishing power flux and a density minimum on the central axis of symmetry. Figure 47 shows early stages of plasma formation after a few microseconds of operation. High energy electron acceleration out of the simulation region with energies exceeding 200eV was observed with subsequent ion acceleration across a band of energies from 20eV to 100eV over the simulation time. This verifies the presence of magnetic expansion and ion acceleration.

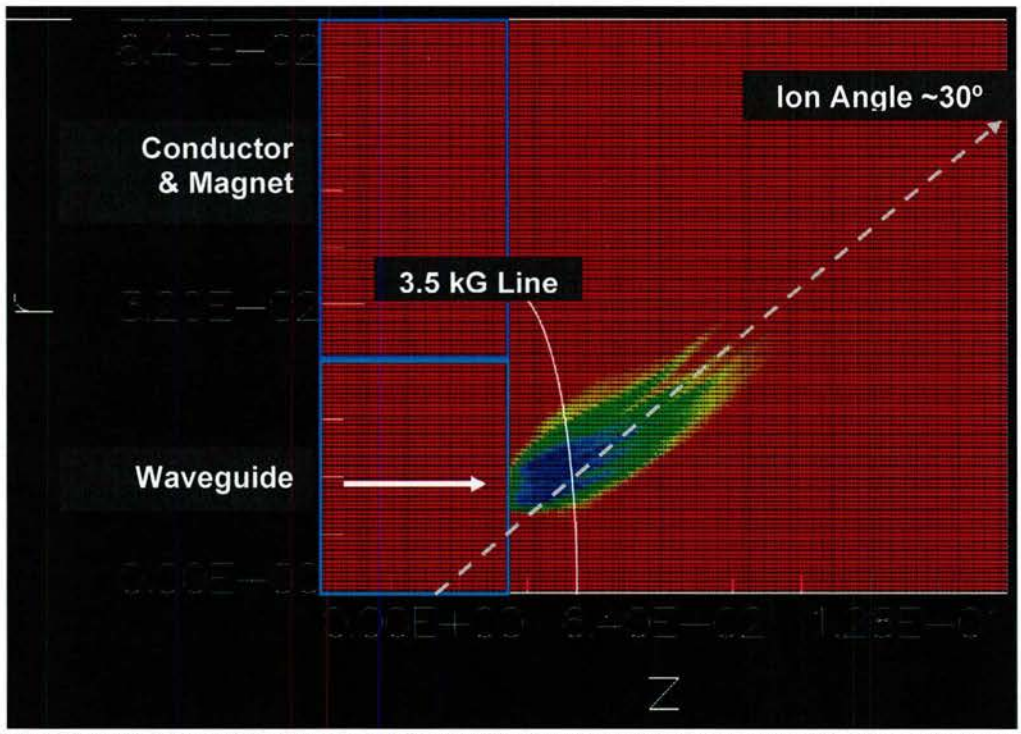

Figure 47: Ring-like plasma density profile for TM01 electromagnetic waves launched into ECR zone. Note the expansion and ion acceleration into a ~30° cone with minimal density on the centerline.

In this simulation an ion divergence angle of 30 degrees was estimated, and this compared well with the measurement of 23 degrees with the RPA and LP diagnostics for the 2.45 GHz experimental apparatus since there is a longer quartz drift tube for ion acceleration without rapid gradient in magnetic field.

These OOPIC simulations would eventually cause the small Dell workstation to crash due to memory overflow errors with high particle count, since microwave breakdown and collective plasma interactions with the EM fields are being simulated. The Linux MPI version of OOPIC-Pro from TechX corporation has not been working properly for EM modeling.

4.2.2 Literature: High-Energy Ion Production Efficiency

A good paper was published by Mark Kushner and one of his graduate students on electron energy distributions in an ECR discharge for application to materials processing.[2] In the late 1980s-early 1990s there was an explosion of growth in the computer manufacturing industry. Multiple approaches were vetted for reactive ion etching and materials modification for silicon wafers for improved speed, uniformity and reliability. Kushner's group performed simulations on these systems for comparative analysis.

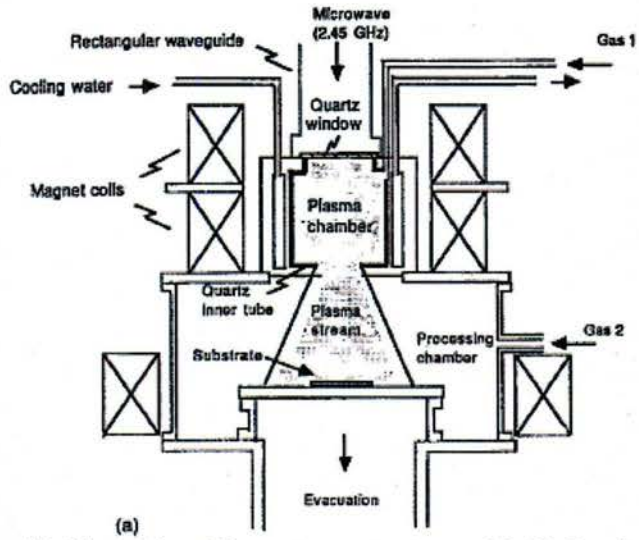

Figure 48: Illustration of the system geometry used in Kushner's paper.

In this paper, he related the EEDF across the discharge and how energy losses are treated from the ECR zone, and then downstream towards the wafer substrate (for processing applications). He finds that the EEDF has two distributions, a low-energy component from inelastic collisions and the high-energy electrons from the resonance zone where they pickup a lot of perpendicular energy. In the simulated chamber and field geometry, he finds that there are some electrons ~120eV at 800W operation. However, the ambipolar potential would max out at about 40eV because the electrons were escaping the plasma and hitting the walls before expanding out of the system.

> *During the time that 30eV electrons (Te = 3/2<E>) which have half of their energy in the perpendicular component move 5-10cm out of the ECR zone, the experience 5-10 collisions, of which 15-20% are inelastic. This decreases the Te outside the resonance zone until the electrons cool and only have e-e collisions. The high-energy tail, which has commensurately lower collision frequencies, takes longer to have these few collisions and therefore persists for a longer time. The lower rate of energy exchanging e-e collisions makes the tail less sensitive to thermalization than the lower portion of the EEDF. The loss of higher energy electrons which climb the plasma potential and escape from the plasma reactor ultimately determines the energy at which the distribution is cut-off....The cut-off in the distribution at approximately 40eV is partly the consequence of higher energy electrons being able to escape the plasma.*

The key finding in this paper (relevant to Starfire Industries' STTR program) is that the ambipolar potential is accelerating ions in the system and electrons are converting their expansion energy into ion energy in the quasi-steady field. Ironically such a high-energy ion population was considered unfavorable for wafer processing since it is preferable to apply an RF bias to the substrate to control the extracted ion energy.

> *The power dissipation in the Ar plasma is dominantly shared between impact ionization and ion acceleration. At 2mTorr and 150W, 21% of the power is dissipated by electronic*

excitation, 36% by electron impact ionization, and 43% by ion acceleration. Since the ion mean free path for charge exchange is <2cm at 2mTorr, approximately 30-40% of this ion energy goes in to gas heating. As pressure decreases, the fraction of power dissipated by ion acceleration increases; at 0.2 mTorr, 67% of the power is dissipated by ion acceleration!

Even in this non-thruster geometry, 67% of injected microwave power is converted into ion acceleration! **It is worthy to note that this jet power efficiency rivals that of modern Hall Effect Thrusters.** If the EEDF was not truncated by the loss of high-energy tail electrons to the walls of the device and perpendicular energy allowed to get into the expansion region, then the ambipolar potential would be higher, more energy would be transferred to ions and a higher fraction of electrical power would go into jet power.

Kushner's results also corroborate Starfire's Monte Carlo simulations with the OOPIC-Pro code, confirming the existence of high- energy electron and ion acceleration. As a side note, this paper also notes that due to the complexity of electron motion in the high B field and multiple electron energy groups there is a lot of noise in the EEDF. This will make interpretation of conventional Langmuir probes difficult.

4.3 Defensive Counter Space Analysis

In the preceding sections, we have established that high energy plasma can be generated with microwave EM coupling, propulsion can be achieved with expansion out of a magnetic nozzle without the need for a cathode neutralizer, a wide range of performance parameters can be achieved by selecting the size and length of the resonance zone for ECR coupling, and nearly 100% ionization fractions can be achieved at high densities.

As mentioned in the Phase I proposal, the microwave thruster has inherent application as a DCS system for object detection, identification and disabling. Starfire identified three possible configurations that utilize these DCS capabilities and they are: 1) remote object detection; 2) x-ray generation; and 3) focused microwave negation. These three concepts are shown schematically in Figure 49. Additionally, there is another defensive screening application where a plasma density gradient can be used to absorb incoming EM radiation to "screen" or "jam" transmissions from reaching a satellite.

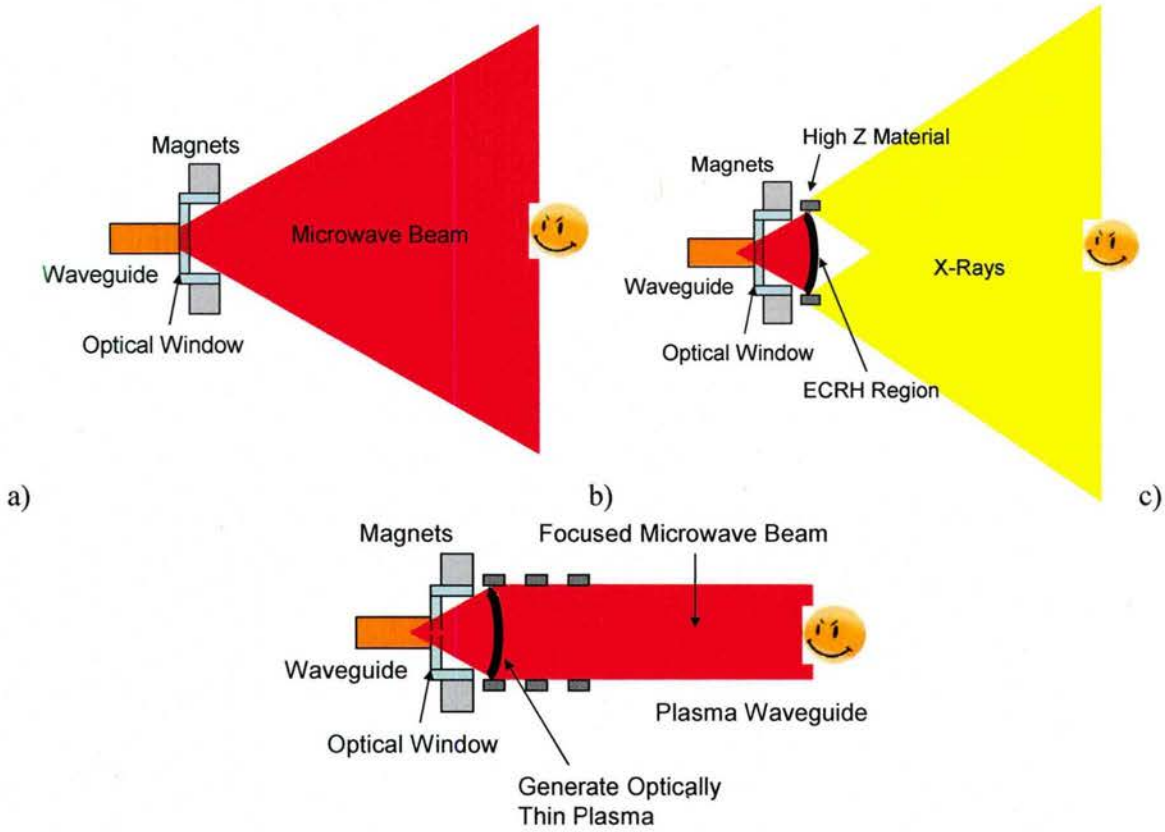

Figure 49: Schematic illustrating the DCS capabilities of the proposed ECR thruster in a) wide-angle microwave, b) x-ray inspection, and c) focused microwave operation.

The Phase I proposal illustrations in Figure 49 do not require waveguides and can be replaced by phased array microwave antenna emitters, other EM launcher configurations, or hardware to take advantage of the onboard microwave power systems for communications and control.

4.3.1 Remote Object Detection

Conventional detection and ranging applications, as shown in Figure 49a, an X-band microwave transceiver system could operate in a multi-mode configuration, switchable from pulse to doppler to pulse doppler. These microwave configurations could allow threat detection at several miles range and velocity detection using CW doppler for close range. There are existing systems and technologies for these applications marketed by Raytheon, TRW, etc. in a well proven and established field.

From the Phase I experimental data, microwave energy can be directed from the object detection array into a static magnetic field nozzle with local propellant injection to achieve propulsion. This could be very attractive for small picosat and nanosat systems where multi-mode operation is very important due to limited mass, power and volume for multiple subsystems.

4.3.2 High-Energy X-Ray Generation

Local x-ray production can be achieved by spinning up electrons in the microwave ECR region to very high potentials in excess of 10keV! Depending on the shape of the magnetic field to produce a "bottle" effect or a very long resonance zone >1cm, it is possible to accelerated electrons to keV energies. If these electrons are directed into a high-Z target material, such as a thin lead strip, then bremsstrahlung radiation will be emitted with a characteristic spectrum that can be used for active interrogation of spacecraft or objects. Since desirable propellants are typically massive atoms, such as xenon, electron interactions with the gas phase propellant can also be used to generate x-rays.

4.3.2.1 Plasma Bremsstrahlung X-Ray Generation

From a review of the literature, the use of ECR plasmas to generate penetrating x-rays with energies ~100keV is feasible. Using the VENUS (Versatile ECR for Nuclear Science) ion source, Leitner and collegues explored the x-ray spectrum generated by 18-GHz and 28-GHz xenon ECR discharges with powers ranging from 500W to 7kW and the effect of magnetic field profile on the resulting bremsstrahlung spectrum[3]. Figure 50 shows some of the x-ray spectra acquired from their experiments. Photon energies ranging from a few keV up to ~1MeV, even for the lowest power case. A large fraction of the resulting x-rays are between 50 and 100keV, which is a typical range of energies for commercial x-ray generators. The source of photons in this experiment was from the plasma itself, rather than electron collisions with a solid high-Z target.

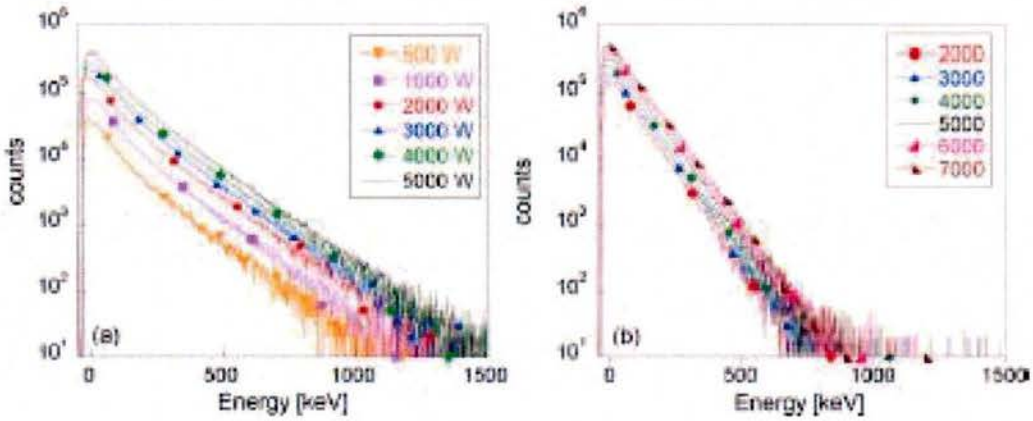

(a) (b)

Figure 50: Bremsstrahlung spectra obtained in the VENUS ion source discharge (a) Bmin=0.7T and (b) Bmin=0.45T.[3]

4.3.2.2 Solid-Target Bremsstrahlung X-ray Generation

Similarly in 1992, Noah Hershkowitz and his graduate students at the University of Wisconsin published a paper on the production of x-rays in ECR processing plasmas.[4] They found

measurable x-ray generation whenever a magnetic field line that passes through the cyclotron resonance surface intersects with the vacuum chamber walls and/or other solid surfaces inside the processing chamber. Since collision frequency drops as the electron energy increases between collisions, then the resonant electrons will "run away" from the bulk portion of the electron energy distribution and become energetic enough to emit x-rays by collisions with solid materials (wall bremsstrahlung) or with ions and/or neutral particles (free-free bremsstrahlung). The following plot (Figure 51) is reproduced from this 1992 paper showing x-ray generation for a nitrogen ECR plasma from the U. Wisconsin processing reactor.

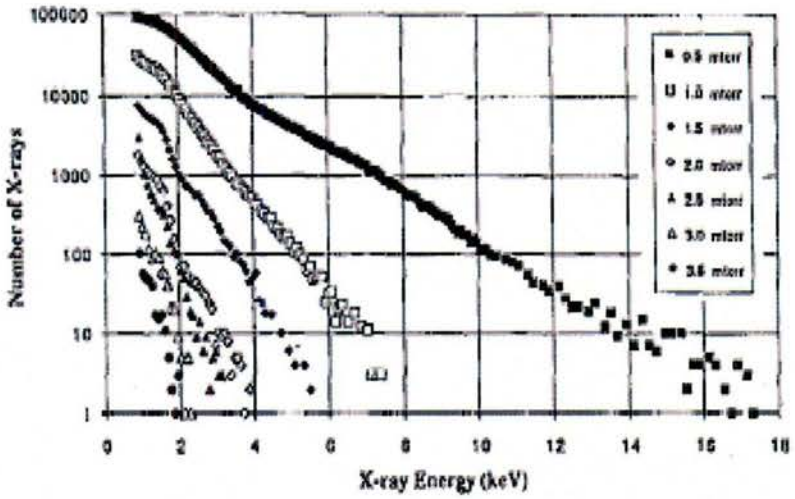

Figure 51: X-ray spectra for 1kW microwave power using nitrogen pressure as a parameter.

Hershkowitz's team also found that minor adjustment to the magnetic field topology to direct electron streams away from solid surfaces had a major impact on x-ray emission yield, as well as variation in pressure as shown in the above plot. This literature reference demonstrates the hypothesized x-ray generation with an ECR-based plasma system. Also note that OOPIC-Pro simulations also show very high electron energy gains in the resonance layer, leading to >1 keV energy if the width zone is long enough for an electron to experience multiple orbits.

4.3.3 Focused Microwave Beam Negation

In Phase I, Starfire operated the microwave ECR system in an underdense mode and the combination of microwave energy and plasma impingement melted cables and interconnects leading to diagnostic failure. Note that the configuration of the magnetic field and magnetic nozzle expansion will greatly affect the shape of the expanding plasma cone and subsequent "focusing" capability.

Interesting data between the underdense and overdense operation modes for the ECR system tested in Phase I is represented in the RPA plot for Figure 30. It exhibits an interesting feature of a high density plasma annulus with a lower density internal core. This is the proper configuration for a plasma waveguide to direct microwave energy onto objects. The RPA result

is encouraging and suggests further study in this area, especially with plasma modeling and simulation tools.

With a general microwave waveguide opening into free space, the EM energy radiates outwards with a $1/r^2$ power law drop in intensity. For directed energy beaming towards a target for disabling and negation, the creation of a low-density plasma waveguide channel will serve to "contain" EM energy and direct it towards an approaching spacecraft.

If plasma is accelerated with a net axially directed momentum with little radial motion, it is possible that this plasma annulus could be extended for several meters away from the spacecraft to guide EM radiation towards an object. The net ion motion can provide "rigidity" to the plasma waveguide to extend it over a longer distance.

4.3.4 High-Density Plasma Screening

Generating high-quality plasma in front of a satellite can disrupt communications and ground transmissions by blocking line of sight. Plasma densities at the $\sim 10^{12}$ cm^{-3} level and below, demonstrated in Phase I, are sufficient to disrupt, absorb or scatter a wide range of communications at frequencies up to 30 GHz (SHF ground data links).

The directed plasma exhaust from the microwave propulsion system can also directly heat spacecraft surfaces, damage solar panels and thin film electronics (thermally and sputtering), and also make opposing spacecraft susceptible to other forms of directed energy. Since microwave propulsion systems can use nearly any propellant, the plasma exhaust could be fouling and coat opposing control surfaces rendering an enemy craft neutralized.

Part 5: Estimates on Technical Feasibility

The Phase I research has shown that there is a clear pathway for efficiency propulsion with DCS capabilities of: (a) Detect, (b) Discern, (c) Disable, and (d) Deceive, in addition to data transmission. On-board microwave power systems for communication can be leveraged into propulsion and DCS activities for a "win-win" for EP. Starfire Industries and the University of Illinois believe that the microwave approach offers the most flexibility to achieve success. In addition, there are near-term commercial applications for microwave-based plasma technology that increase the chance for technology development and success in the marketplace.

5.1 Feasibility With MILSATCOM

Current space-based communications systems utilize a series of discrete frequency bands for ground-space uplinks, space-ground downlinks, and space-space crosslinks. Figure 52 shows a list of communications platforms and frequency ranges.

SYSTEM	UPLINK	DOWNLINK
UFO MUOS	290-320 MHz 300-320 MHz	240-270 MHz 360-380 MHz
Commercial Ku Band	13.75 - 14.50 GHz	10.95 - 12.75 GHz
Global Broadcast Service (GBS)	N/A for ship	20.2 - 20.7 GHz
MILSTAR	43.5 - 45.5 GHz	20.2 - 21.2 GHz
Advanced Extremely High Frequency (AEHF)/EHF	43.5 - 45.5 GHz	20.2 - 21.2 GHz
Interim Polar System (IPS)	43.5 - 45.5 GHz	20.2 - 21.2 GHz
Wideband Global Satellite (WGS) (includes GBS)	7.9 - 8.4 GHz 30 - 31 GHz	7.25 - 7.75 GHz 20.2 - 21.2 GHz

Figure 52: MILSATCOM communications platforms and frequency ranges.

For example, the Wideband Gapfiller constellation will supplement military X-band (roughly 7–8 GHz) communications capability now provided by the Defense Satellite Communications System and the military Ka-band (about 20–21 gigahertz down, 30–31 gigahertz up) capability of the Global Broadcast Service. In addition, the Wideband Gapfiller includes a high-capacity two-way Ka-band capability to support mobile and tactical personnel, see Figure 53.[5]

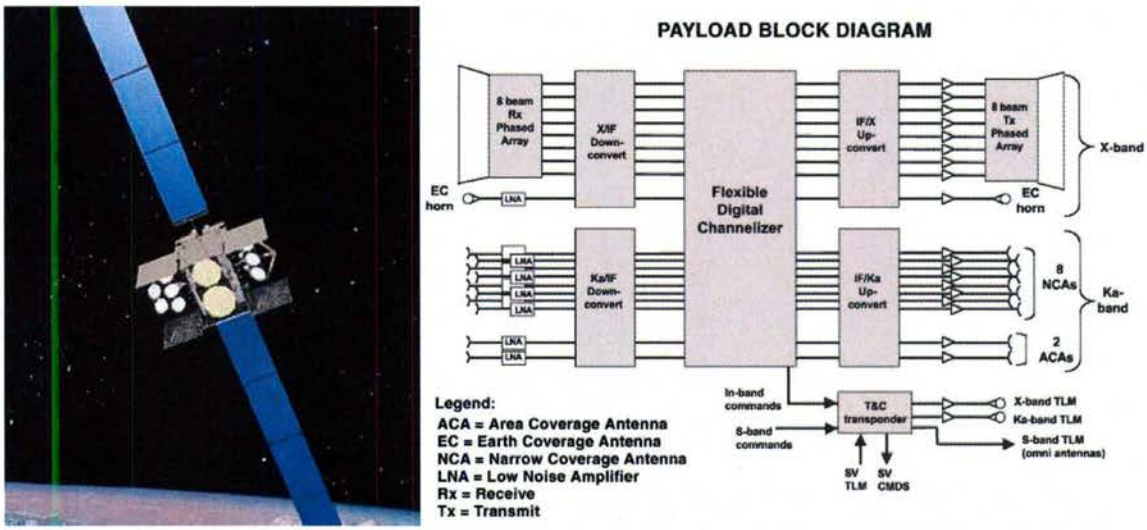

Figure 53: Wideband gapfiller satellite (left) with phased-array antennas payload diagram (right).

The AEHF satellite, due for launch in 2008, will offer an order-of-magnitude increase in protected communications capability to augment the aging MILSTAR platforms using over 10,000 RF/microwave/millimeter wave modules with ~10kW power available.[6] The AEHFs will carry several advanced 4.5kW HET thrusters suitable for orbit raising and station keeping in GEO orbit. While the actual thrusters are not too large and massive, the power processing unit needed to service several EP thruster systems is massive. Even with this additional weight and size, there is a significant 1000-kg savings compared to an all-chemical system due to the high Isp from the HET.

Defense satellite systems scheduled over the next few years will include more microwave hardware than ever before with high-levels of on-board electrical power in the 15-35kW range. A large amount of research and development has gone into lowering the cost of the solid-state

power amplifier and antenna circuitry[7], including digital combiners and dividers to active phased array antennas.[8]

Phased arrays will use thousands of microwave modules per satellite, and some satellite constellations will consist of as many as 20-30 satellites. DARPA has actively funded progress in this area to drive the cost down and increase the functionality of phased array systems.[9] These systems have the capability to generate spot beams with different frequencies to service thousands of ground stations and orbiting satellites for communications relay. Active phasing can create modal EM structures and standing wave patterns that could be directed into a magnetic nozzle system for plasma generation and propulsion.

Thus, there is a great opportunity for further technical feasibility and evaluation with specific frequency and power platforms.

5.2 Multi-Mode Microwave Propulsion w/Secondary DCS

Since microwave energy can be directly beamed into the propellant for heating, ionization and acceleration, innovative microwave thrusters with multi-mode propulsion capability are possible for operationally-responsive and DCS space missions. Such a system could operate as: (1) an straightforward cold-gas thruster for rapid-response high-thrust maneuvers, (2) an electro-thermal thruster for moderate-thrust large-ΔV maneuvers, by direct microwave propellant heating for expansion out a conventional nozzle in the 500-800 sec range, and (3) an ambipolar ion thruster for high-I_{sp} propellant-conserving maneuvers, by an ambipolar/magnetic nozzle expansion technique for ion acceleration into the 10-200 eV range (with and without ECR).

Since the microwave thruster is electrode-less, a wide variety of propellants can be used including liquid-storable or vaporizable solids. This opens the door for increased flexibility with satellite design, especially with the use of water or ammonia propellants that are easily utilized. Furthermore, this system is a plasma thruster, meaning no external neutralizer cathode is needed. As stated, this class of microwave propulsion system could leverage existing on-board microwave power from communications infrastructure; thereby obtaining a significant mass savings by avoiding an additional power processing unit.

Starfire Industries proposes advancing this propulsion system further with the addition of the diverging magnetic nozzle for thruster operation in the ambipolar regime for higher Isp and achieving dual mode operation, as shown in Figure 54.

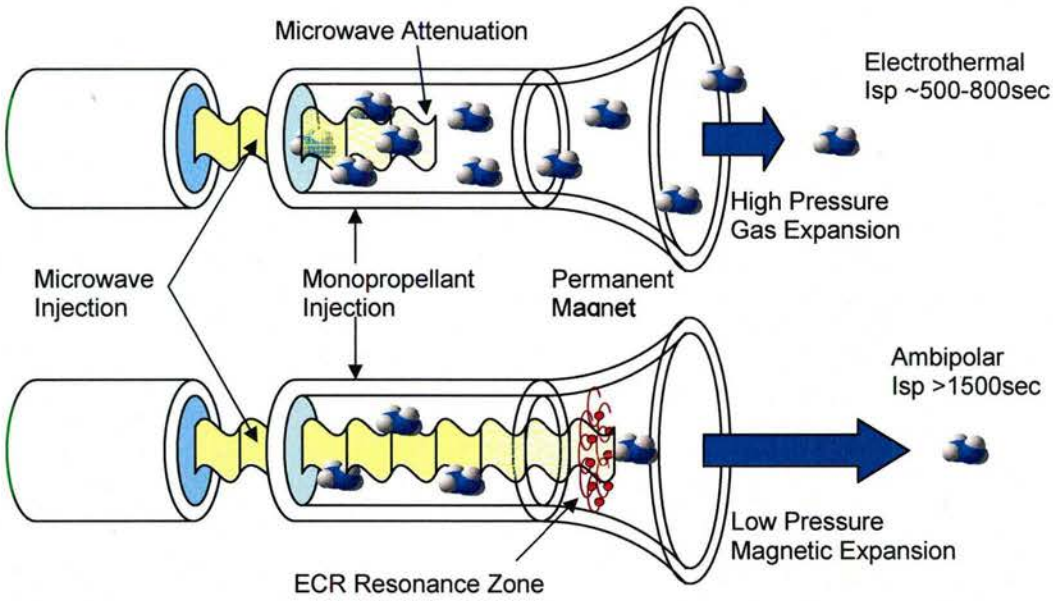

Figure 54: Illustration of electrothermal (top) and ECR-driven ambipolar (bottom) acceleration modes.

Microwave plasma generation has been researched at Penn State University by Micci et al. for application to supersonic combustion ramjet engines and electrothermal electric propulsion at 7.5GHz[10] and 14.5GHz.[11] Moderate Isp ranges have been demonstrated with no erosion and long thruster lifetime. Additionally, their team has demonstrated microwave thruster operation with nitrogen, ammonia, hydrazine and other storable propellants.[12]

The components of this type of multi-mode microwave thruster are fairly straightforward. There are no electrodes in contact with the plasma since it is a resonant wave interaction phenomenon which generates and sustains ionization. The ionization zone is located in the diverging section of the magnetic nozzle such that nearly all ions which are formed from electron impact will be utilized and accelerated downstream in the ambipolar potential; this minimizes ion wall loss and decreases ΔE/ionization cost.

When the gas density is sufficiently high, depending on the microwave driver frequency, the electron density will exceed a critical value through ionization collisions and bulk build up.[13] At this point, electrons begin collective action in response to the applied EM field and begin to absorb microwave energy directly into thermal motion of electron in the gas. Instead of a resonant layer for cyclotron action and ambipolar acceleration, microwave energy is now transferred to plasma near the waveguide inlet port. Using the critical density function for microwave propagation as a function of frequency, Table 2 shows the estimates for magnetic field for ECR and collective attenuation. Note that this critical density function is simply when the electron plasma frequency is equal to the driver frequency, microwave absorption occurs in a continuous spectrum about this point.

Table 2: Critical density for bulk microwave absorption and magnetic field required for ECR.

Applied Frequency [GHz]	ECR Magnetic Field [kG]	Critical Density [electrons/cm^3]
2.45	0.875	7.5E10
7.5	2.7	7.0E11
14.5	5.2	2.6E12
20.5	7.3	5.2E12
44.5	15.9	2.5E13

For electrothermal gas expansion and acceleration, this process is ideal and can maximize thermal energy transfer to the propellant. Design of the microwave inlet, propellant injection, fluid dynamics properties and gas residence time are important to determine overall coupling to the exhaust gas.

In summary, there are four different modes of operation of a microwave thruster: (1) ambipolar acceleration with ECR for very-high Isp, (2) ambipolar magnetic expansion without ECR (direct microwave heating) for high Isp, (2) electrothermal for moderate-Isp and moderate thrust, and (3) cold gas expansion for quick high impulse adjustments at low Isp. Based on this understanding, Starfire Industries is highly optimistic about the potential for a microwave-driven thruster technology to achieve highly-efficient electric propulsion at multiple thrust and specific impulse levels.

Microwave energy can be fed into a waveguide and injected into a cavity for direct heating of the propellant. Different microwave applicators, such as axial injection, co-axial injection, or transverse injection, all have different advantages. One aspect of a future Phase II project could focus on development of these systems for a multi-mode propulsion system with inherent DCS capability for both low power and high power applications.

5.2.1 Low Power Propulsion

This multi-mode microwave system could be developed with small-size high-temperature permanent magnets for used with solid-state high-frequency microwave communication circuits.

By augmenting the electrothermal thruster concept with the ambipolar magnetic nozzle expansion technique, a simple thruster geometry can be built for integration on spacecraft serving the: (1) auxiliary role of station keeping and minor attitude adjustments (drag correction), or (2) serving as the primary propulsion on nanosats or picosats.

Simple gas/liquid feeds that vaporize propellant, such as hydrazine, will work well. Samarium-cobalt high field magnets with temperature levels up to 350C make this system realizable at small size.

5.2.2 High-Power Propulsion

The multi-mode architecture is ideally suited for scale up for high-power main propulsion on large satellite systems or even for an orbital transfer vehicle with an "all microwave" system bus. Phase I testing with a 750W magnetron yielded measureable plasma acceleration results in a non-optimized configuration for producing and generating thrust. Multi-kilowatt thruster levels will be limited by EM transmission equipment and magnet configuration.

For very high power systems large permanent magnets are not feasible due to size and weight concerns; thus, an electromagnetic solenoid and field shaper will be necessary to accommodate the dense plasma exhaust. HET systems typically use a hybrid approach with high-current electromagnets generating magnetic flux and steel pole pieces guiding the field into a radial annulus for electron trapping. Similar configurations are possible for high-power microwave systems and will require engineering design studies.

The University of Illinois has a 6kW continuous microwave power supply at 2.45GHz that could be used for testing high-power propulsion in a Phase II program. Improved vacuum infrastructure would be needed for this level of continuous power, such as Chamber 3 at AFRL Edwards.

5.3 DCS/Communications w/Secondary Propulsion Capability

The previous section was focused on developing a propulsion system that could be used for DCS activities as a secondary benefit. The other design approach is to focus on the DCS system as the primary system, and then augment such a system with propulsion as an additional side-benefit.

5.3.1 Phased Array Propulsion

In wave theory, a phased array is a group of antennas in which the relative phases of the respective signals feeding the antennas are varied in such a way that the effective radiation pattern of the array is reinforced in a desired direction and suppressed in undesired directions. Such an array could be augmented with a permanent magnet structure to produce one or more magnetic nozzle regions with individual propellant feeds. The result would be a simple thruster concept.

A near-term feasibility and test demonstration could be performed with a phased-array microwave antenna and a magnetic nozzle and propellant feed system that could be mounted to a satellite. This system could be a part of a nanosatellite system for Operationally Responsive Space (ORS), such as local detection and ranging of potentially hostile craft approaching within the vicinity of large DoD assets, e.g. the AEHF communications and data relay network. For this system, a phased array microwave transmitter array with receiver capabilities for remote detection could be designed with a secondary propulsion capability.

Figure 55 is an illustration of an example thruster configuration with a phased array antenna structure. The steerable EM radiation beam can be swept spatially, in frequency and power, and can be directed into a magnetic nozzle mounted to the spacecraft surface. In the lower figure, two separate phased antenna arrays are beaming microwave power just above the propellant injector port near a permanent magnet assembly. Plasma is generated and heated at the top of the magnetic field and expanded to produce thrust.

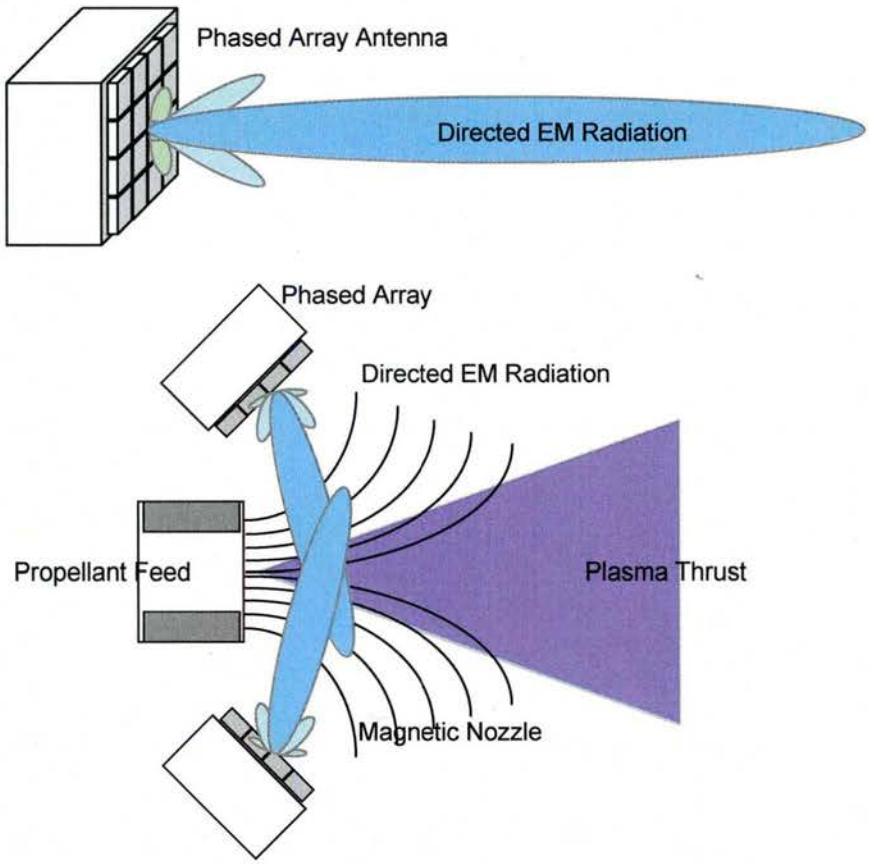

Figure 55: Phased array antenna with directed EM radiation (top) and on example configuration magnetic nozzle thruster configuration (bottom).

Note that there are many other configurations with magnetic nozzles that are possible, and future research and selection of optimal configuration will depend on the satellite mission, on-board array capabilities and mission goals.

5.3.2 Defensive Counterspace Feasibility

From the Phase I testing, DCS activities with microwave sources and plasmas are plentiful, and there is considerable opportunity to demonstrate DCS and dual-use feasilbility in Phase II and beyond for:

- Remote Object Detection: phase-array microwave transceiver scanning
- Illumination and Evaluation: x-ray and plasma illumination
- Disable and Negation: focused microwave beam with plasma waveguide
- Screening and Protection: local high-density plasma shielding and fouling

Remote object detection and ranging is a well established art within the wavelength bands of interest. Transceiver arrays and synthetic aperture nanosat and picosat clusters could provide Space Situational Awareness (SSA) and object negation.

An X-band source can easily produce a 4-degree beam width with small aperture antennas that could be used to direct a high-power microwave beam at a target. The beam would desensitize the transponders making it "deaf" or unable to receive signals. Thus, a focused microwave could render an opposing spacecraft unable to receive ground or space commands, e.g. rendering it immobile. In addition, suitable plasma conditions could allow focusing of microwave energy onto a close target for neutralization. In this scenario, the microwave energy is "contained" by the weak plasma column to focus on an opposing satellite to disrupt solar cells, cause local heating and melting of critical components, and disrupt electronics.

Demonstration of a focused beam of microwaves on a characteristic solar array panel could be performed with a microwave plasma setup. In Phase I, diagnostics, cabling and materials were locally melted by high-power microwave impingement at <50cm. Testing beyond Phase II could actually show this in a characteristic environment.

Another DCS application is to deploy a wide-area plasma screen around the satellite to block incoming communications or diagnostic sensors, such as a targeting lock. Or local plasma generation can be used to defeat "nulling" antennas and circumvent anti-jamming capability without actually harming an enemy satellite. With sufficient density gradient in plasma, including communication transmissions can be blocked or attenuated to prevent communications with another satellite or ground station. These systems can be operated for defensively, but impede the operation of an enemy satellite.

With ECR electron acceleration, x-rays can be generated on-orbit and used for interrogation of objects and even to overwhelm sensors and sensitive electronics. Bremsstrahlung targets and specially-shaped magnetic bottle geometries can enable a simple high-flux x-ray source. There is an opportunity for demonstration of such a system in Phase II and beyond.

5.4 Compact Plasma Sources

Generating high-density plasma is particularly important for directed ion sources, since extractable (usable) current is a function of local plasma density near an orifice with an separate extraction or focusing electrode providing the extraction of ions into a useable beam. In this Phase I research, we have shown that electron energy (velocity) perpendicular to the magnetic nozzle field can be resonantly excited by microwaves and directed downstream with very high plasma ionization fractions and density. A microwave plasma source would be superior to conventional methods because of:

- Low radial plasma loss due to axial field
- High power coupling efficiency for complete ionization
- Net-directed axial plasma momentum
- Electrode-less plasma generation

The low radial loss and high-power coupling efficiency directly translate into very high plasma densities and extractable current capability for a given pressure of operation. More importantly, the net axial momentum generated by the magnetic nozzle expansion serves to eliminate the need for a separate extraction electrode or grid to form and direct the ion beam. This removes a physical electrode that depletes the beam current (% transparency) and is a sputter erosion target for heavy ions that affect lifetime of the ion source. With EM power coupling it is possible to have an electrode-less system with long lifetime. There are multiple applications in semiconductor manufacturing, surface preparation, materials processing, etc.

5.4.1 Compact Neutron Source

Starfire Industries has an active program related to developing compact neutron sources for industrial non-destructive testing and materials assay. The current state-of-the-art neutron source uses a Penning Ion Source to produce an ion beam that is accelerated into a target for the production of deuterium-deuterium or deuterium-tritium fusion reactions to generate neutrons. The key requirements for these devices is that they are small in diameter (to fit down oil well boreholes or in medical applications) and have low power requirements. Figure 56 shows a diagram of a conventional system.

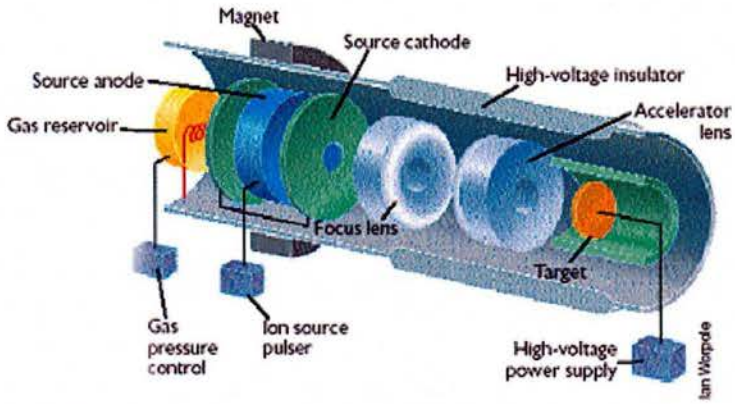

Figure 56: A traditional neutron generator source uses a Penning Ion Source which must operate at ground potential and is lifetime limited by electrode erosion.

The lifetime of these systems are limited by degradation of the ion source (ion bombardment and sputtering erosion) that degrades the high-voltage insulator and the target.

Also, the target region producing the neutrons has to be electrically isolated from its surroundings since it is elevated to high negative voltage (~100-150kV). This is unfortunate

since the neutron flux rapidly decreases with distance from the source (1/r2 power law). Ideally, a neutron source would be constructed with the ion source at high voltage and the target grounded so the source of neutrons could be located as close as possible to the object being interrogated (maximum neutron flux).

Since the Penning ion source (with multiple electrodes) requires several power supplies for operation in addition to an extraction/focusing electrode, it is extremely difficult to elevate the ion source to high voltage. ThermoFisher Scientific (developer of neutron sources) accomplishes this with a 1000kg specialty power supply that is very large in size and not practical for most applications.

The microwave ECR ion source would allow high-density plasma generation at voltage without an extraction electrode for superior performance. This would be an enabler for compact neutron source technology with high neutron flux capability. In addition, a compact co-axial geometry or resonant cavity source would reduce the ion source size for very high currents >10-100mA.

An important defensive space application where this technology could be important is active interrogation of other satellites for special nuclear materials and treaty compliance. An on-board compact neutron source could generate pulses of neutrons and look for signatures showing the presence of U, Pu, Th, etc.

5.5 Commercialization Strategy

Starfire Industries is planning to take a three-point strategy to commercialization of microwave plasma source and propulsion technology in the following areas:

- Near-Term Compact Plasma Source Technology (i.e. Non-Military)
- Mid-Term Nano/Pico-Sat Microwave DCS Propulsion Technology
- Long-Term High-Power Multi-Mode ECR Spacecraft Bus

Protecting US space-borne assets is becoming an increasing priority for both military and civilian satellites. Long-term commercialization efforts will depend on a DARPA-like technology demonstrator or DoD acquisition program geared towards the production of a medium-to-high-power propulsion technology for standardized EP-based upper stage replacement or satellite power, propulsion and navigation platforms. This STTR program and subsequent follow-on effort provides the basis for evaluating this concept to meet future USAF/DoD mission planning requirements.

Near-term investment dollars can be directed into compact microwave systems for industrial plasma sources, specifically for plasma neutron generation where high power efficiency is critical with a simple architecture that can survive harsh temperature environments similar to space.

The long-term future of electric propulsion will lie in the ability to integrate multi-mission functionality into a standard package for spacecraft design. The advantages of a highly-efficient

multi-mode electric propulsion system are: (1) increased dry payload to orbit (30-50% @ $10,000/kg) with more mission flexibility and (2) significantly lower launch costs by using cheaper launch vehicles, such as Delta 4 vs. Atlas 5 ($60M vs. $100M per launch). Adding in the defensive counter-space and diagnostic capabilities further increases the value proposition and acts as a tactical multiplier with reducing risk.

Starfire Industries is optimistic about the potential commercial opportunities that will result from successful demonstration of a "multi-mode" next generation EP system. To reach this level of readiness, Starfire's near-term development efforts are geared towards concept validation through the STTR program and high-power technology demonstration in a subsequent SBIR or T&E effort. Approximately $10M will be needed to bring this technology to market readiness.

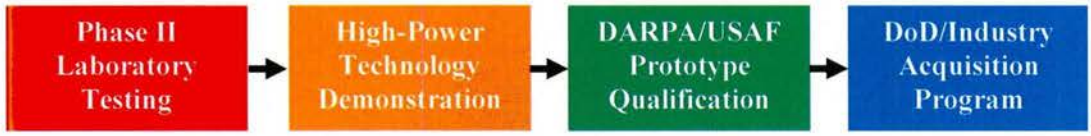

Figure 57: Defensive counter-space technology development pathway.

Due to the historical 10-15 year time horizon for electric propulsion concepts to reach maturity, (e.g. Aerojet and Busek Hall thrusters), it is very difficult for small business to continue technology development without incubation and support from the end-user/customer. This pattern of technology commercialization is present in many high-tech industries where capital and product development costs are high.

Part 6: Conclusions and Phase II Development Plan

With the conclusion of this report, Starfire Industries has met all of the Phase I objectives and demonstrated a clear pathway towards an electrode-less plasma thruster with multi-mode capability (i.e. high thrust and high Isp) and defensive-counter space activities (i.e. detection and disablement). The dual-use advantages using high-power microwaves make the argument for advanced electric propulsion stronger.

The results from the Phase I evaluation indicates multi-modal propulsion capability:

- ECR-driven ambipolar acceleration and magnetic expansion for high specific impulse (Isp)
- Direct microwave heating magnetic expansion for moderate-Isp levels and moderate thrust
- Electrothermal physical nozzle expansion for moderate-Isp and high thrust.

There are multiple avenues for this technological approach to be effective both big and small. Small nanosat and picosats with integrated microwave propulsion and detection/ranging could serve as the basis for deployable guardian (ANGEL) satellites to protect and monitor the local space around DoD assets, such as the AEHF network. A high-power primary microwave propulsion system can disable rogue satellites and perform additional on-orbit maneuvering at higher Isp for longevity.

The proposed microwave thruster could leverage even more functionality to existing spacecraft systems laden with communication systems. Microwave sources, such as phased-array solid-state power amplifiers (and older traveling wave tube amplifiers and klystrons), are already employed on satellites for communication and data link operations in the 2-50GHz range. A large amount of mass, volume, and power are already devoted to these microwave generators for communications. If the microwave plasma thruster system could be used for propulsion, DCS applications, and communications…this would truly constitute a "multi-use" system and be a win-win scenario.

Multiple configurations for DCS operations are envisioned with microwave plasma systems:

- Remote Object Detection: phase-array microwave transceiver scanning
- Illumination and Evaluation: x-ray and plasma illumination
- Disable and Negation: focused microwave beam with plasma waveguide
- Screening and Protection: local high-density plasma shielding and fouling

Based on a successful future Phase II, Starfire Industries would be positioned to rapidly commercialize a technology that would lead to near-term, flexible, efficient, and compact EP systems to meet Air Force mission requirements. We also envision concepts for low-power, ECR-based systems that could be useful for nano-satellite architectures.

For microwave systems in the 2-15 GHz range, permanent magnet solutions exist for ECR-driven thruster configurations that can achieve very high Isp with excellent system efficiency. For higher-frequency systems in the Q-band, where conventional electron resonance is difficult due to lack of magnetic field strength, additional research into improving transverse electron heating will be needed for efficient magnetic nozzle expansion. Microwave thruster configurations are possible without ECR, but maximum achievable efficiency will be lower. One area of research of further interest is active phased array antenna modulation for microwave energy concentration, wave beating, and harmonic electron acceleration.

An ambitious goal stemming from a successful STTR (and follow on research) would be to develop an advanced EP-based power, propulsion, guidance, navigation, control, and communication module to serve as the basic building block for future satellites. Essentially, this would be a new spacecraft bus that would serve as a common platform for mission planners and satellite designers. As of this date, no show-stoppers have been found towards this concept.

Starfire has also identified a near-term commercial opportunity for compact ion source technology based on the electron cyclotron plasmas, for simple plasma fusion neutron generators. Since ions are directed out of the ECR resonance zone with net forward energy, an efficient directed ion source can be manufactured for operation at high voltages needed to produce fusion reactions. Commercial prospects are excellent for a compact ECR plasma source for neutron generators, and Phase II STTR research can be leveraged into a near-term product. This technology could be suited for deployment on small satellites for active interrogation of foreign spacecraft for detection of special nuclear materials for treaty compliance.

Starfire has identified a near-term approach for such a technique and has established a relationship with a commercialization partner, ThermoFisher Scientific (NYSE: TMO), as a potential partner for Phase II testing.

Part 7: References

[1] A.V. Phelps, J. Appl. Phys. 76, July 1994, 747-753.
[2] J. Appl. Phys. **72** (1) July 1992, 33
[3] D. Leitner, J.Y. Benitez, C.M. Lyneis, et al, "Measurement of the high energy component of the x-ray spectra in the VENUS electron cyclotron resonance ion source," Rev. Sci. Instrum., 79 (2008).
[4] Appl. Phys. Lett., Vol. 60, No. 23, June 1992, 2856
[5] http://www.aero.org/publications/crosslink/winter2002/08.html
[6] http://www.afcea.org/signal/articles/templates/SIGNAL_Article_Template.asp?articleid=988&zoneid=4
[7] http://www.ottawa.drdc-rddc.gc.ca/html/tm_2005_055_e.html
[8] http://www.globalsecurity.org/space/systems/aehf.htm
[9] http://ucsdnews.ucsd.edu/newsrel/science/10-07PhasedArrayChipDK-L.asp
[10] S. Bilen et al., 41st JPC AIAA, 2005, 3699-937.
[11] K. Goovaerts et al., 43rd JPC AIAA, 2007, 5293-713.
[12] D. Clemens et al., 42nd JPC AIAA, 2006, 5156-842.
[13] J. Roth, Industrial Plasma Engineering Vol. 1, IOP Publishing, Philadelphia.